ROMA TRE
UNIVERSITÀ DEGLI STUDI

Dipartimento di Scienze Geologiche

The contribution of brittle deformation processes on improving hydrocarbon carbonate reservoirs: the Jandaíra Formation (Turonian - Campanian) as analogue.

by Aline Theophilo Silva

PhD Thesis in Geologia dell'ambiente e delle Risorse
XXIII ciclo

Tutor: Prof. Francesco Salvini
Dipartimento di Scienze Geologiche, Università degli Studi Roma Tre

Co-Tutor: Dr. Paola Ciafarra
Dipartimento di Scienze Geologiche, Università degli Studi Roma Tre

March, 2011

*To my parents **Alliria Theophilo Silva** and **Antonio Silva***
For all the support and love they have always given me.

*In memory of **João Baptista Filho** (1949 - 2009)*
My first professor of Geology, an example of love for this science, and someone that marked my personal development.

Acknowledgements

I acknowledge Petrobras for allowing me to do this PhD and for the financial support.

I also acknowledge the Roma Tre University, for receiving my PhD project, and my tutor Francesco Salvini.

I am especially grateful to my manager Maria José Resende Oliveira (Petrobras / Cenpes), for the support she always gave me, and to Professor Francisco Hilário Rego Bezerra (University of Rio Grande do Norte, Brasil), who gave me very useful advices and collaborated a lot for the field work. Their support was crucial for the successful completion of this work.

I am thankful to Paola Cianfarra (Roma Tre University), for her patience for teaching me the softwares I used on this thesis, and for her friendship and concern on making me feel that I was not alone in a strange country.

Many thanks to my colleague Anderson Moraes (Petrobras / Cenpes), for the technical discussions, the great help with the numerical models, and for his sense of humor. His contribution was essential for this thesis to reached a good result.

I acknowledge Petrobras / UN-RNCE, represented by Silmara Campos (manager of EXP/ABIG), for authorizing the use of the four seismic lines presented in the thesis and the geophysicist Pedro Xavier Neto, for having recovered the seismic lines sent to me.

I also thank the geophysicist Amin Murad (Petrobras / Cenpes) for the time to depth conversion of the seismic data, and to his manager Eduardo Lopes de Faria, for authorizing Amin to dedicate some of his time to do this conversion. The geophysicist Paulo Eduardo Miranda Cunha for your help on understanding some interference features on the carbonates imaged by the seismic lines, which were interpreted as karstic evidences.

To Diego de Medeiros Bento, regional coordinator of the IBAMA/CECAV – Rio Grande do Norte, for having provided the map of the cave studied in this thesis.

Many thanks to the staff of the Cenpes' library, who spared no efforts to obtain the articles, books, and public data I requested.

My colleagues Isabella de Oliveira Carmo, Mario Neto Cavalcanti de Araujo and Paulo Cezar Santarém da Silva (Petrobras / Cenpes), who allocated part of their time to read the chapters of the thesis. Thanks for the comments and suggestions.

Thanks to Cláudia Maria Andrade de Sousa and Rafael Duarte (respectively Graduation and M.Sc. students at the University of Rio Grande do Norte) for their assistance on the field work. Special thanks to Cláudia for doing the manual detection of fracture lineaments at the study area scale.

My psychologist Patricia Wasserman (Brasil) and my yoga teachers Flavia Melo Seabra (Brasil) and Patrizia Gelli (Italy) for helping me to maintain my equilibrium.

Thanks to Irene Manino, for her friendship, sincerity, and perspicacity.

Special thanks to all my friends who cheered me, supported me when I was too anxious, shared their own experience with me, and, after all, became happy because I have completed this challenge.

I am grateful to the Buddha Shakyamuni and to the Dalai Lama, whose teachings have helped me keep focus and remember that there still are many others objectives to achieve.

I am deeply grateful to Sri Krishna, Gurudeva, who certainly has been conducting me and will be forever.

“(…) Think of all the outcrops of sedimentary rocks that you have ever seen and try to recall a layer that was completely unfractured, with the possible exception of extremely ductile rock, such as salt or certain shales, you will not be able to recall any unfractured rocks simply because they don’t exist. (…)”

(David W. Stearns, in R.A. Nelson, 2001, p. XIII)

Abstract

Nowadays, hydrocarbons are the most important source of energy. In 2008 they represented 60% of the main types of fuel consumed worldwide (oil – 36%; natural gas – 24%; coal – 29%; nuclear energy – 5%; hydroelectric – 6%). In this context carbonate reservoirs are significant for the global oil and gas supply, as long as more than 60% of oil and 40% of gas reserves are found in this type of rock. But the knowledge about the key elements controlling the porosity and permeability on these reservoirs is incomplete. What is especially true regarding the understanding of fracturing contribution to secondary porosity creation and permeability increases.

The goal of this thesis was to contribute for the investigation of the actual role of fractures on carbonate reservoirs. To accomplish this commitment were studied a great exposition of Jandaíra Formation carbonates (Potiguar Basin, NE Brasil) where are located a well-developed cavern system named Furna Feia (linear development of 739m, maximum depth of 30m) and other karstic features (e.g. sinkholes; minor caverns), all of them presenting strong evidences of structural control. Such karstic environment was used as analog to investigate the relation between fracturing and high permeability corridors on carbonates, based on the generally accepted concept that caverns on carbonates are mostly formed by erosion due to natural acid in groundwater, which seeps through bedding-planes, faults, joints, etc.

The methods used in this study were: compilation of public data; lineament analysis (regional and local scales); outcrops structural analysis; structural measurements analysis; numerical modeling. Below, the sequence of analysis performed and theirs main results are described.

1. Information about the Potiguar Basin evolution and available data about the nowadays stresses were compiled from the literature. The state of stress operating today on the Basin was understood from earthquakes focal mechanisms, borehole breakouts analysis, and fracturing testes results from wellbores. These data demonstrated that: (i) the nowadays state of stress predominant through the Basin is strike-slip, with some reverse or normal mechanisms; (ii) the orientation of the maximum horizontal stress component ranges from NW-SE to E–W. Given such stress regime, it was considered

that the NE-SW faults through the Potiguar Basin are favorably oriented to be reactivated as inverted faults, while the NW-SE, E-W and N-S faults are favorably oriented to be reactivated as strike-slip faults.

2. Lineament analysis were performed at regional-scale (using SRTM3 data) and at local-scale (using GooglePro^{TM} high resolution satellite images). From the regional-scale analysis, the main azimuth frequency of lineaments obtained that for the Potiguar Basin is oriented NE-SW (N65^{o}E). From the local-scale analysis, the main azimuth frequency of lineaments is oriented NW-SE (N49^{o}W). These two directions are nearly orthogonal (114^{o} divergent), putting into evidence that at the study area some particular structural evolution exists and it could be related or not to the regional tectonic-structural history.

3. From the analysis of outcrops and structural measurements, the NW-SE direction was confirmed as the principal structural trend at the study area. By using specific fault inversion methods included into the Daisy software, two stress tensors that possibly generated the observed deformation were calculated: (i) using the "inversion by rotax analysis" method it was obtained a stress tensor oriented NW-SE (N330^{o}E), compatible with a strike-slip fault regime, which could only explain the observed faults; (ii) using the "Direct Inversion" method it was obtained a stress tensor also oriented NW-SE (N318^{o}E), but compatible with a reverse fault regime, which could explain the whole deformational elements observed through the area (i.e. faults; joints; bedding). Both stress tensors are in conformity with the present day regional state of stress given by the seismology and the borehole data analysis. But the second stress solution was assumed to be the most reliable because the Monte Carlo test included on the algorithm presented a well constrained distribution of the possible stress tensors.

4. A comparative analysis between the azimuth distribution of the Furna Feia principal galleries axis and the statistical analysis (Azimuth by Frequency distribution) of the local-scale lineaments and structural elements (i.e. faults; joints) was done. Such comparison evidenced a clear coincidence between the principal trends obtained for the study area and the cavern's galleries axis.

5. On the basis of all available information the following tectonic-structural model for the study-area was proposed:

   a. A major not outcropping NE-SW normal fault exists somewhere toward NW from the study area;

b. Given the estimated nowadays stress regime, the hypothetical NE-SW normal fault was reactivated as an inverted fault;

c. This inversion movement caused the exhumation of the Jandaíra Formation, on the returning hanging wall of the main NE-SW fault;

d. Minor NW-SE strike-slip faults result from the accommodation movements due to the major NE-SW fault activity;

e. Minor NE-SW strike-slip faults constitute conjugated pairs with the NW-SE strike-slip faults, or are related to oblique movements of the main NE-SW fault.

f. The fracturing associated to this deformation history was responsible for the creation of oriented high fractured corridors. These corridors control the meteoric water circulation through the Jandaíra carbonates, conducting the dissolution process and the formation of the Furna Feia caverns system.

6. Afterwards a sequence of numerical models was run in order to examine the reasonability of the theory proposed for the permeability increase in the Jandaíra carbonates. Such numerical models are based on mechanical analysis by finite element method for 2D simulation, comprised in the TECTOS program.

At the end of this work it was accepted that the faults and joints observed through the whole study area, associated to a dilatancy effect, led to a porosity increase in the Jandaíra carbonate rocks and controlled the creation of high permeability corridors. Such high permeability zones focalized the water percolation into the carbonate rocks and conditioned the growth of the Furna Feia cavern system.

Keywords:

Carbonate reservoirs; brittle deformation; Jandaíra Formation; Potiguar Basin; karst; lineaments; structural analysis; numerical models.

Units Glossary

Petrophysics

md – Millidarcy; unit of measure of permeability equivalent to one-thousandth of Darcy.

A porous medium has a permeability of 1 Darcy when differential pressure of 1 atmosphere across a sample 1 centimeter long and 1 square centimeter in cross section will force a liquid of 1 centipoise of viscosity through the sample at the rate of 1 cubic centimeter per second.

Time

M.y. - million years

Volume

MBOE - Thousands of Barrels of Oil Equivalent

MMBO - Million Barrels of Oil

MMBOE - Million Barrels of Oil Equivalent

MCF - Million cubic feet

OOIP - Original Oil In Place

Table of Contents

Chapter 3 - Lineament Analysis

Chapter 4 - Structural Analysis

Chapter 5 – Numerical Modeling

List of Figures

Page

Chapter 1

Chapter 2

Chapter 3

Chapter 4

Chapter 5

Chapter 1

Problem Presentation

1. Introduction

Nowadays hydrocarbons are the most important source of energy in the world. Only in 2008 they represented 60% (36% oil and 24% gas) of the main types of fuel consumed (Figure 1.1; BP, 2009). According to the IEA report (2006) fossil fuels will remain the dominant source of energy to 2030, accounting for 83% of overall increase demand. The report also predicts that global oil demand reaches 99MMBO/day in 2015 and 116MMBO/day in 2030. In this context carbonate reservoirs have a great importance, as long as more than 60% of the World's oil and 40% of the World's gas reserves are found in this type of rock (Schlumberger, 2007; Montaron, 2008).

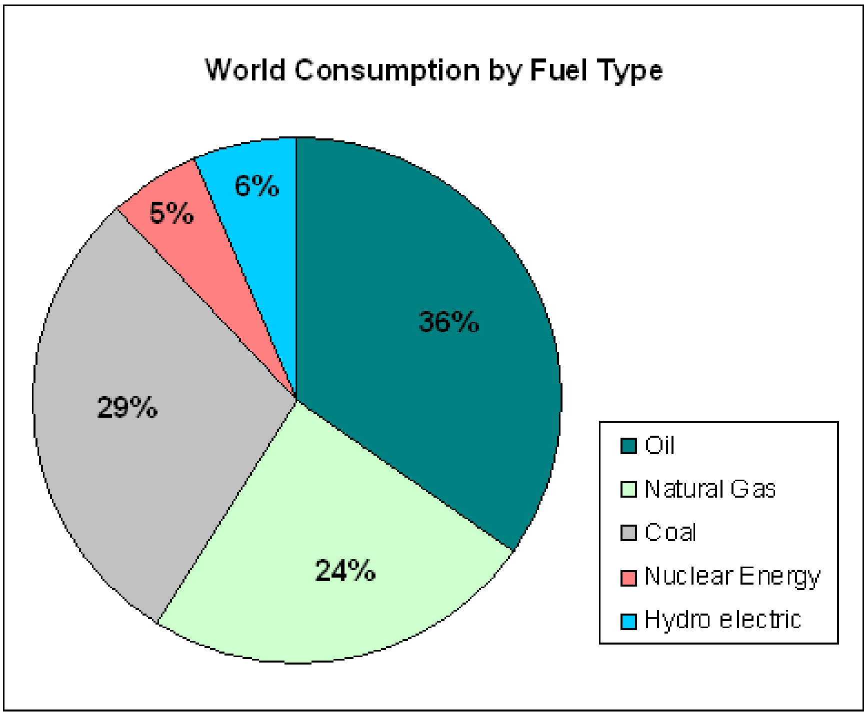

(Source: BP Statistical Review, June 2009)

Figure 1. 1. Participation of main fuels in the global energy supply.

According to a C&C Reservoirs[Appendix, 1.1] report (1998), despite their relevance for the global energy supply, during the 80's and 90's carbonate plays have not been receiving much attention from the industry and only a few number of discoveries were made in this type of rock. The report points out the complexity of carbonate systems, combined to economic and market aspects and exploration opportunities, as the most possible reason for the avoidance of these exploratory targets.

The complexity of carbonate systems is mainly due to the depositional conditions of carbonate sediments and to the greater chemical reactivity of carbonate minerals. Carbonate sediments have been deposited in shallow warm oceans since the Proterozoic to the Present, and the sedimentation is mostly done by biological activity (e.g. stromatolites; coral reefs; accumulation of shells and skeletal material). Once carbonate deposits are closely related to the evolution of life on Earth, their depositional conditions present a great variability in the space (Figure 1.2) and through the geological time. It results into a wide range of composition, textures, and, consequently, pore-space distribution (Choquette and Pray, 1970; Sarkisyan et al, 1973; Lonoy, 2006; Lucia, 2007).

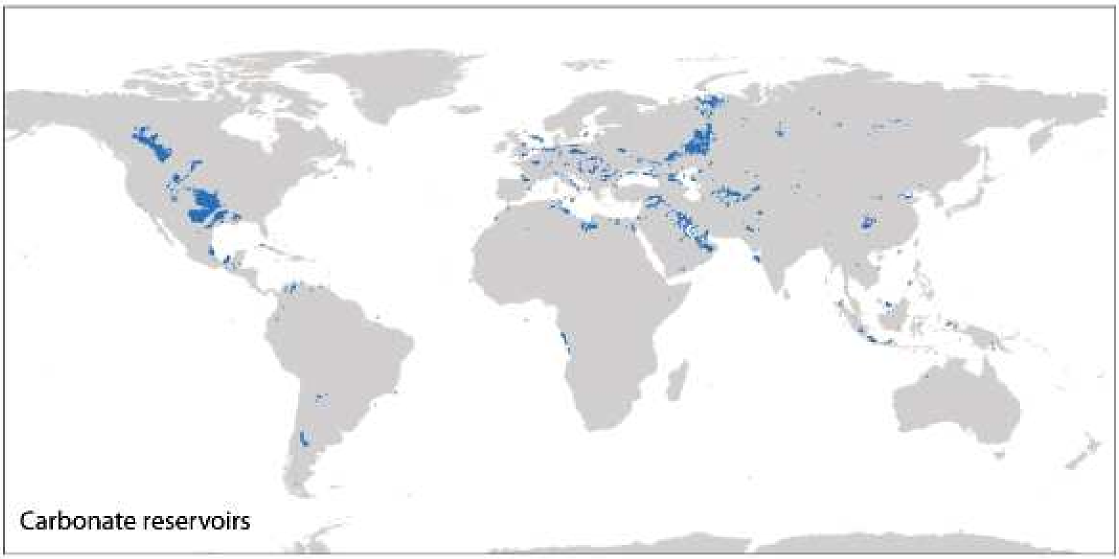

(Modified from: Ehrenberg and Nadeau, 2005)

Figure 1. 2. General distribution of carbonate reservoirs worldwide.
The blue areas correspond to carbonate reservoirs.

Primary sedimentation environment and postsedimentation process, like dissolution, mineralization, stylolites, and fracturing, are considered the main factors controlling the carbonate rocks porosity. But the relation between porosity and permeability for carbonate reservoirs is actually poorly defined. Therefore, in many carbonate reservoirs predictive models for reservoir-quality distribution are difficult to generate, resulting in significant uncertainty in hydrocarbon reserve calculations or in reservoirs management planning (Choquette and Pray, 1970; Sarkisyan et al, 1973; Lonoy, 2006; Lucia, 2007).

2. Fractures contribution for reservoirs productivity

The reservoir characterization job aims to build a volumetric model of a reservoir that incorporates all its petrophysics characteristics (e.g. grain size; porosity; permeability). This model is the base to simulate the flow of fluids within the reservoir under different sets of circumstances and find the optimal production techniques that will maximize the production.

Regarding carbonate reservoirs characterization the major challenge is to understand the relation between pore type and porosity and permeability. For the industry, this knowledge has a strong impact on the capability of building predictive models for quality distribution of reservoirs and fluids circulation (Ehrenberg and Nadeau, 2005; Lonoy, 2006; Montaron, 2008). It is common that porosity-permeability cross plots for carbonate reservoirs present a significant variability (Figure 1.3), which demonstrates that factors other than porosity are important on modeling permeability (Lucia, 2007).

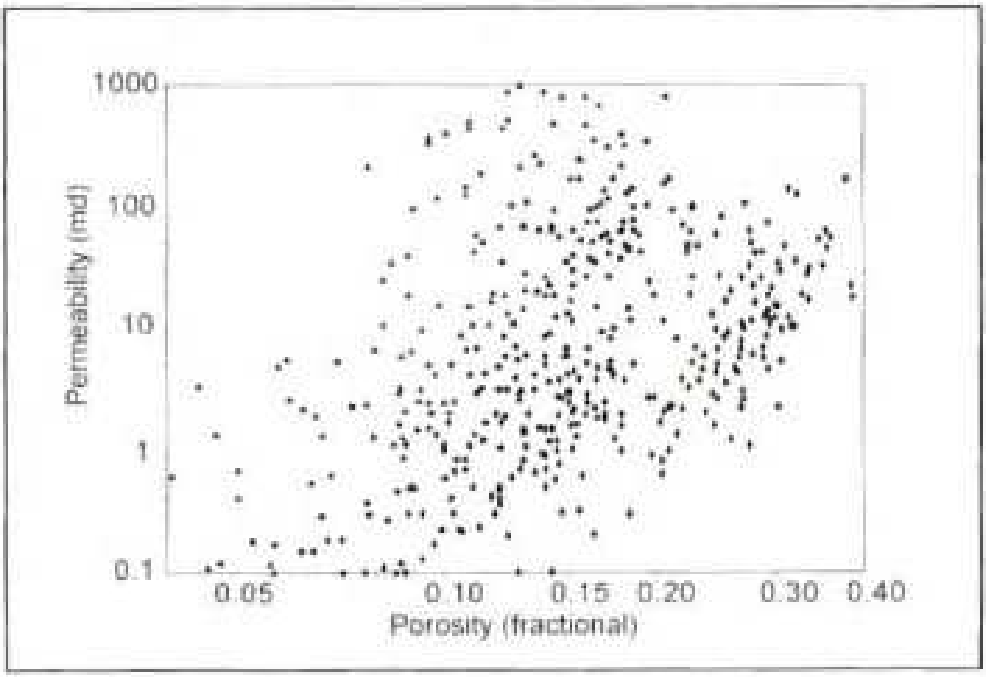

(From: Lucia, 2007)

Figure 1. 3. Example of variability in porosity-permeability relationship.

For some authors (Ehrenberg and Nadeau, 2005; Peacock and Mann, 2005; Aguilera, 2006; Montaron, 2008), in addition to the pore-space provided by depositional conditions and postsedimentation process, the fracturing affect significantly the permeability and the flow of fluids and production rates of reservoirs.

Peacock and Mann (2005) affirm that as carbonate reservoirs get mature, it is increasingly evident the significant role of natural fractures[Appendix, 1.2] in controlling hydrocarbon production and water breakthrough[Appendix, 1.3].

Ehrenberg and Nadeau (2005) noticed that although the fundamental depositional and chemical differences between sandstone and carbonate reservoir rocks seem widely accepted and commonly motivate the adoption of distinct treatment for carbonate reservoirs, the actual nature and magnitude of these differences suffer from little or no quantitative documentation. To address this void the authors analyzed the average porosity versus depth and the average permeability versus average porosity available for 30122 siliciclastic reservoirs and 10481 carbonate reservoirs, covering all petroleum-producing countries, except Canada. From this study they stated that: (i) carbonate reservoirs have a greater relative proportion of high permeabilities at low porosities; (ii) both lithologies include a subordinate group of reservoirs with multidarcy permeabilities at porosities below 15%, which the authors suspect to reflect fracture instead of matrix values; (iii) the relative paucity of low-porosity (0–8%) siliciclastic reservoirs at all depths compared with carbonates may reflect the most common occurrence of fractures in carbonates and the effectiveness of these fractures for facilitating economic flow rates in low-porosity rock.

Aguilera (2006) presents the analysis of the cross-plot average porosity versus weighted mean oil recovery for 5915 pools in Alberta Field (Canada). The data presents a wide variation in porosities and recoveries (Figure 1.4), following the same general idea of Ehrenberg and Nadeau (2005). Based upon this analysis and his own experience on studying many other naturally fractured reservoirs around the World, Aguilera (2006) made some important considerations: (i) the presence of natural fractures in lower porosity carbonates, especially when dolomitized, is probably responsible for the larger oil recovery and the lowest values of water saturation; (ii) low porosity intervals in naturally fractured reservoirs should never be neglected - the use of a porosity cutoff can leave as undiscovered a reservoir that, if tested, could prove to be commercial.

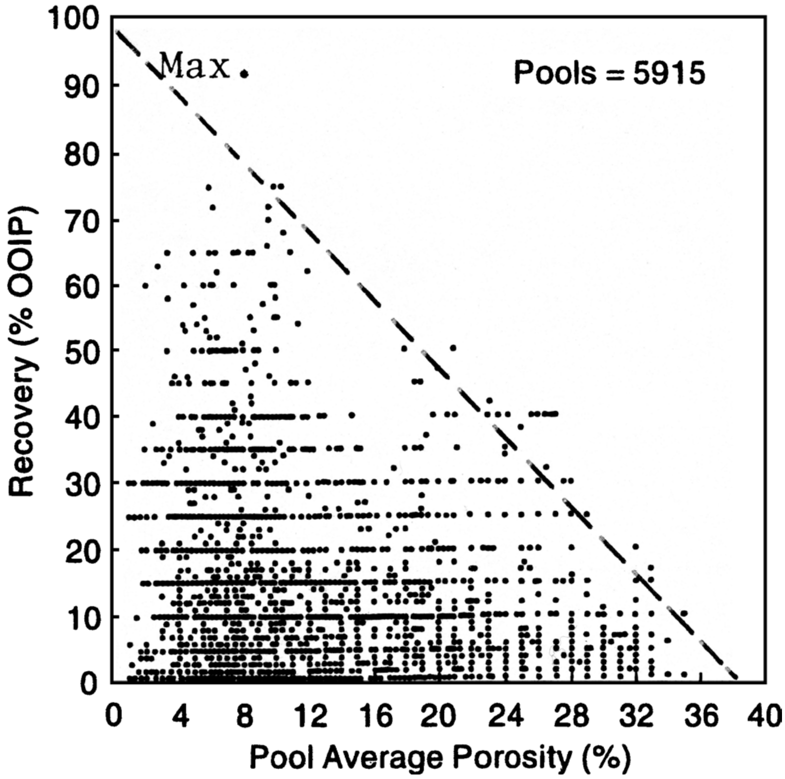

(From: Aguilera, 2006)

Figure 1. 4. Oil recovery versus porosity for 5915 pools in Alberta (Canada).

The high oil recovery in low-porosity reservoirs suggests natural fracturing. Without natural fractures the opposite behavior would be expected.

Montaron (2008) affirms that to take fracturing into consideration is very important for reservoir management, because the permeability along major fracture corridors can be a thousand times greater or more than the surrounding rock matrix. The effects of this increasing in permeability can be positive or negative. The author gives as examples of negative effects the risk of earlier breakthrough and the occurrence of problems during drilling, like mud[Appendix, 1.4] losses. Providing highways for draining the reservoirs is indicated by Montaron (2008) as the most positive effect for the presence of fractured zones.

3. Problem outline

Concerning the key elements controlling the porosity and permeability in carbonate reservoirs the number of publications in Structural Geology is really few, principally if compared to Stratigraphy and Sedimentology.

Anyhow, some reputable experts in the petroleum world consider natural fracturing fundamental to improve permeability and productivity in carbonate reservoirs. They assume this rule to be especially true for low permeability rocks (e.g. chalks) and mature reservoirs. But the real relevance of fractures is not completely clear yet, probably due to the so small amount of published quantitative studies as well noticed by Ehrenberg and Nadeau (2005).

4. Thesis objective

The porosity-permeability ration on carbonate reservoirs is a complex subject. The objective of this study is simply to contribute to the investigation about the actual role of fractures on the carbonate reservoirs permeability. To accomplish this commitment some excellent carbonate rocks expositions of the Jandaíra Formation, occurring close to the Baraúna village (onshore Potiguar Basin, Northeast Brasil), were studied. At this area exist a very well developed cavern system (739m of linear development, achieving 30m of depth) and some minor karstic features, all of them presenting strong evidences of structural control.

The term karst designate a general category of landforms, characterized by numerous closed depressions, caves, collapse features, and diversion of drainage underground. These landforms result from the chemical reaction of slightly acidic groundwater with soluble rocks, such as carbonate rocks (limestone and marble), dolomite (magnesium carbonate), gypsum (calcium sulfate), and some evaporites (Easterbrook, 1999; Burcham, 2009). Easterbrook (1999) affirms that the optimum conditions for karst development include more than just the carbonate rocks mineralogy. According to the author secondary porosity produced by intersecting joint sets play an important role in karst formation, because they permit rocks to hold more water and facilitate groundwater circulation through the system by increasing permeability.

Considering the arguments above I assumed that the karst terrain at the study area represents a good analog to investigate the relation between brittle deformation and the creation of high permeability zones on carbonate rocks. The following steps were taken in this investigation:

1. The information available from earthquake focal mechanisms, breakouts and fracturing testes was compiled to estimate the nowadays state of stresses at the Potiguar Basin (**Chapter 2**);
2. A multi-scalar lineament analysis was performed to determine the principal structural trends at the Potiguar Basin and at the study area (**Chapter 3**);
3. Outcrops structural analysis, structural measurements analysis, and information from four seismic lines were used to define the structural regime on the Jandaíra limestones at the study area (**Chapter 4**);
4. The distribution of azimuth by frequency of the galleries axis of the main cavern was compared with the statistical analysis of structural measurements and the study-area lineaments, to verify if there is any coincidence between the structural trends at the study area and the cavern's galleries (**Chapter 4**);
5. In light of all information available, a tectonic-structural model for the study area and a theory to explain the development of the main cavern system were proposed (**Chapter 4**);
6. Numerical models were employed to examine the reasonability of the theory proposed for the permeability increase in the Jandaíra carbonates (**Chapter 5**).

All these complementary results support the assumption that the faults and joints observed at the study area led to the formation of high permeability corridors, which conditioned the cavern development. If there were a real hydrocarbon reservoir at that place, a superior productivity zone would possibly be found instead of a cavern system.

Chapter 2

The Potiguar Basin

1. Introduction

In this chapter the main tectonic-structural and stratigraphic characteristics of the Potiguar Basin are presented. The objective is to introduce the non-familiarized reader to the depositional and deformational processes involving the Jandaíra Formation (a Turonian to Campanian tide-dominated carbonatic platform) that were taken in this study as analogue to fractured carbonate reservoirs.

The Potiguar Basin is the easternmost basin at the Brazilian Equatorial Margin (Figure 2.1). It comprises an area of 48000Km^2, which is divided in 21500km^2 onshore and 26500km^2 offshore. The basement of the Basin is composed of Archean-Paleoproterozoic terrains (orthogneisses and metamorphosed supracrustal sequences), marked by polyphase deformation events and a large number of plutonic intrusions, that constitutes the Borborema Province (Almeida et al., 1977). The Fortaleza High defines its limit with the Ceará Basin and the Touros High defines its limit with the Pernambuco-Paraíba Basin (Figure 2.1) (Matos, 1992; Araripe and Feijó, 1994; Pessoa Neto et al., 2007).

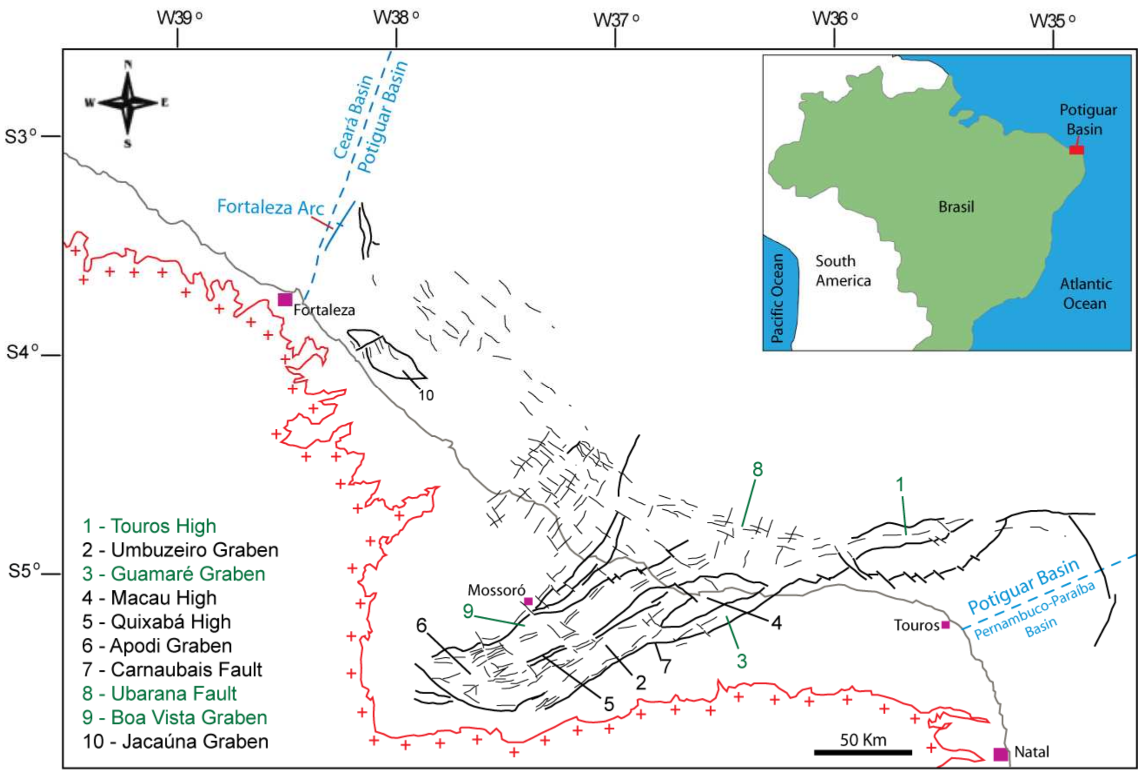

(Modified from: Bertani et al., 1991; Mattos, 1992)

Figure 2. 1. Localization and Tectonic Framework of Potiguar Basin.

The first oil discovery at the Potiguar Basin took place in 1973 on the Ubarana Field (offshore). Ever since more than 4000 wells have been drilled (92% onshore) and more than 115000km of seismic lines were acquired (78% offshore). The interpretation of data obtained from these wells and seismic lines was fundamental to build the actual knowledge about the basin's lithostratigraphy and structural framework (Bertani et al, 1991; Matos, 1992; Araripe and Feijó, 1994).

2. Tectonic-Structural Development

The Potiguar Basin started to be formed during the early Cretaceous, as a result of the South America/African plates breakup and subsequent South Atlantic opening (Figure 2.2) (Françolin and Szatmari, 1987; Matos, 1992; Cremonini et al., 1996). It is part of an intracontinental rift system that opened from South to North in the southern South Atlantic branch, and from West to East in the Equatorial Atlantic branch (Matos, 1992).

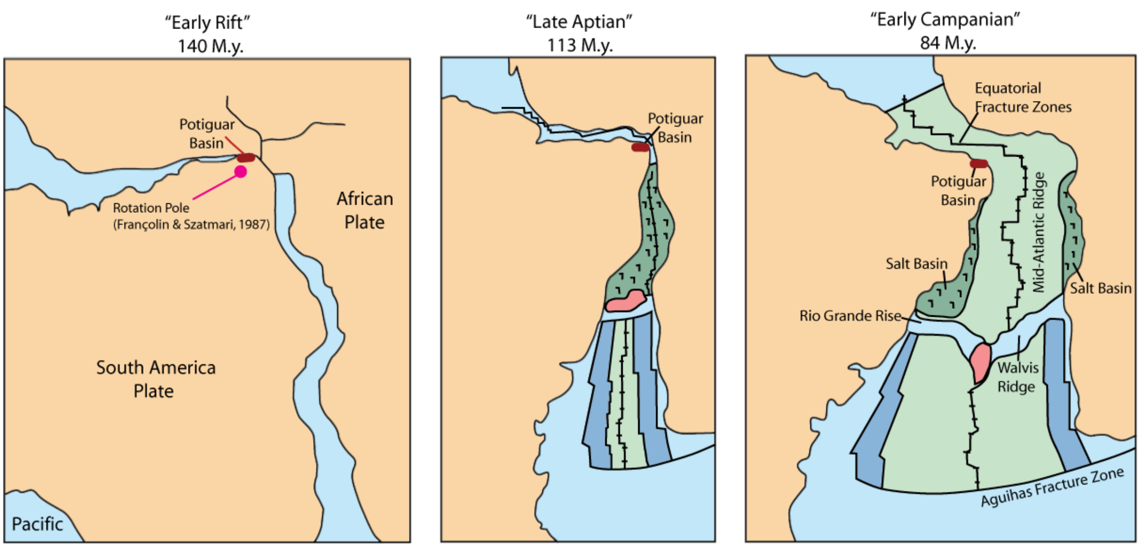

(Modified from: Fainstein et al., 1998)

Figure 2. 2. Schematic chart of South Atlantic opening.

Since the Potiguar Basin is located at the corner between the Southern and Equatorial branches of the Atlantic rift system, it contains important registers for the understanding of the opening processes. But this history is not easy of being reconstructed and several models have been proposed, as illustrated by the examples of tectonic models below. The most controversial subjects among authors are the stresses orientation during the breakup and the relative movement between the two plates at that time.

Françolin and Szatmari (1987) proposed that during the Neocomian (Rio da Serra to Early Aratu local Stages[Appendix, 2.1]) the South American Plate rotated clockwise relative to the African Plate, with respect to an eulerian pole located at 7°S and 39°W (Figure 2.2). This rotation created a singular stress field, divided into two domains: (i) a E-W compression operating at the tip of rotating South America, pressed against the western African margin (actual Republic of Cameroon); (ii) a N-S extension operating where South America pulled away from the northwest African margin (actual Nigeria). According to these authors, this stress field was responsible for the reactivation of numerous NE-SW and E-W preexisting Precambrian shear zones as strike slip faults. They explain the frequent creation of half grabens on Potiguar Basin as a compensation for the imperfect fit between the blocks laterally dislocated and rotated.

Matos (1992) criticises some previous reconstructions and tectonic models, on which were assumed a rigid plate rotation between South America and Africa (Bullard et al., 1965; Rabinowitz and LaBrecque, 1979; Szatmari et al., 1987; Françolin and Szatmari, 1987), or that recognized the importance of major structural discontinuities during the South Atlantic opening but did not consider in detail nonuniform deformations within the intracontinental Northeast Brazilian rift basins (Popoff, 1988; Unternehr et al., 1988, Conceição et al., 1988). He proposes a model in which is assumed that major kinematic changes occurred during the rift evolution and takes in account the role of major discontinuities within the extensively deformed Proterozoic continental crust. The author argues that during the Neocomian-Barremian (Rio da Serra to Buracica local Stages) the early extensional pulses were oriented toward NW-SE, and during the Barremian-Aptian (Buracica to early Alagoas local Stages) the extensional axis rotated counterclockwise toward a general E-W direction. Based on this model, Matos (1992) suggests that the Paleoproterozoic NE oriented structural trends were reactivated as normal faults and the E-W and NW-SE trends become potential sites for transfer faults and/or accommodation zones.

Cremonini (1993) and Cremonini et al. (1996) recognized an important transfer zone oriented nearly WNW-ESE close to the Ubarana Field, named Ubarana Transfer Zone (Figure 2.1). The authors interpreted this transfer zone as being sub parallel to the maximum extensional effort. The former was responsible for the reactivation of several NE-SW and E-W structural trends on the Borborema Province as ENE-WSW normal faults and WNW-ESE transfer faults - resulting in the Potiguar Rift implementation during the Neocomian. They proposed a second rifting pulse controlled by an extension E-W, operating from the Barremian to the early Aptian (Buracia to early Alagoas local Stages). Such second pulse is recognized just along the submerse portion of the Basin and is associated with the Equatorial Margin breakup, when the rift stage of Potiguar Basin was aborted and the drift stage began.

From the different reconstructions and tectonic models the fundamental common point is the assumption that the Paleoproterozoic structural grain controlled the Potiguar Rift geometry. But it is still being controversial subjects - that will not be discussed in this thesis - the first relative movement between the South America and African plates (rotation or simple drifting), and the principal stresses direction operating during the breakup and initial rift.

3. Tectonostratigraphy

The Potiguar Basin stratigraphic record (Figure 2.3) is deeply related to its tectonic evolution stages and comprehends three Supersequences: Supersequence Rift; Supersequence Pos-rift; Supersequence Drift (Pessoa Neto et al., 2007).

3.1. Supersequence Rift

The Supersequence Rift, mainly composed by continental sedimentation, is sub-divided into two phases: Rift I and Rift II (Pessoa Neto et al., 2007). The phase Rift I (Neocomian) is characterized by a crustal stretching regime with high rates of mechanics subsidence. Major normal faults were developed at this moment (reaching 5000m of offset) defining asymmetric half-graben and internal highs mostly oriented towards NE-SW. The low areas were filled by lacustrine, fluvial-deltaic and fan-delta deposits that constitute the Pendência Formation (Figures 2.3 and 2.4). The occurrence of Rift I sediments on the offshore portion of the Basin is limited to an elongation of the emersed rift towards NE (Araripe and Feijó, 1994; Pessoa Neto et al., 2007).

At the phase Rift II (Barremian to Aptian) a strike-slip/transform faulting regime was imposed along the future Brazilian Equatorial Margin, causing a significant changing on the rift's kinematics. This event moved the rift axis to the immersed portion of Basin while induced the elevation of the emersed portion that becomes the new rift's bulge and source area. At this moment the direction of tectonic transport changes from NNW-SSE toward E-W, what is interpreted as the very beginning of the continental drift process. The sedimentary register at this phase is dominated by alluvial deposits, fluvial-deltaic deposits, lake sediments, and turbidites, that constitute the Pescada Formation (Figures 2.3 and 2.4). This sequence is limited to the offshore portion of Potiguar Basin (Araripe and Feijó, 1994; Pessoa Neto et al., 2007).

3.2. Pos-rift Supersequence

The Pos-rift Supersequence (Aptian-Albian) was deposited under a relative tectonic quietening regime dominated by thermal subsidence, that followed the end of the rift phase (Pessoa Neto et al., 2007). The Alagamar Formation comprises the lithological register of this stage and is characterized by a gradual transition from the continental to a shallow marine environment, with predominant fluvial-lacustrine deposits (Figures 2.3 and 2.4). This formation was deposited directly against to the top of the rift sequence in a strong angular discordance. Black shales, calcarenites and ostracod limestones (CPT layers; Figure 2.3), deposited in a sabkha environment[Appendix, 2.2], correspond to the first evidence of marine transgression on Potiguar Basin (Araripe and Feijó, 1994; Pessoa Neto et al, 2007).

Despite being a quiet tectonic period, at the very beginning of the Pos-rift Supersequence (Early Aptian) there are evidences of a strong structural control on the fluvial deposits at Boa Vista and Guamaré grabens (Figure 2.1). This indicates that some faults from the rift phase have been active until that time (Pessoa Neto et al., 2007).

3.3. Drift Supersequence

The Drift Supersequence (Albian to the Recent) corresponds to the end of the Atlantic opening process. This supersequence is subdivided into Marine Transgressive and Marine Regressive Sequences (Pessoa Neto et al., 2007).

During the **Marine Transgressive Sequence** (Albian to Campanian) the basin had its less significative subsidence rates and the main depocenter was a large fluvial channel oriented toward NE, passing gradually to a shallow siliciclastic platform. On these environment were deposited the Açu Formation (Figures 2.3 and 2.4) which contains the main hydrocarbon reservoir rocks on the onshore basin, composed by medium to coarse sandstones with layers of shales. At the edge of the siliciclastic platform a carbonate sedimentation (Ponta do Mel Formation) was implanted, while a slope/basin system marked by canyons and associated turbiditic deposits (Quebradas Formation), was developing sideward. The transgression achieved its maximum at the Cenomanian-Turonian limit, being marked by the deposition of a continuous shales sequence (Ubarana Formation) at the immersed portion of Basin and the drowning of the fluvial/estuary system on the emersed portion (Araripe and Feijó, 1994; Pessoa Neto et al., 2007).

Between the Turonian to Middle-Campanian was implanted a tide-dominated carbonatic platform/ramp corresponding to the **Jandaíra Formation** (Figures 2.3 and 2.4). In this environment the lithologies deposited were calcarenites with bioclasts (planktonic foraminifera, green algae, bryozoans and echinoids), calcarenites with miliolids, calcilutites with bioclasts and calcilutites with bird's eyes (Tibana and Terra, 1981). The deposition of these carbonates marks the end of the Marine Transgressive Sequence (Araripe and Feijó, 1994; Pessoa Neto et al., 2007). Nowadays the Jandaíra Formation crops out in almost all the emersed portion of Potiguar Basin, constituting the largest exposed Cretaceous carbonate platform along the Brazilian continental margin. Apart from its wide area of occurrence the Jandaíra Formation commonly presents intense post-rift deformation, frequently associated to karstification processes, in a tectonic context equivalent to other Brazilian reservoirs. In this way the Jandaíra Formation represents an excellent analog to the investigation proposed in this thesis.

The **Marine Regressive Sequence** (Campanian to Recent) comprises shallow platform systems (Tibau Formation) with carbonatic edge (Guamaré Formation) and slope to basin system (Ubarana Formation), that are limited from the actual coastline to the offshore region (Figures 2.3 and 2.4). From the Miocene to the Pliocene continental alluvial sediments were deposited along the coast (Barreiras Formation) being replaced by fluvial and eolian/beach sediments in the Holocene.

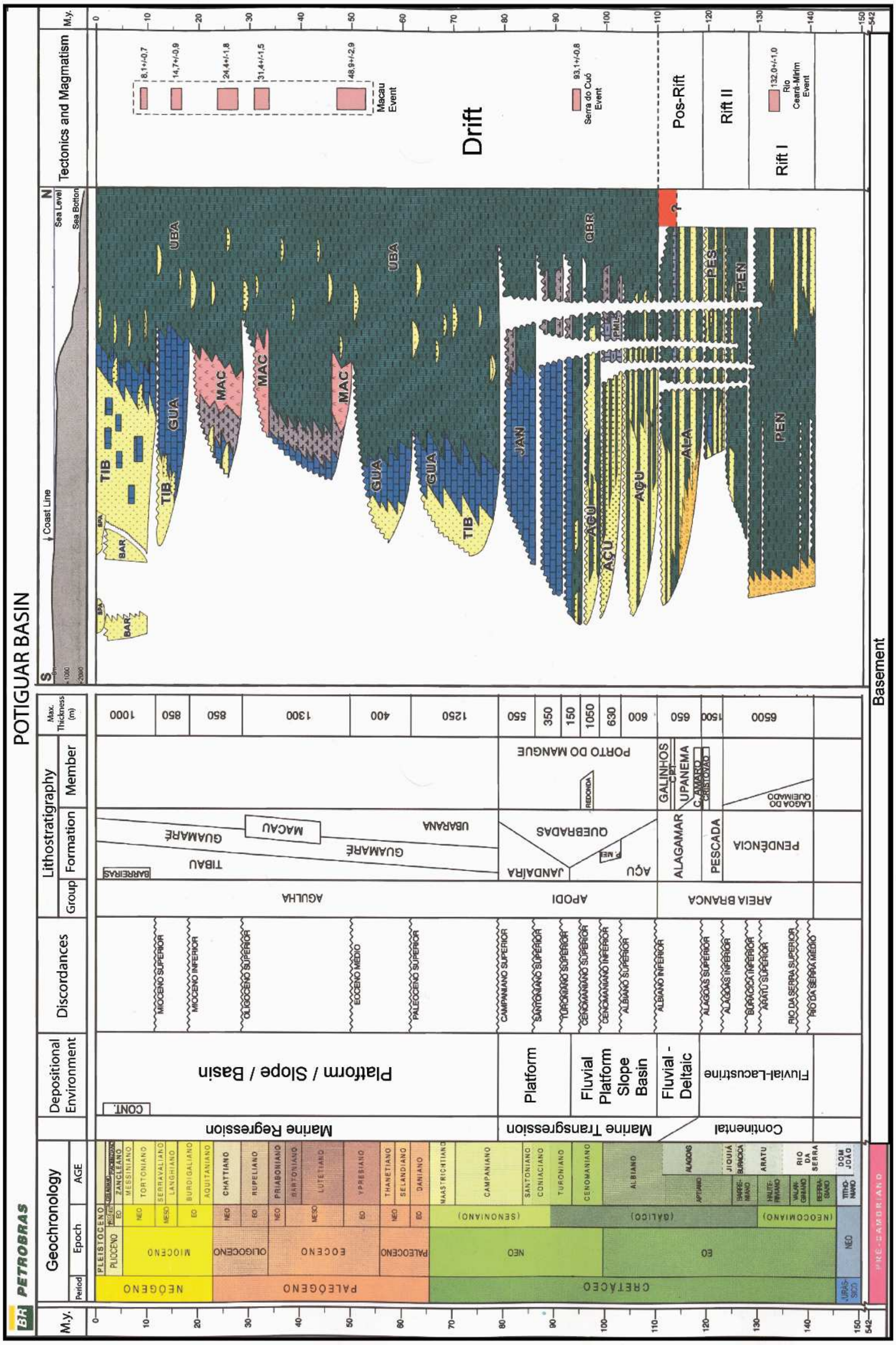

(Modified from: Pessoa Neto et al., 2007)

Figure 2. 3. Potiguar Basin stratigraphic chart.

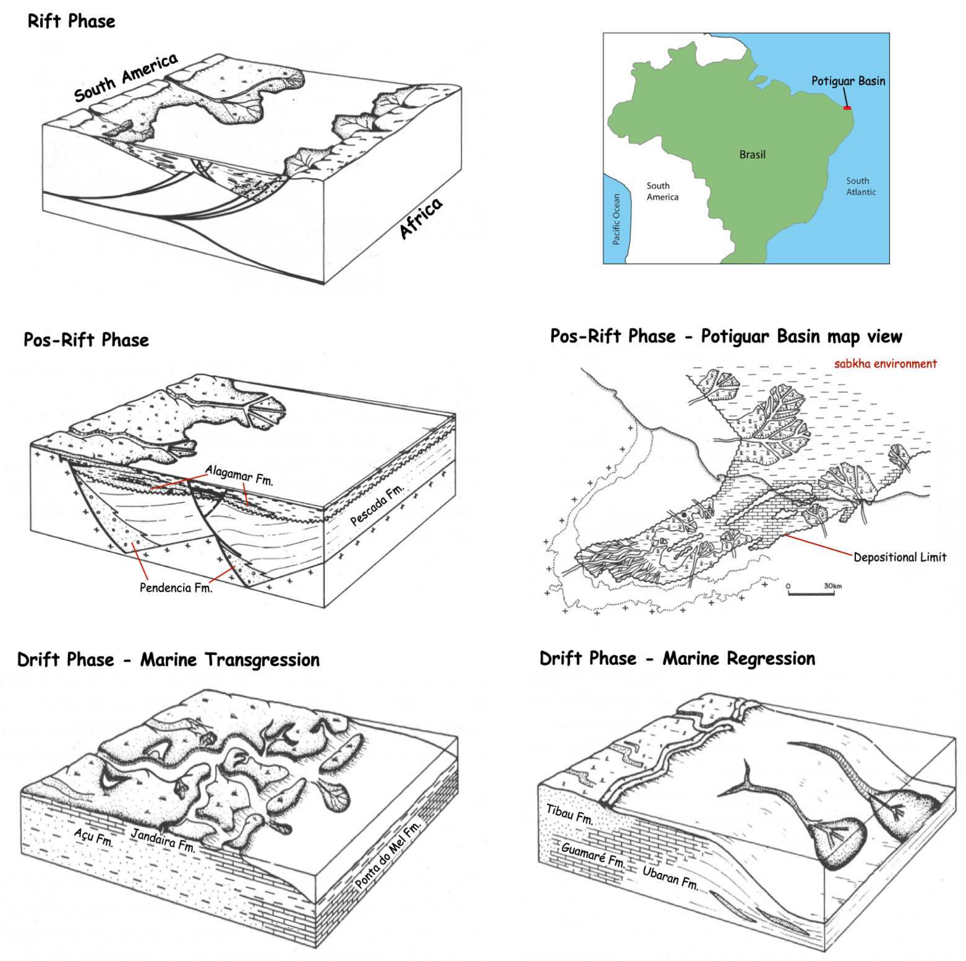

(Modified from: Bertani et al., 1991)

Figure 2. 4. Schematic evolution of Potiguar Basin

As previously said the available information from wells (e.g. samples, cores, logs) and seismic lines were fundamental to build the stratigraphic and structural knowledge about the Potiguar Basin. These data are even more important if considering that from the entire stratigraphic register only the Formations Barreiras, Tibau, Jandaíra, and Açu outcrop at the onshore basin.

4. Magmatism

Three main magmatic events (Figure 2.3) are identified on the Potiguar Basin:
(i) Rio Ceará Mirim event corresponds to the occurrence of tholeiitic dike swarms, mostly E-W oriented, intruding the Pre-Cambrian bedrock at the southern edge of the

onshore Potiguar Basin. The age of these dikes was estimated by the Ar/Ar method in 132.2 ± 1 M.y.; or ranging between 130 and 125 M.y. by the K/Ar and Fission Track methods, being related to the basin's opening process. The occurrence of vulcaniclastic rocks interlayered with the basal Pendencia Formation at the emersed portion of Basin is correlated to this event too (Matos, 1992; Pessoa Neto et al., 2007).

(ii) Serra do Cuó event comprises alkali-basalt overflows outcropping on the south portion of the onshore basin. The age of these basalts was estimated by the $^{40}Ar/^{39}Ar$ method in 93.1 ± 0.8 M.y. (Souza et al., 2004).

(iii) Macau event occurred as volcanic pulses of ages from 70-65 M.y. to 9-6 M.y., with strongest activities from 48.9 ± 2.9 M.y. to 31.4 ± 1.5 M.y. (Eocene/Oligocene). interlayered to the Marine Regressive Sequence sediments and at some specific regions in the bedrock.

5. Seismology

The seismicity at Northeast Brasil is one of the most important in the country. It occurs mainly on the exposed Precambrian basement around the onshore border of Potiguar Basin and between the Potiguar and Parnaíba basins (Figure 2.5). According to the instrumental registers recorded over the last 40 years, the seismic activity on the region is characterized by low magnitude events (maximum instrumental register mb = 5.2, in Cascavel event; Figure 2.5) tending to occur in swarms that continue from several months to some years (Takeya et al., 1989; Assumpção, 1992; Ferreira et al., 1998; Bezerra and Vita-Finzi, 2000).

It must be noticed that, up to the present time, ground-ruptures caused by earthquakes are not known at the region, even if some events have registered magnitudes over 5.0 (instrumental and historical record), serious damage to buildings have been reported in the last 200 years, and several liquefaction features are observed on Pliocene deposits (Barreiras Formation) and Quaternary continental siliciclastic deposits (Assumpção, 1992; Bezerra et al., 2008; Nogueira et al., 2010).

Another characteristic of seismicity at NE Brasil is that the epicenters usually occur confined among 1-5km depth. Events like the João Câmara earthquake sequence (event **a**; Figure 2.5), which had its maximum epicenter depth around 8 to 10km, are very rare (Takeya et al., 1989; Assumpção, 1992; Ferreira et al., 1998).

From the available focal mechanisms instrumental register, the Potiguar Basin exhibits a predominant strike-slip stress regime with some reverse and normal events (Figure 2.5). Ferreira et al. (1998) explains the occurrence of focal mechanisms indicating different stress regimes in a same area as a possible result from different orientations of pre-existing fault planes reactivated under the same uniform crustal stress field. The focal mechanisms also furnished the maximum compressive stress orientations[Appendix, 2.3] through the basin, that ranges from NW-SE to E–W, roughly parallel to the coastline (Assumpção, 1992, 1998; Ferreira et al., 1998; Bezerra and Vita-Finzi, 2000).

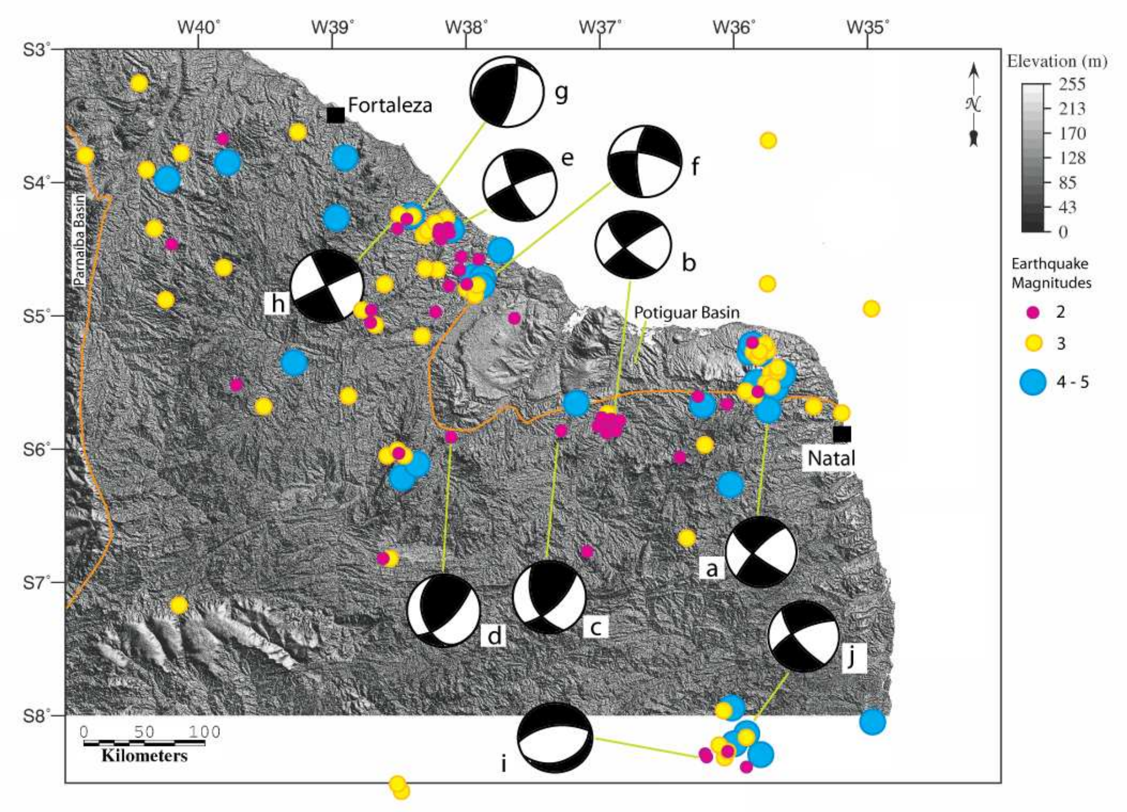

(Modified from: Ferreira et al., 1998; Nogueira et al., 2010)

Figure 2. 5. Seismicity at Potiguar Basin area.

On the beach ball diagrams the write zones correspond to compression while the black zones correspond to traction. The focal mechanisms refer to the following events: (a) João Câmara, 1986 to 1988; (b) Açu reservoir, 1990 to 1991; (c) Augusto Severo, 1990; (d) Tabuleiro Grande, 1993; (e) Cascavel, 1994; (f) Palhano, 1989; (g, h) Paracajus, 1980; (i, j) Caruaru, 1991.

6. Present day Stresses on Potiguar Basin

The stress tensor acting at any point on the Earth's crust can be described by three mutually perpendicular components, σ_1, σ_2, σ_3, which refer respectively to the maximum, intermediate and minimum principal stresses ($\sigma_1 > \sigma_2 > \sigma_3$). To describe the stress tensor at a point is necessary to determine the orientations and magnitudes of the three principal stresses (Hubbert and Willis, 1957; Bell, 1990).

For the oil industry the knowledge of the operating stresses in a given area is an important parameter for several exploitation and exploration activities. On drilling activities it is strongly recommended to consider the in-situ stress condition since the wellbore design phase (e.g. mud drilling weight programming; calculation of ideal inclination and azimuth for directional wells), to avoid stability problems like unexpected formation fracturing or borehole collapse (McLean & Addis, 1990; Peska & Zoback, 1995; Aadnoy & Bell, 1998). To predict which faults or fracture families behave as seal or as conduits for fluids is fundamental on seeking new targets in a basin (exploration activities) and on planning reservoirs management (exploitation activities). This task is also deeply influenced by the knowledge about the in-situ stresses (Barton et al., 1995; Finkbeiner et al., 1997; Wiprut and Zoback, 2000).

The needed information to estimate the in-situ stresses is usually obtained from ordinary tests and logs performed in wellbores. Even if at first these data are acquired for different purposes, they can be used to detect and measure mechanic phenomenon occurring on the borehole walls as a function of the principal stresses. Breakouts and drilling-induced fractures are well known borehole stress-related failures, commonly used by petroleum geologists and engineers to determine stresses orientation (Zoback et al., 1985; Zoback, 1992; Bell, 1990).

However measuring reliable in-situ stress magnitudes is not easy. With certain simplifying assumptions it is possible to estimate the minimum stress magnitude (σ_3) from hydraulic fracturing procedures and other usual fracturing tests (Hubbert and Willis, 1957; Bell, 1990; Aadnoy, 1990; Addis et al., 1998; Brudy, 1998). As in sedimentary basins the topography is usually gentle, the vertical stress (Sv) is generally considered equivalent to the overburden pressure and is calculated by the integration of formation density logs data (Bell, 1990). None of the existing tests or logs is able to measure the magnitude of intermediate principal stress (σ_2). Its assessment is possible only by using computer algorithms, which calculate the complete in-situ stress tensor based on information from borehole failures and rock strength, other than fracturing tests, density logs and formation fluid pressure tests (Peska and Zoback, 1995; Zoback and Peska, 1995).

On the Potiguar Basin Lima Neto, 1998, 1999 and Lima et al., 1997 accomplished the most comprehensive efforts to estimate the present-day stresses based on wellbore data. Lima Neto (1998, 1999) contributed very much to the understanding of Potiguar Basin's stresses regime based on the analysis of approximately 187 leak-off tests results and 69 hydraulic fracturing data, obtained from the onshore and offshore portions of Basin. Lima et al. (1997) performed a regional scale analysis of breakouts, detected from four-arm dipmeter caliper data available for 541 vertical wells distributed on the Brazilian onshore and offshore basins. As for the Potiguar Basin the authors analyzed 129 wells, of which 65 wells presented enlarged intervals due to the occurrence of breakouts.

6.1. Stresses Orientation on Potiguar Basin

The analysis of breakouts is the most usual method to estimate the orientation of maximum and minimum horizontal principal stresses (SHmax and Shmin respectively).

Breakouts are shear fractures induced on wellbore walls, resulting from the principal stresses redistribution around a borehole during perforation due to the substitution of rock by drilling mud (Figure 2.6). In such redistribution a maximum stress concentration is naturally localized in two specific regions around the borehole section, parallel to the Shmin direction (Figure 2.6). If at a given depth the rock strength and the pressure induced by the drilling fluid are not sufficient to compensate the shear stress at these regions, a breakout will occur. As breakouts are aligned to Shmin, determining its direction is the same as measuring the Shmin orientation (Zoback et al., 1985; Bell, 1990; Zoback and Peska, 1995). Once the three principal stresses components are assumed to be mutually perpendicular, the SHmax direction can be automatically obtained at 90^{o} from Shmin (Figure 2.6).

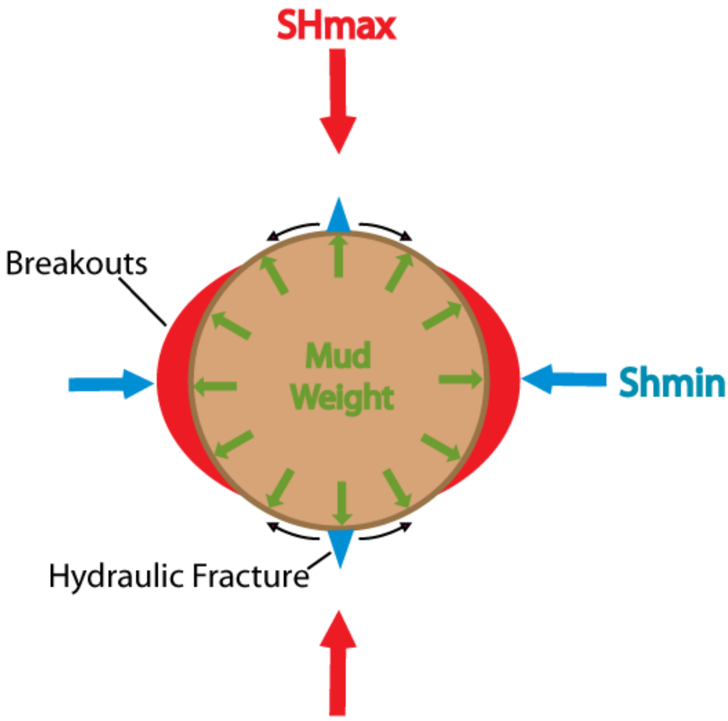

Figure 2. 6. Deformations occurred around the borehole section.

SHmax is the maximum horizontal principal stress; Shmin is the minimum principal stress. Breakouts are shear fractures induced when the pressure of the drilling fluid is not sufficient to compensate the shear stress on wellbore walls. Hydraulic fractures are traction fractures that occurs when the pressure of the drilling fluid overcomes the rock strength and the pressure of the Formation's fluid (i.e. water; oil; gas).

There are two methods for identifying and measuring breakouts orientation:

(i) The caliper analysis of four-arm dipmeter tools, which has two pairs of arms orthogonally arranged (Figure 2.7) and maintained in contact with the borehole walls while the tool rotates and is pulled up from the wellbore button. When a breakout is encountered, one pair of arms becomes trapped and the rotation ceases. At this depth interval the orientation of the largest caliper is recorded as the breakout's orientation (Plumb and Hickman, 1985; Bell, 1990; Zoback, 1992).

(ii) The image logs are a new technology that allows to observe the failures on borehole walls (breakouts or induced fractures) in a direct manner, enhancing significantly the interpreter's capability to determine the orientation of principal in-situ stresses (Shmin parallel to breakouts and SHmax parallel to induced fractures). The reliability of breakouts data has also improved with this technology, since it made possible to distinguish without a doubt breakouts from other types of enlargement induced by factors not related to in-situ stresses (Figure 2.7) (Zoback et al., 1985; Peska and Zoback, 1995).

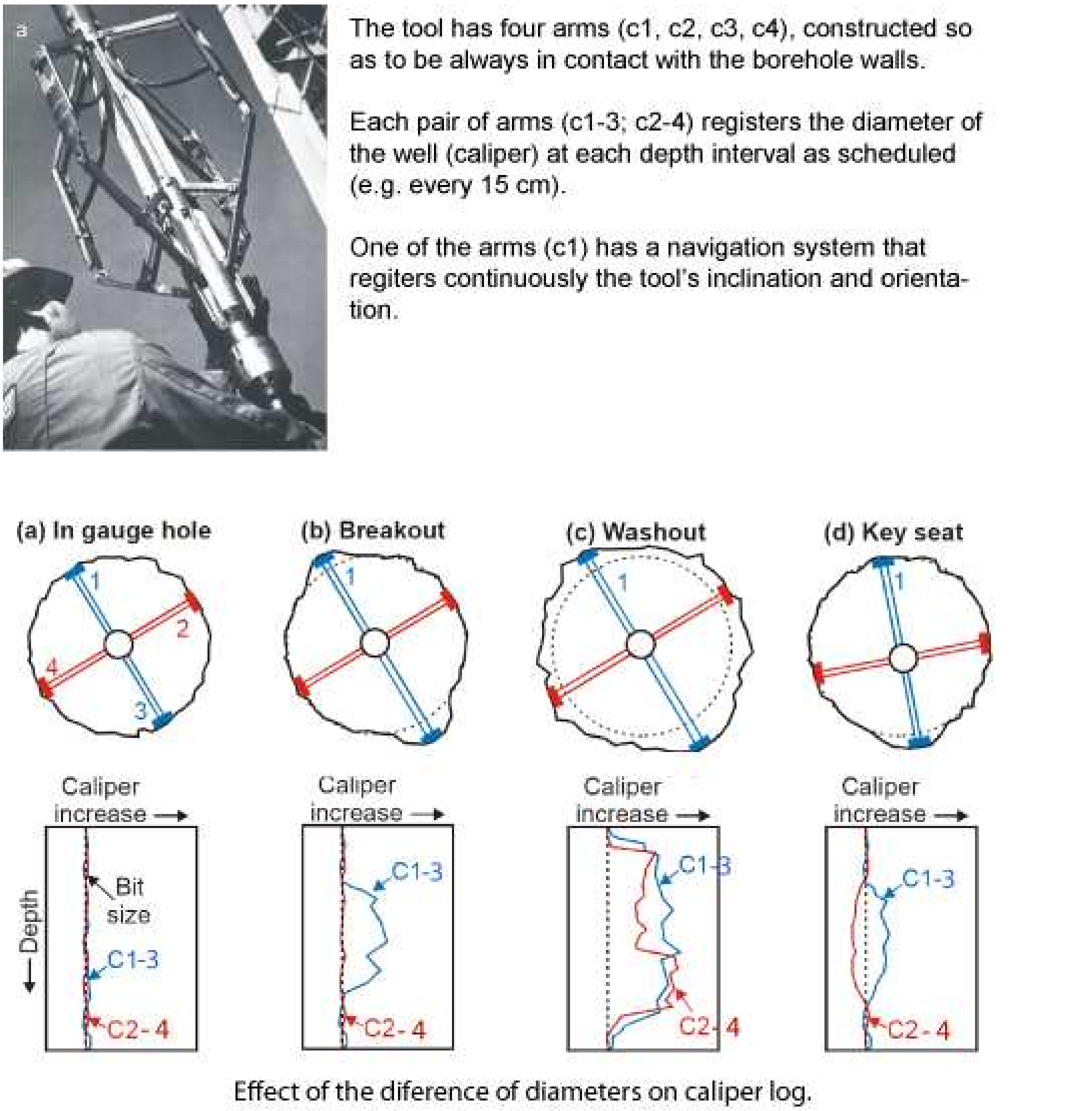

(Modified from the World Stress Map site)

Figure 2. 7. Four-arm caliper tool and types of borehole section enlargement.

Bit size is the borehole diameter planed for a given depth. For World Stress Map (WSM) definition consult Appendix [2.4].

The breakouts data analyzed for the Potiguar Basin by Lima et al. (1997) exhibit a NW-SE to E-W general SHmax orientation, roughly parallel to the coastline (Figure 2.8). This is coincident to the direction indicated by several of the earthquake focal mechanism available for the surrounding area of Basin. According to Mastin (1988), in strike-slip stress regimes the breakouts occurrence is more controlled by the far-field tectonic stresses than by the local stresses near the wellbore. As earthquake focal mechanisms indicate a predominant strike-slip regime through the Potiguar Basin, the hypothesis of Mastin (1988) seems suitable for the area and the SHmax orientation estimated from breakouts can be considered reliable indicators of the direction of maximum compression through the Basin.

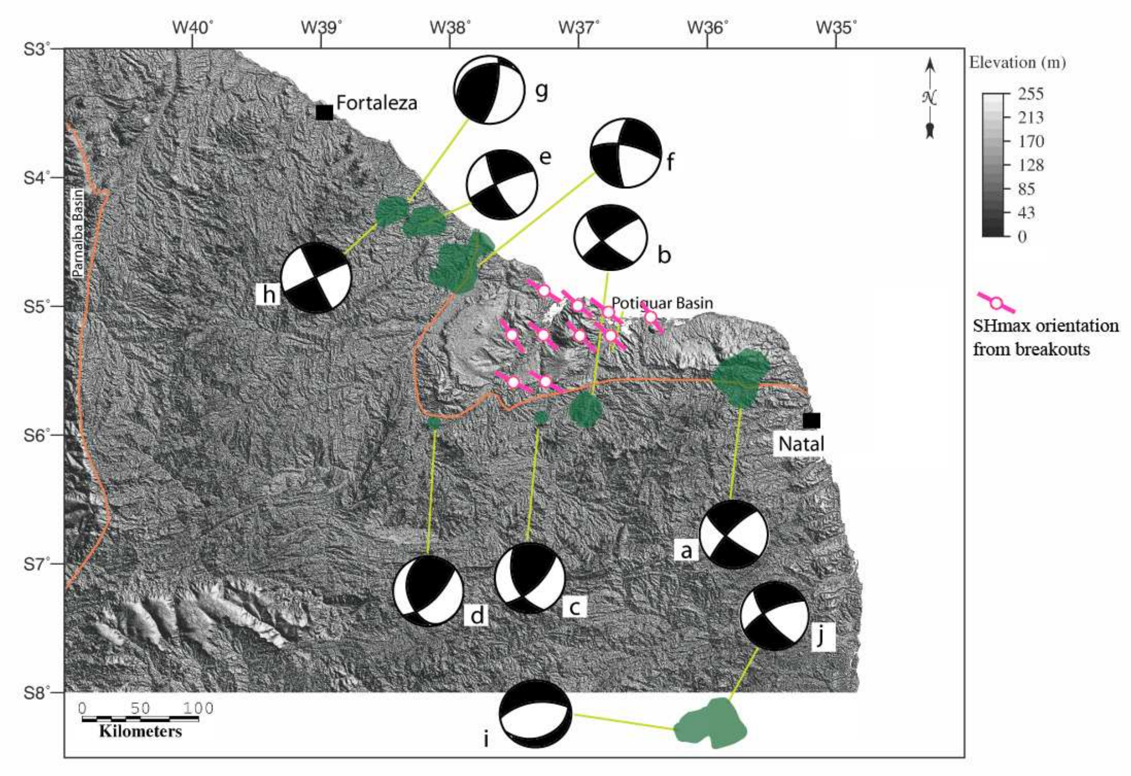

(Source: Lima et al., 1997; Ferreira et al., 1998; Nogueira et al., 2010)

Figure 2. 8. SHmax orientation at Potiguar Basin area.

The focal mechanisms refer to the same events of figure 2.5. The green areas correspond to the regions where the earthquakes that furnished the focal mechanisms occurred.

6.2. Stress Regime on Potiguar Basin

Several operations in the petroleum industry involve the formation fracturing at given depth intervals of interest. Fracturing tests (e.g. leak-off test; extended leak-off test) are routinely used in drilling activities, to evaluate the maximum pressure of drilling fluid (mud weight) which can be withstand by the formation in the next hole phase (Ervine & Bell, 1987; Addis et al., 1998). The hydraulic-fracturing is a well-known technique used to enhance the production on low permeability reservoirs (Hubbert and Willis, 1957; Brudy, 1998). All these methods involve isolating a section of the borehole over a known depth interval, with inflatable packers, and then increasing the pressure within the interval by pumping in fluids until they induce a fracture in the surrounding rocks. The pressure at which this occurs, named instantaneously shut-in pressure, is considered equivalent to the in-situ minimum principal stress (Hubbert & Willis 1957; Ervine & Bell, 1987; Bell, 1990).

The studies performed by Lima Neto (1998; 1999) for the Potiguar Basin show a predominant strike-slip stress regime. The author also observed a secondary reverse stress regime, appraised from the shallowest available data (between 313 and 2500m depth) and from data deeper than 3700m (these obtained offshore). At these depths the registered shut-in values (taken as equivalent to Shmin magnitudes) are very close to the calculated Sv values at the same depth interval.

Again, the results obtained from wellbore data corroborate the nowadays stress pattern indicated by the earthquake focal mechanisms.

Summary

The Potiguar Basin was implemented at early Cretaceous, in the context of the South America/African plates breakup and the subsequent opening of the South Atlantic. The stratigraphic record at Potiguar Basin is deeply related to its tectonic evolution.

The present knowledge about the lithostratigraphy and tectonic-structural evolution of Potiguar Basin results from the analysis of data obtained from petroleum wells and seismic lines. These data were fundamental to build this knowledge, since just the Barreiras, Tibau, Jandaíra, and Açu Formations outcrop in the the onshore portion of the Basin.

Nowadays the stress regime operating through Potiguar Basin is predominantly strike-slip, with some minor reverse and normal events. The maximum compressive stress orientation through the Basin ranges from NW-SE to E–W, roughly parallel to the coastline. This information was obtained from available earthquake focal mechanisms and from specific tests and logs performed on hydrocarbon wellbores.

The Jandaíra Formation is a Turonian to Campanian tide dominated carbonatic platform that crops out in almost all the emersed portion of Potiguar Basin. It presents intense

Post-rift deformation, frequently associated to karstification processes, in a tectonic context equivalent to other Brazilian reservoirs. Because of this it was used on this thesis as analogue to naturally fractured carbonate reservoirs.

Chapter 3

Lineament Analysis

1. Introduction

For more than a century the observation of linear patterns in the topography has been attracting the attention of geoscientists (Wise, 1982; Wise et al., 1985). At the very beginning of the 20^{th} century "german writers" established the expression "*tektonische linien*" to describe rectilinear features correlated to planes of faults or joints (Hobbs, 1904; page 485 – author's note). But this definition was insufficient to explain the origin of all aligned elements observed in the topography, principally considering how difficult it was to establish the correct observation perspective by only using terrain investigation methods. Because of this, Hobbs (1904) opted to use the term **lineament** to describe "(…) nothing more than a generally rectilinear earth feature".

The development of the aircraft-derived images between the two World Wars (Figure 3.1) and the development of the satellite-derived images during the 1950's, revealed how surprisingly frequent and pervasive are the aligned features on the Earth's surface, achieving lengths of tens to hundreds of kilometers (Wise et al., 1985; Liu, 2007).

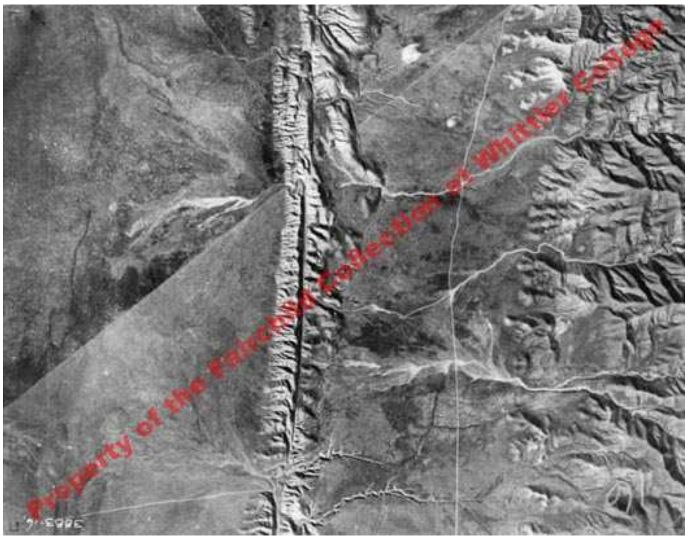

Figure 3. 1. – San Andreas Fault from aircraft-derived image (1936).

This image shows the Elkhorn Scarp, San Andreas Fault Carrizo Plain, close to San Luis Obispo Co., CA. (http://web.whittier.edu/fairchild/san_andreas.html).

With the improvement of imagery technology the concept of lineaments improved too. Today the term lineament is applied to any mappable linear topographic features which constitute the expression of tectonic-structural processes and/or crustal stresses on the Earth's surface (Wise *et al.*, 1985; Jordana & Schottd, 2005; Pradhan, *et al.*, 2006; Rahiman & Pettinga, 2008).

Despite the significant amount of satellite images available nowadays, attesting unequivocally the lineaments' existence, the analysis of lineaments is still one of the most controversial subject on the modern structural geology. The main reason for such controversy is the inefficiency of traditional field methods in matching at outcrop scale the aligned features observed on images. It is due to a natural limit imposed by the scale variation, that produces different perception about the existing elements (Figure 3.2). Furthermore, unequivocal information about the lineaments' age, tectonic settings, and stress fields responsible for their origin are usually lacking (Wise *et al.*, 1985).

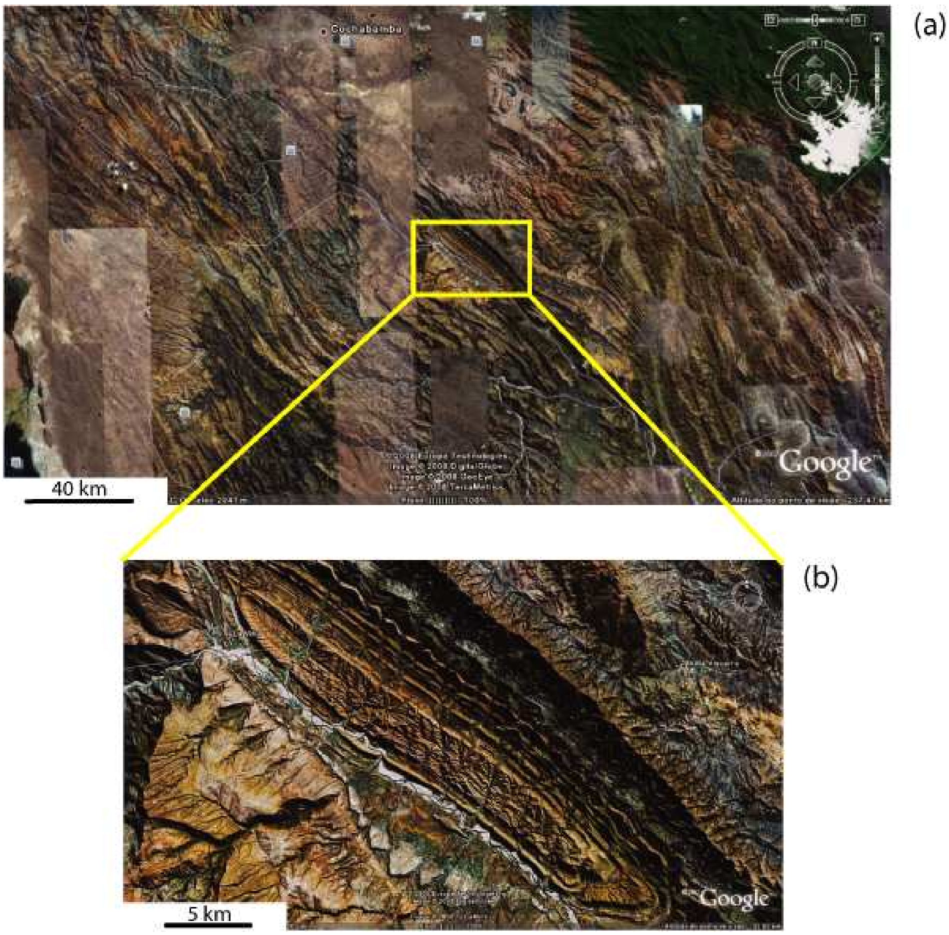

Figure 3. 2 – Lineaments perception from different scales.

These images refer to the Andes Range central part, in Bolivia, at the Pacific Margin of South America. In the image (a) it is possible to observe many topographic aligned features but it is not possible to individualize any specific structure, which can be described as the original Hobbs' concept of lineament: "(…) nothing more than a generally rectilinear earth feature". The yellow rectangle indicates the area from which was obtained the image (b). On (b) it is already possible to individualize several geomorphologic, structural and stratigraphic aligned elements (e.g., valleys; drainage channels; faults; beddings). Despite the high resolution image allows us to see perfectly the regional structures, it is not certain that it will be possible to identify all single elements on the terrain.

On the other hand the detection and analysis of lineaments and lineament domains (i.e. clusters of lineaments oriented along preferential directions) is an ongoing subject of interest for science, industry, and society. It has been considered a practical and economically advantageous tool when investigating large areas, or regions where conventional field mapping techniques of structural geology are impractical due to difficult approach conditions or limited amount of outcrops. In these circumstances the use of lineaments information can reduce significantly the risks, costs, and time involved in a given project (Solomon & Ghebreab, 2006; Rahiman & Pettinga, 2008).

Several studies using lineament data derived from multiple sets of remote sensing imagery, mapping them at local and regional scales, as well as linking lineaments to detailed field mapped structures, have been providing a better comprehension about the structural and tectonic evolution in many areas worldwide (Jordana & Schottd, 2005; Solomon & Ghebreab, 2006; Rahiman & Pettinga, 2008). The results of these studies find useful applications on: (a) improving hazard analysis on landslide prone areas (Pradhan, *et al.*, 2006); (b) seismic or volcanic active regions (Arellano-Baeza *et al.*, 2006); (c) groundwater exploration (Onyedim & Norman, 1986; Masoud & Koike, 2006; Gleeson & Novakowski, 2009); (d) mineral exploration (Onyedim & Norman, 1986; Balaji & Ramasamy, 2005; Masoud & Koike, 2006); (e) oil and gas exploration (Babcock & Sheldon, 1976; Onyedim & Norman, 1986; Guo *et al.*, 1999; Masoud & Koike, 2006).

2. The use of lineaments analysis on this thesis

As it was explained on Chapters 1 and 2, the Jandaíra Formation was adopted in this thesis as the analogue to fractured carbonate reservoirs for its plenty exposition on the Potiguar Basin and its tectonic context equivalent to other carbonate reservoirs along the Brazilian margin. However, the common occurrence of karstic processes on Jandaíra Formation (Figure 3.3) often makes the structural analysis a very complicated task. The principal problems caused by the karstic framework are: (i) the access to the outcrops is difficult, exhausting, and moderately danger; (ii) the high density of non-tectonic fractures associated to the karst usually obliterate the tectonic fractures, making it difficult to observe the continuity and relationship of structures from the terrain point of view.

Figure 3. 3. Karstic fabric at the study area.

Great part of the blocks seen on the image is mobile - they easily rotate and tilt when a person step on -, making difficult to walk and increasing the risk of serious injures in case of tumble. It is possible to distinguish long and aligned holes, but is very difficult to individualize joint or fault plains to measure.

Due to these adverse conditions for fieldwork, the structural analysis of outcrops has become a very difficult task. To overcome this difficulty a multi-scale analysis of lineaments was done: (i) outcrop-scale lineaments (i.e. local-scale) were extracted from satellite high resolution images, available in Google Earth Pro (resolution 0.6 m); (ii) basin-scale lineaments (i.e. regional-scale) were extracted from SRTM3[Appendix, 3.1] data (resolution 90 m). The objective was to obtain a broad perspective about the distribution of structural trends in local and regional scales. From this understanding was possible to verify the interdependence between the deformational events imprinted on the Basin and the study area.

3. Lineaments detection methods

The most usual method to detect topographic lineaments is the manual tracing, based on human interpretation. However this technique is not completely reliable due to conditional factors like experience, knowledge about the area, and mood. These factors may affect the interpreter's capability on detecting lineaments, resulting in the introduction of bias in the database (Wise et al., 1985). This risk is another source of disagreement involving the use of lineament data in studies of structural geology.

To overcome this problem, with the increasing use of synthetic images, in recent years some computer programs have been developed to automatically detect lineaments. These algorithms allow to obtain lineaments exempted from the interpreter's influence and save time when the study area is too large or contains too many details (Wise et al., 1985; Raghavan et al., 1995).

Another technique that improves significantly the work of lineaments detection in both manual and automatic methods is the variation of lighting condition. On synthetic images this is done by the variation of the azimuth and elevation angles of the simulated (i.e. numerical) illumination source (Wester and Lundén, 1996).

3.1. Lighting condition

The lighting applied to a given image affects the orientation and the area of the shadow zones as a function of the topography represented in this image. Basically the shadow technique (Wise, 1969) allows to decrease the variation of the grey levels according to the simulated light azimuth and elevation angles, resulting in a pronounced minimum in the strike diagram of the recognizable lineaments (Wise et al., 1985).

The fundamental effect of this technique is the relative enhancing or attenuation, up to vanishing, of the lineaments directions. This means that the aligned features on a synthetic image became more evident as more perpendicular they are to the light direction (Figure 3.4). On the other hand, the features aligned parallel or nearly parallel to the direction of illumination became less evident on the image (Figure 3.4).

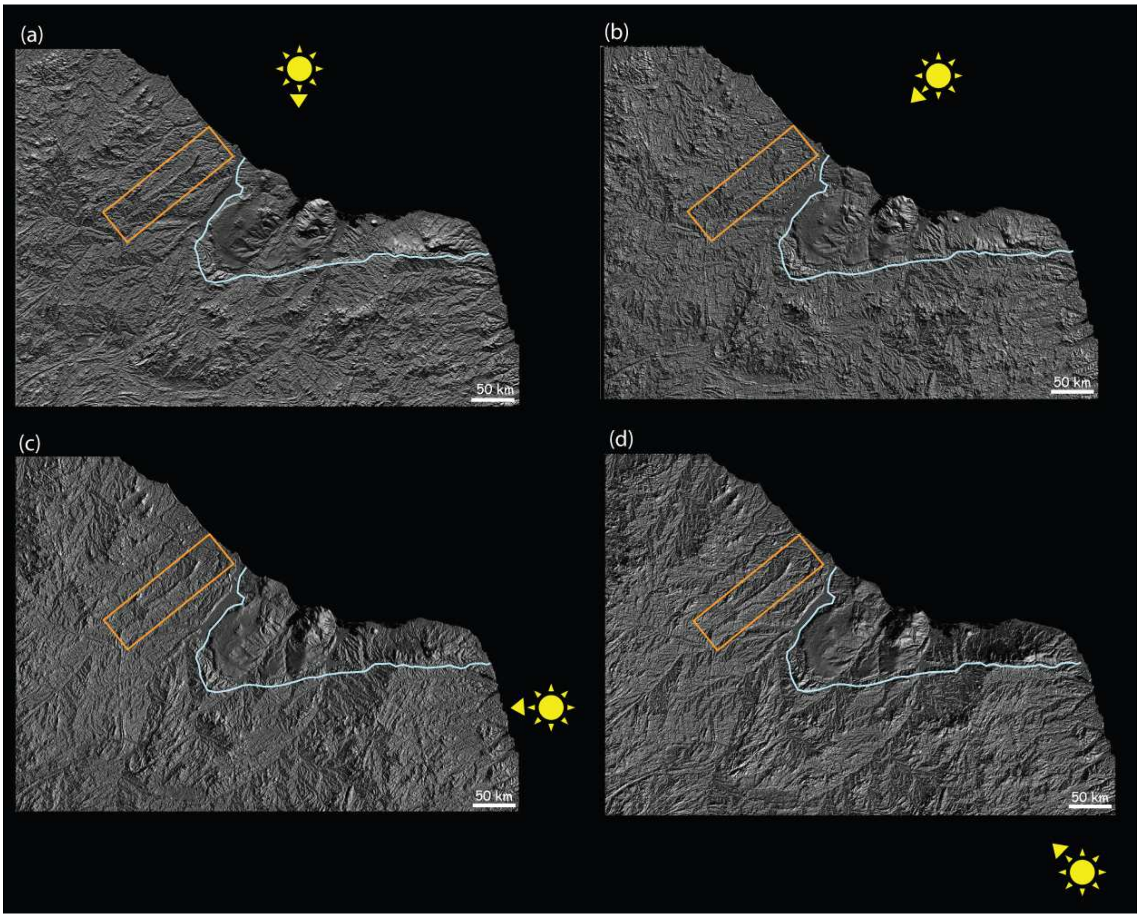

Figure 3. 4 – Lighting effect on topography image.

The pale blue line represents the general limit of the Basin's onshore portion. The yellow sun and arrow symbols show the light direction applied on each image: (a) azimuth N0° and elevation 10°; (b) azimuth N45° and elevation 10°; (c) azimuth N90° and elevation 10°; (d) azimuth N135° and elevation 10°. The orange rectangle individualizes a linear NE topographic feature, that is evident on images (a), (c) and (d) but almost disappears on image (b) where the light is nearly parallel to this aligned element.

Another interesting piece of information that can be estimated when varying the light condition on a same image is the relative age of tectonic activity. Assuming that active or recent tectonics usually creates relief faster than erosion smooths it, lineaments related to the youngest tectonic pulse are supposed to be longer and narrow than the previous (P. Cianfarra and F. Salvini oral communication). The result is a reduced scattering on lineaments azimuth measurements (Figure 3.5).

In this way the most frequent lineaments direction appearing under different lightings for the same image is considered indicative of the more recent or more penetrative tectonic activity.

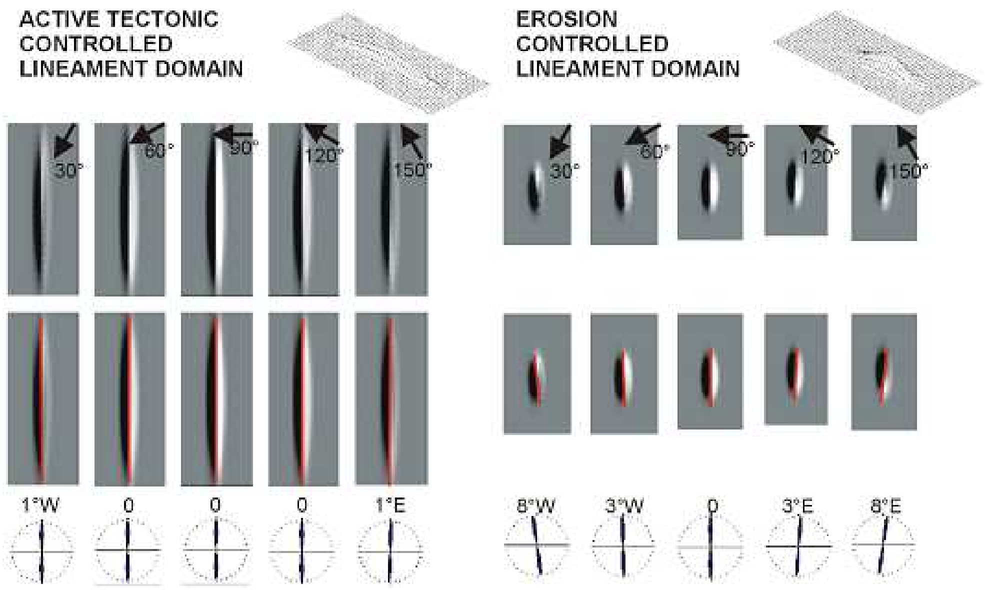

(A courtesy from P. Cianfarra and F. Salvini)

Figure 3. 5 – Young lineaments compared to old lineaments.

The black and light grey elliptic symbols are related to two synthetic aligned topographic features (the mashed 3D surfaces). The left object illustrates an active tectonic event, while the right object illustrates an older tectonic event. They are submitted to five different light directions, indicated by the black arrows and degree annotations. The red lines represent the lineament traces for the elliptic objects as a function of each light direction. The object related to the active event, and not yet affected by erosion, presents almost any scattering on the azimuth measurements (rose diagrams), but the lineament azimuths obtained for the object related to the oldest tectonic event have an evident scattering behaviour.

3.2. Automatic detection methodology

Most of the automatic lineaments detection methods are based on edge enhancement and filtering techniques using digital filters. These techniques enable to detect adjacent pixels abruptly changing in gray level, generating processed images composed by numerous lineament segments (VanderBrug, 1976).

In this study the automatic detection of lineaments was done on SRTM3 data, by using the software SID3 (©Prof. F. Salvini). The input file to SID3 are grayscale images generated from SRTM data or other satellite derived images, after the application of the most favorable light conditions (Figure 3.4) and digital filters (Figure 3.6a and b). The sequence of filters applied was: (i) Smoothing Average (3x3 matrix) – it reduces the intensity of variation between one pixel and the next by replacing each pixel value with the average value of neighboring pixels in the matrix and its own value; (ii) Gaussian Blur – it has the effect of reducing the image's high-frequency components by applying a Gaussian function; (iii) Laplacian filter - it produces a picture of all edges in the image by highlighting areas where the intensity changes rapidly; (iv) Threshold, converts grayscale or color images into high-contrast black-and-white images.

At the end of the filtering process it is very common that some pixels unrelated to real topographic lineaments are generated from low contrast areas on image. They represent spurious data. To eliminate the useless pixels the algorithm LIFE (©Prof. F. Salvini) was developed. It must be applied to each filtered image before importing it into SID3 (Figure 3.6c and d). The parameters LIFE used to clean the image are: (i) Threshold - the pixel equivalent size in meters (i.e. if the image resolution is 90m, one pixel is equivalent to 90m); (ii) Minimum Neighbours - the minimum number of white pixels within an area; (iii) Neighbour Threshold - the minimum distance between white pixels; (iv) Life Window Size - the number of pixels defining the filtering window that will scan the image (in this case a window 5x5 pixels).

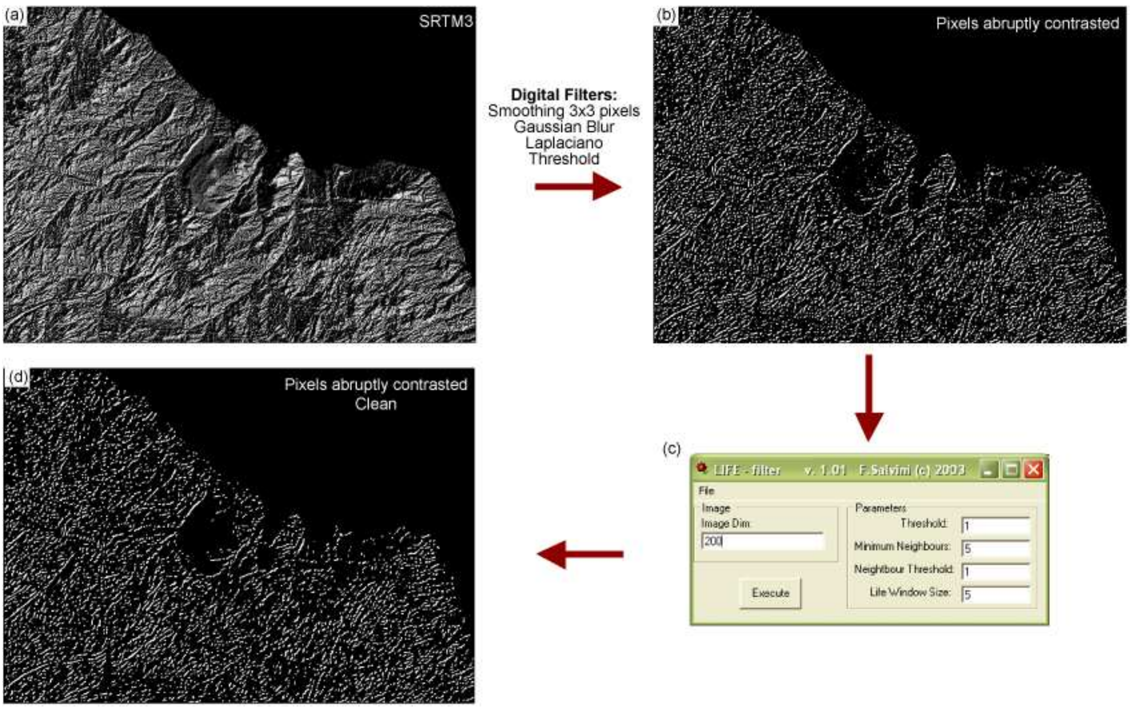

Figure 3. 6 –Routine to create input images to SID3.

(a) the original SRTM3 image from which one wants to detect lineaments; **(b)** the abruptly contrasted pixels image after digital filtering; **(c)** the LIFE algorithm, to eliminate spurious pixels remained on low contrast areas; **(d)** the output image generated by LIFE, that is the input file to SID3.

SID3 will systematically search for all possible aligned segments on the new image, according to an eleven-parameter list (Figure 3.7a): (1) Minimum Length is the minimal number of pixels along a lineament; (2) Maximum Length is the maximum number of pixels along a lineament; (3) Width is the number of pixels along the lineament strike (defines the lineament thickness); (4) Threshold is the pixel value in meters (Threshold equal to 1, the pixel has the original resolution of image); (5) Along Length Integration is the width, in pixels, of the smoothing along the potential lineament; (6) Density is the minimum number of pixels at a lineament point; (7) Separation is the maximum distance, in pixels, between two lineament segments; (8) Min. Segments Length is the minimum length in pixels of each lineament segment; (9) Azimuth Step Resolution is the angular interval in degrees according to SID will search for lineaments; (10) Max % Double Overlap is the percentage of superposition allowed for the scanning process; (11) Double Search Angle is the angular interval according to SID verify if a lineament is detected twice. Those parameters simply describe a standard lineament (Figure 3.7b), which constitutes a model to orient the program on seeking lineaments.

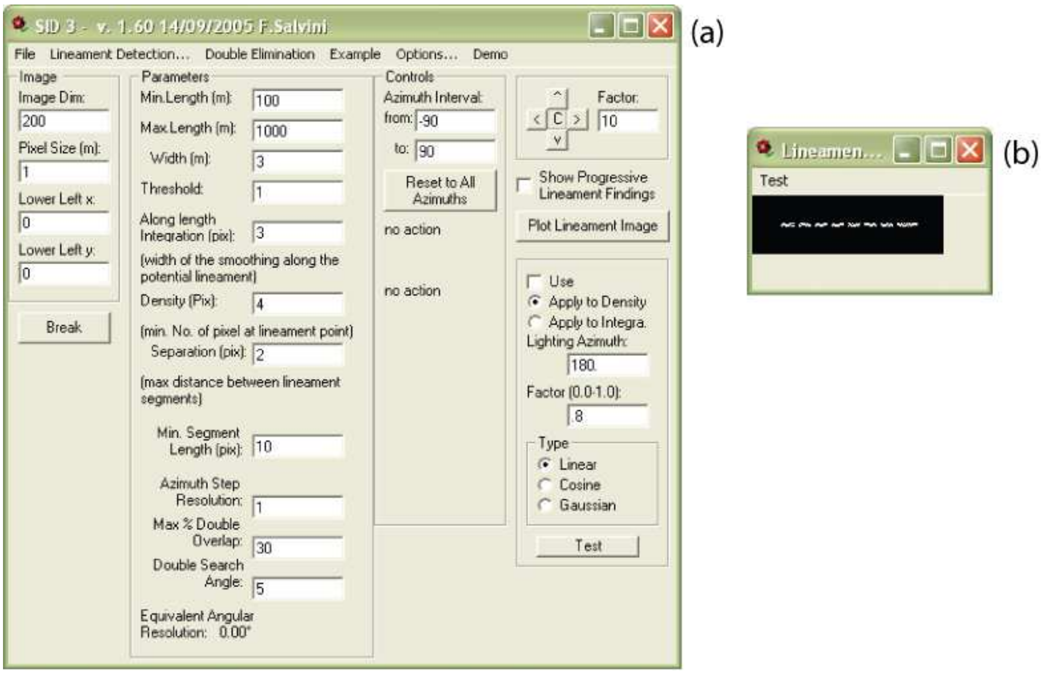

Figure 3. 7 – SID's parameters describing a standard lineament.

(a) The main SID's window, where are established the eleven parameters to create the standard lineament to be searched. (b) This is the lineament model created according to the parameters defined in (a). The Azimuth Interval control tool allows specifying the desired angular interval in which SID will scan the image.

After the parameters are established the software examines the whole image and traces a line segment where exist a sequence of pixels equivalent to the model, independently of its azimuth.

The final output is a map of all possible lineaments found (Figure 3.8) and an ASCII file containing the information about these lineaments: length; azimuth; coordinates on the raster image (Figure 3.9). This ASCII file is the input to the software Daisy (©Prof. F. Salvini) in which will be carried on the statistical analysis.

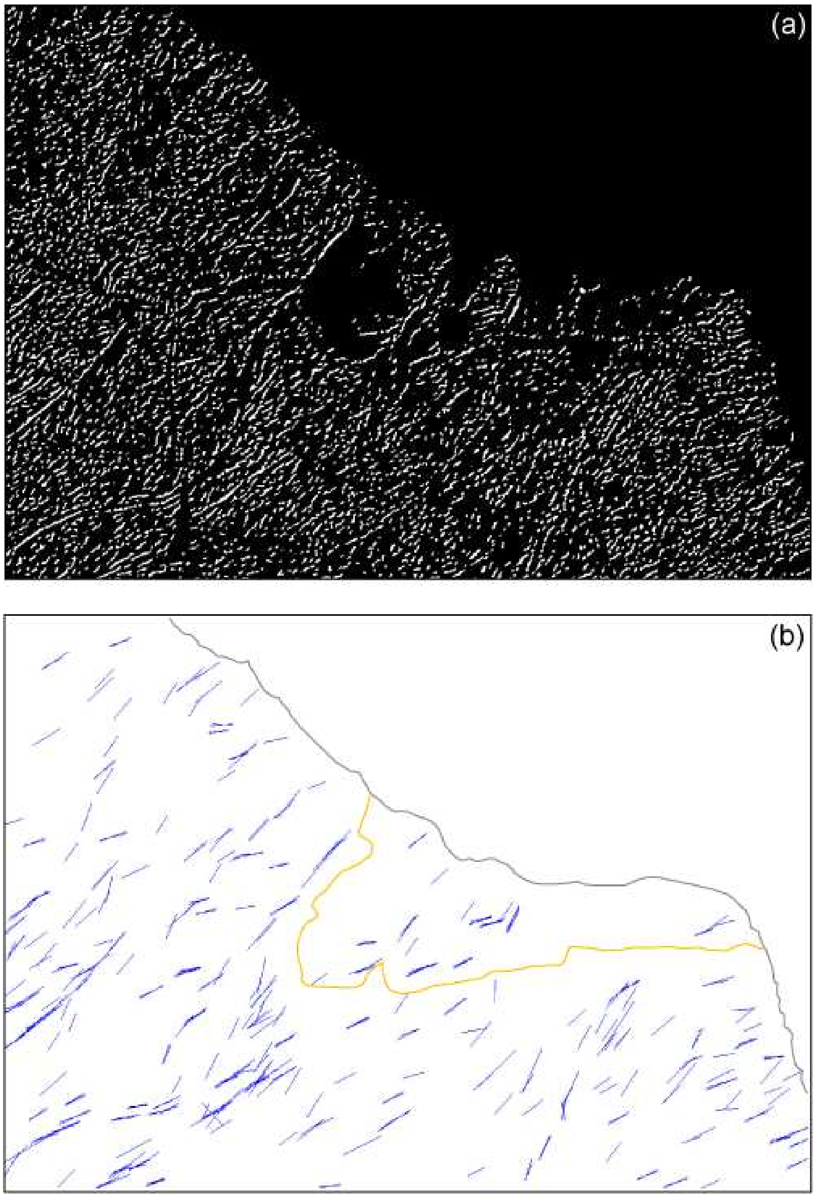

Figure 3. 8 – Example of automatically detected lineaments from SID3.

(a) Pixel abruptly contrasted image, obtained from the original SRTM3 image - lighting N135^o/elevation 10^o. (b) Blue traces represent lineaments automatically detected by SID3. The yellow line is the general limit of Potiguar Basin, and the gray line is the coast limit. These two lines were added to the original lineaments map from SID3.

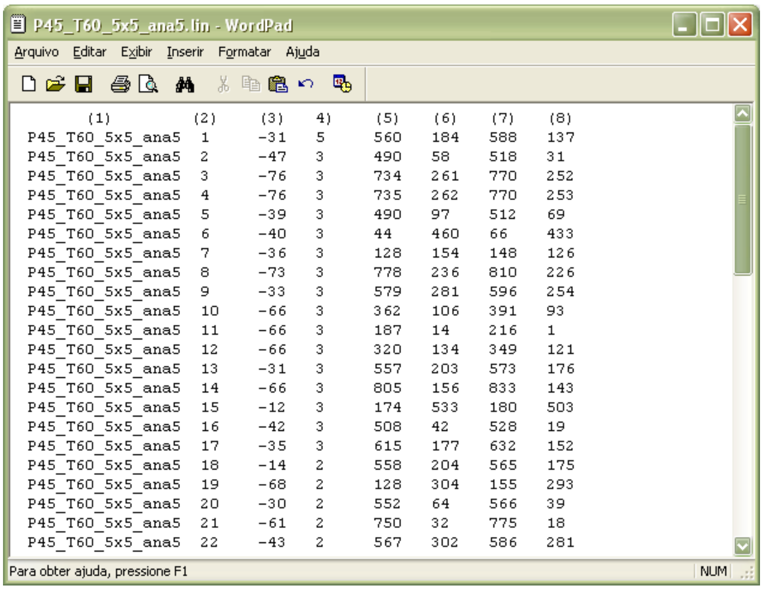

(1)	(2)	(3)	4)	(5)	(6)	(7)	(8)
P45_T60_5x5_ana5	1	-31	5	560	184	588	137
P45_T60_5x5_ana5	2	-47	3	490	58	518	31
P45_T60_5x5_ana5	3	-76	3	734	261	770	252
P45_T60_5x5_ana5	4	-76	3	735	262	770	253
P45_T60_5x5_ana5	5	-39	3	490	97	512	69
P45_T60_5x5_ana5	6	-40	3	44	460	66	433
P45_T60_5x5_ana5	7	-36	3	128	154	148	126
P45_T60_5x5_ana5	8	-73	3	778	236	810	226
P45_T60_5x5_ana5	9	-33	3	579	281	596	254
P45_T60_5x5_ana5	10	-66	3	362	106	391	93
P45_T60_5x5_ana5	11	-66	3	187	14	216	1
P45_T60_5x5_ana5	12	-66	3	320	134	349	121
P45_T60_5x5_ana5	13	-31	3	557	203	573	176
P45_T60_5x5_ana5	14	-66	3	805	156	833	143
P45_T60_5x5_ana5	15	-12	3	174	533	180	503
P45_T60_5x5_ana5	16	-42	3	508	42	528	19
P45_T60_5x5_ana5	17	-35	3	615	177	632	152
P45_T60_5x5_ana5	18	-14	2	558	204	565	175
P45_T60_5x5_ana5	19	-68	2	128	304	155	293
P45_T60_5x5_ana5	20	-30	2	552	64	566	39
P45_T60_5x5_ana5	21	-61	2	750	32	775	18
P45_T60_5x5_ana5	22	-43	2	567	302	586	281

Figure 3. 9 – Example of ascii output file from SID3.

The numbers between parentheses indicate the columns sequence in the file: (1) the files' name; (2) the lineament identifier; (3) the lineament azimuth, raging -90^{o} to 90^{o}; (4) the lineament length, in number of pixels; (5), (6), (7), (8) are the lineament raster coordinates on the image.

This processing chain, from the original image to the SID3's output files, must be repeated for each illumination condition used. Then the results for each lighting condition are converted into a single database. It is assumed then that this collection has the best possible distribution of lineaments for the study area.

3.3. Manual tracing methodology

In this study the manual tracing of lineaments was executed on high definition satellite images (average resolution 0.60m), exported from Google Earth Pro^{TM} as raster images.

As explained on the previous topic 3.1, the use of a multiple lighting directions on relief maps reduces in a systematic manner the effects of shadow zones. But this process is not so easily accomplished using satellite images (Wise et al., 1985). Concerning the study area (Figure 3.10) the impossibility to vary the lighting on the images is not significative for the lineaments analysis, once the topography is gentle enough to be considered flat – the maximum elevation is nearly 112 m.

To enhance the interpreter capability to detect lineaments, the area was divided into eighteen sub areas (Figure 3.10). For each sub area a maximum zoom to obtain the best visualization possible of the outcrops was applied (Figure 3.11a).

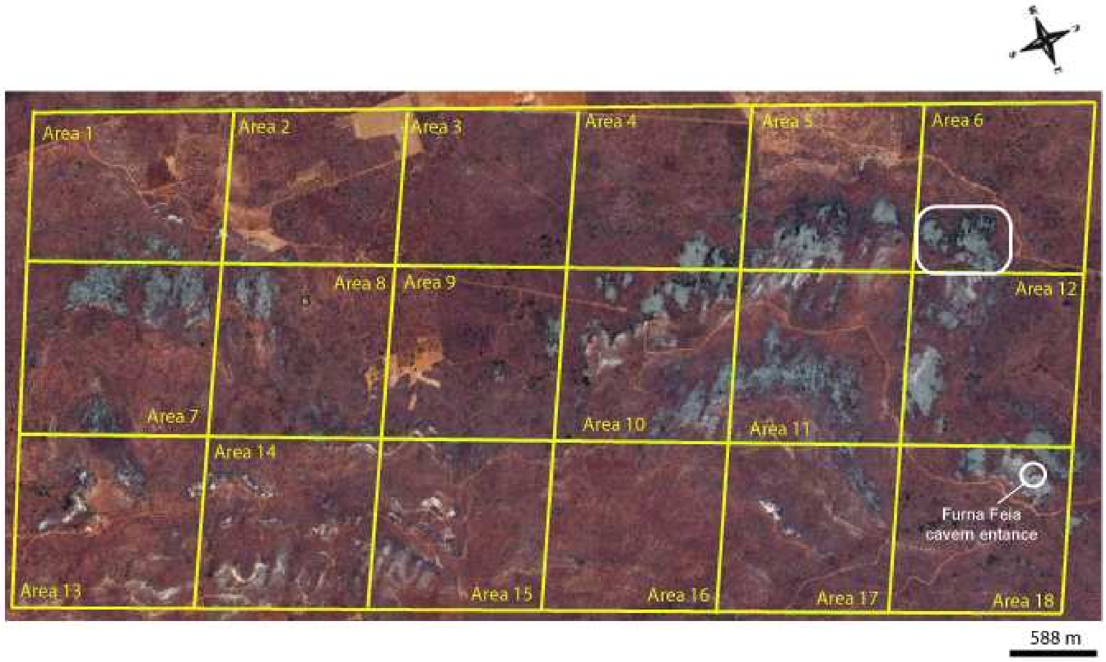

Figure 3. 10 – Subdivision of the study area.

The grey colors correspond to the Jandaíra Formation carbonates expositions. The white circle indicates the Furna Feia cave entrance. The white polygon indicates the area from which was obtained the Figures 3.11 and 3.12.

The only filtering applied to the images were a color filter (converting RGB colors into grayscale) and a bright and contrast filter (Figure 3.11). The objective was to emphasize the detectable lineaments, which at this area are evident fractures and faults.

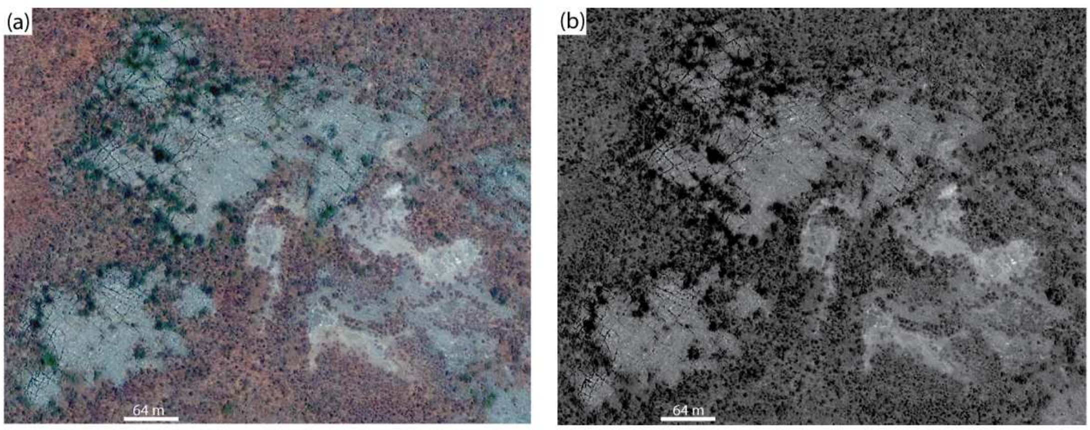

Figure 3. 11 – Outcrops raster image from Area 6.

(a) Original RGB colors satellite image. (b) The same image shown on (a) after applying the color and the bright and contrast filters. Both images are oriented toward North.

The tracing work (Figure 3.12) was done using a common commercial software. To create an ASCII file in a format compatible to be imported into Daisy (Figure 3.9) the detected lineaments were digitalized using the algorithm LinDig (©Prof. F. Salvini) written for this purpose.

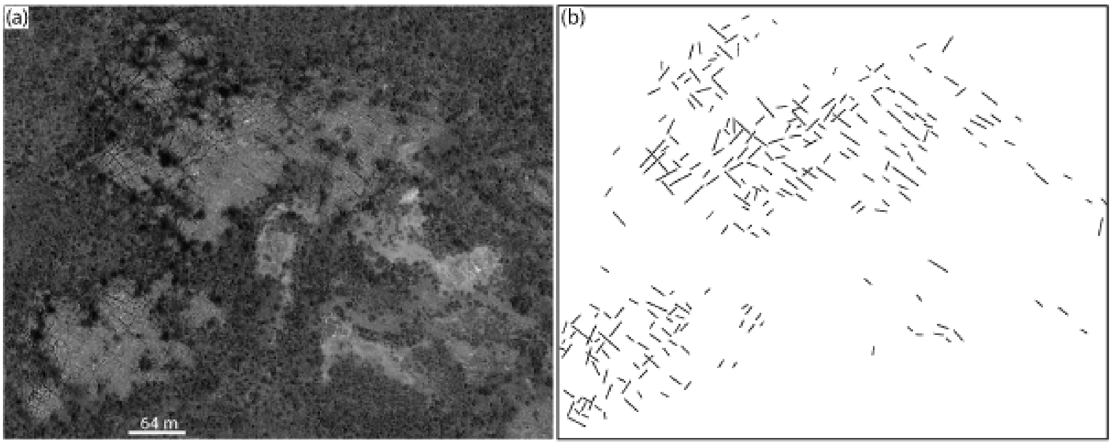

Figure 3. 12. – Example of manual tracing of lineaments (Area 6).
On (b) the lineaments manually traced on (a) are shown. The areas of both images are identical.

4. Results for Regional-scale Lineaments

The detection of lineaments on the regional-scale was performed on four images, obtained from the SRTM3 data available for the Potiguar Basin and part of the surrounding Archean-Proterozoic basement. Each image corresponds to a specific lighting condition (Figure 3.13): (a) azimuth N0^o and elevation 10^o; (b) azimuth N45^o and elevation 10^o; (c) azimuth N90^o and elevation 10^o; (d) azimuth N135^o and elevation 10^o.

The area involved is very large (approximately 144.000 Km^2) and the resolution of the SRTM3 data (90m) offers a significant amount of detail. The manual execution of comprehensive maps of lineaments for each image would require a lot of time. The methodology for automatic detection of lineaments, included in the SID3 program, reduced the working time and allowed to build a database free of bias.

The results (Figures 3.13 and 3.14) show that lineaments oriented NE-SW are the most frequent. On the lighting azimuth N135^o this tendency is more evident (Figures 3.13d and 3.14d), since the largest number of lineaments was detected on this image (380 lineaments, comprising 50% from the total).

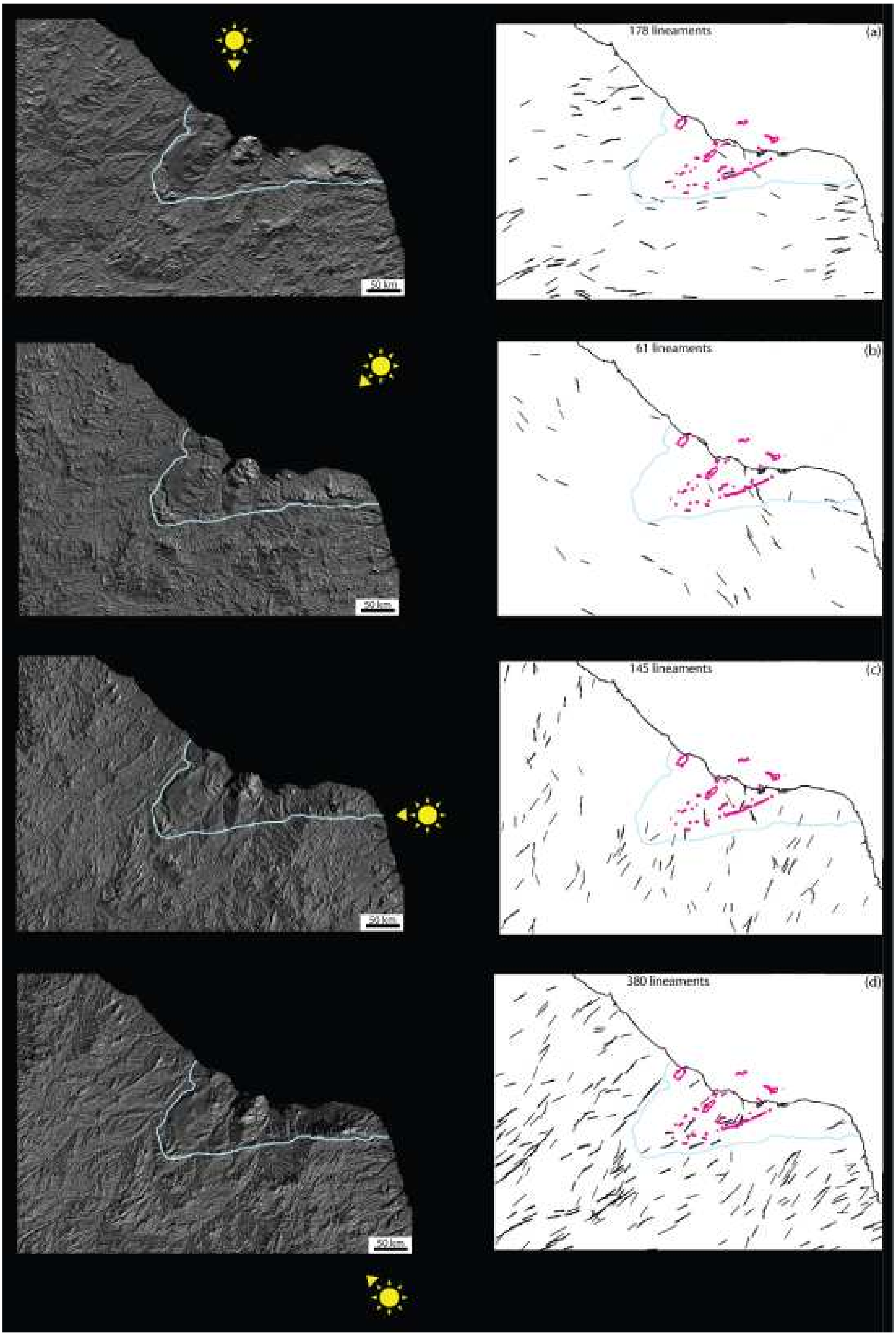

Figure 3. 13 – Automatically detected lineaments for each light condition.

The pale blue line represents the general onshore limit of Potiguar Basin. The yellow sun and arrow symbols always show the light orientation applied for each image. The rose polygons represent oil fields. The numbers inform how many lineaments were find for each light condition.

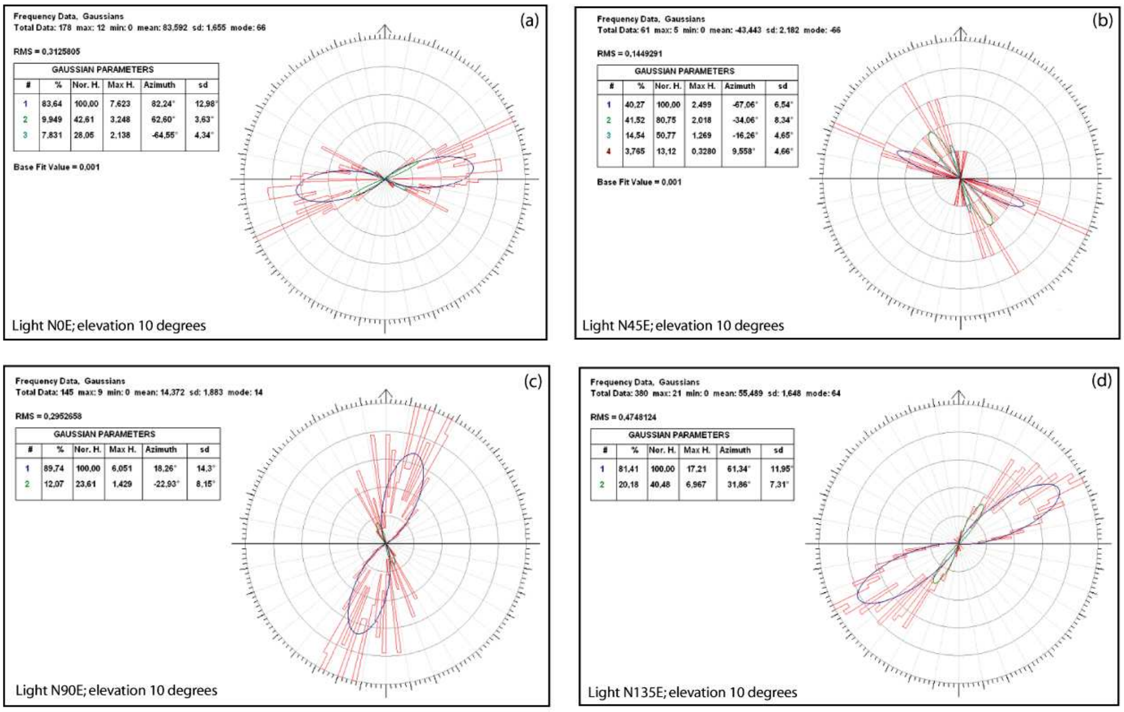

Figure 3. 14. Lineament domains for each light condition.

The rose diagrams correspondent to the frequency analysis of the lineaments on Figure 3.13. The statistics parameters are: **max,** is the maximum frequency comprising all data; **min**, is the minimum frequency comprising all data; **mean**, is the average azimuth comprising all data; **sd**, is the mean azimuth stander deviation; **mode**, is the most frequent azimuth in the dataset; **RMS** (Root Mean Square), is a statistical measure of magnitude of a varying quantity, that in this case defines the number of gaussians that better fit the data distribution; **%**, the percentage of lineaments included in each domain; **Nor.H.** (Normalization High), is the maximum frequency value used to normalize the dataset, bringing them to a common scale; **Max H.** (Maximum High) defines the gaussian maximum length related to the **Nor.H.**; **Azimuth**, the mean orientation referred to the North calculated to each lineament domain; **Base Fit Value**, the cutoff value accepted as a reference to eliminate data that present a high level of scattering. The red lines represent the data distribution and the colored petals are equivalent to the gaussians correspondent to each domain.

After merging these four data sets a collection of 764 lineaments was obtained (Figure 3.15). Three main domains were identified on the azimuths by frequency analysis of these lineaments (Figure 3.16): N65^{o}E (66% of total); N6^{o}W (19% of total); N27^{o}E (9% of total).

Notice that the **Base Fit Value** had its better profit (0.001) for this dataset. Only 6% of total data (46 lineaments in 764) were automatically rejected due to the high scattering level.

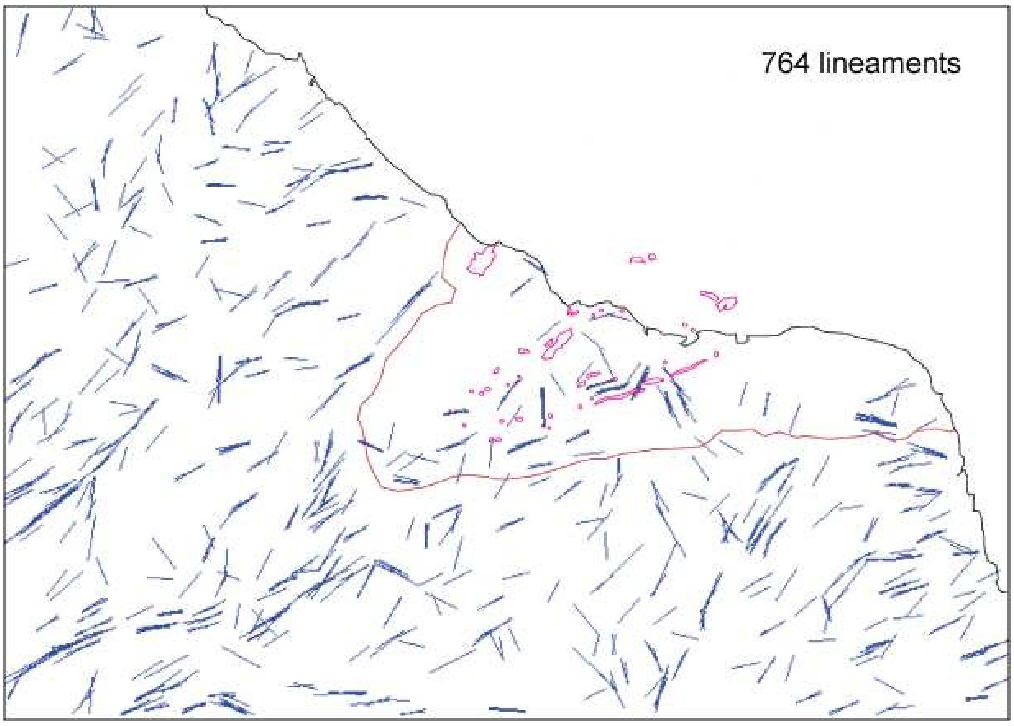

Figure 3. 15 – Merged lineaments obtained from the four light condition.

The blue lines represent the 764 lineaments automatically detected.

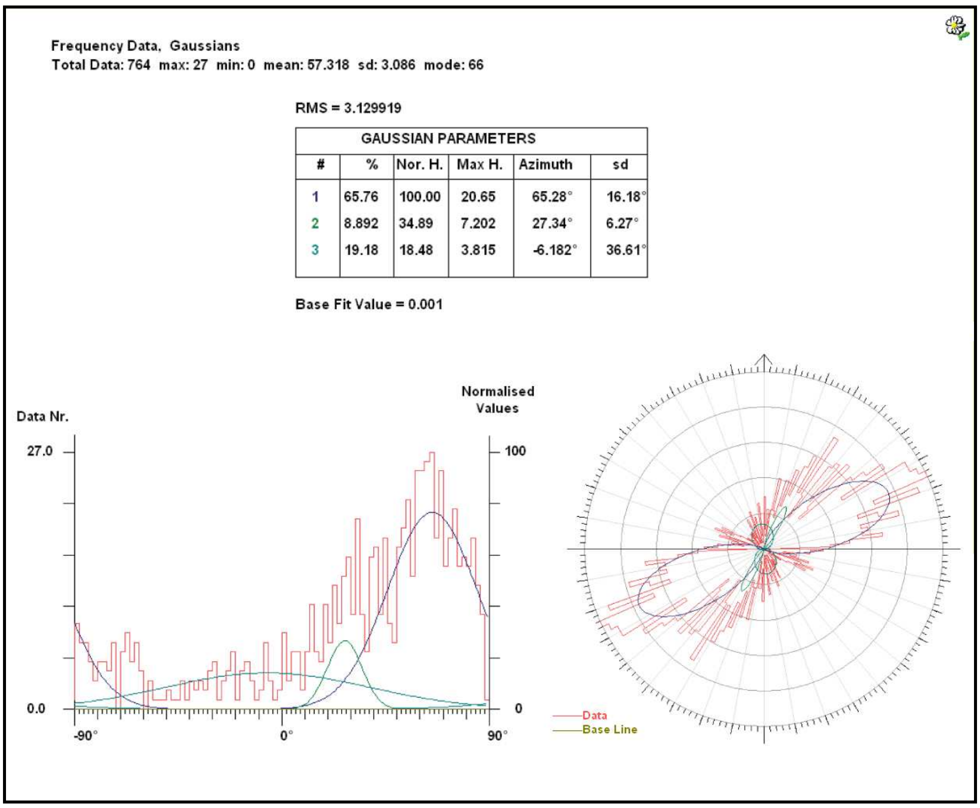

Figure 3. 16. Frequency diagrams merging the four lighting results.

On the histogram (bottom left) and on the rose diagram (bottom right) the red lines represent the data distribution, the colored curves and petals represent the gaussians correspondent to each domain.

5. Results for Local-scale Lineaments

The automatic method for lineaments detection available in SID3 did not work well on the outcrop-scale analysis. The high resolution of images demonstrated to be unappropriated for this type of program, since a large amount of non-geological aligned elements (i.e. paths; fences; vegetation) become too much evident. The attempt to clear these features, besides being a very difficult process, could have damaged the data of interest. Because of this, some useless lineaments were accidentally taken as true geologic ones.

Although the useless data the frequency domains calculated for each sub-area show a trend NW-SE (Figure 3.17).

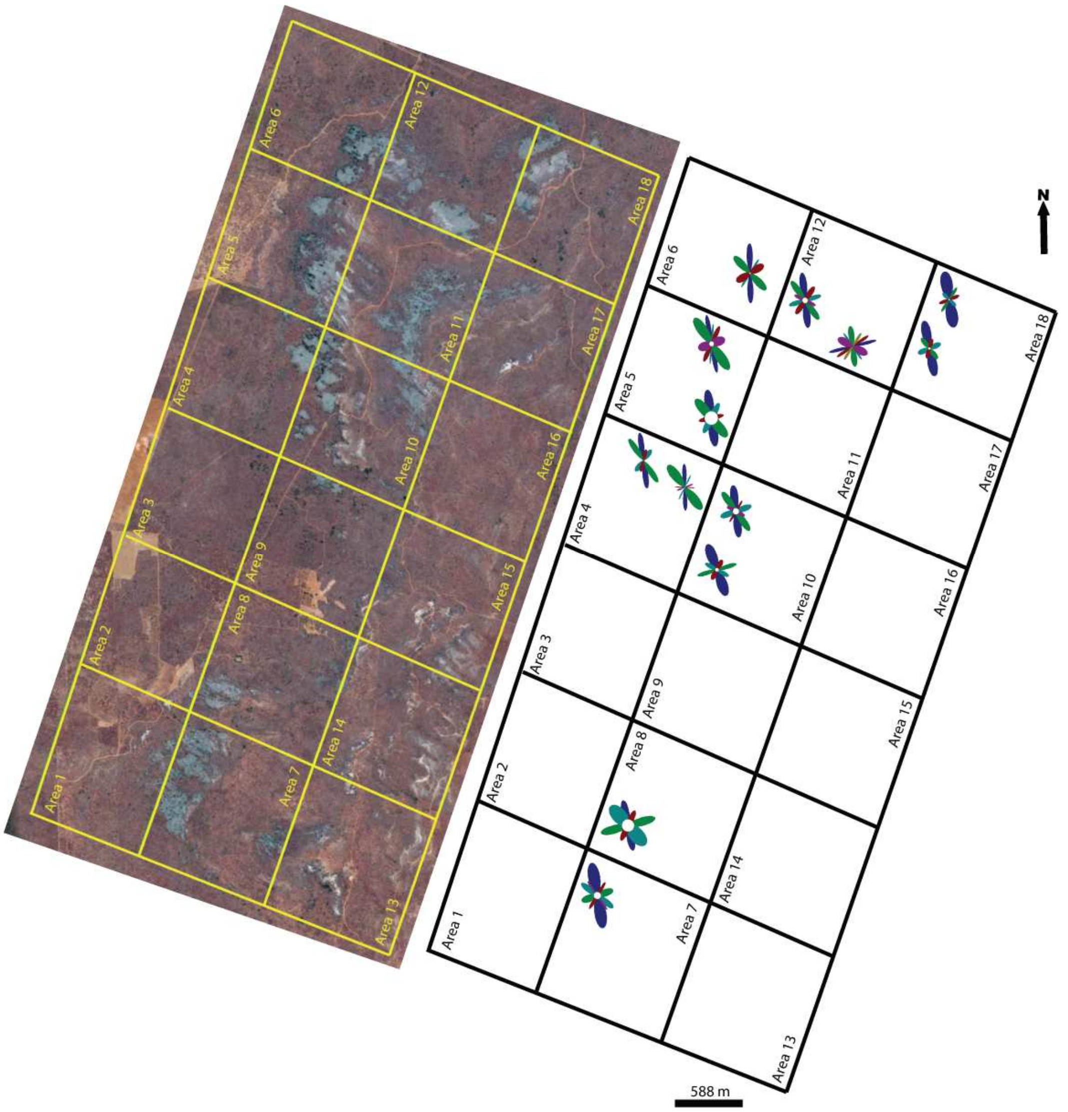

Figure 3. 17. Lineament domains distribution for each sub-area.

Each rose diagram (petals only) is located on the central position of the outcrop image used for the analysis. The areas with no rose diagrams are those from which it was not possible to extract images with good definition to identify lineaments.

On the other hand, these spurious data caused important scattering on the overall statistics of the complete automatically detected lineaments collection (Figure 3.18). The best **Base Fit Value** obtained for this dataset was too much high (more than 100), what is indicative of a very high dispersion level. To corroborate to this perception of the useless lineaments interference, from 22226 detected lineaments only 60% (13308 lineaments) were considered by the software Daisy as being reliable for the statistics.

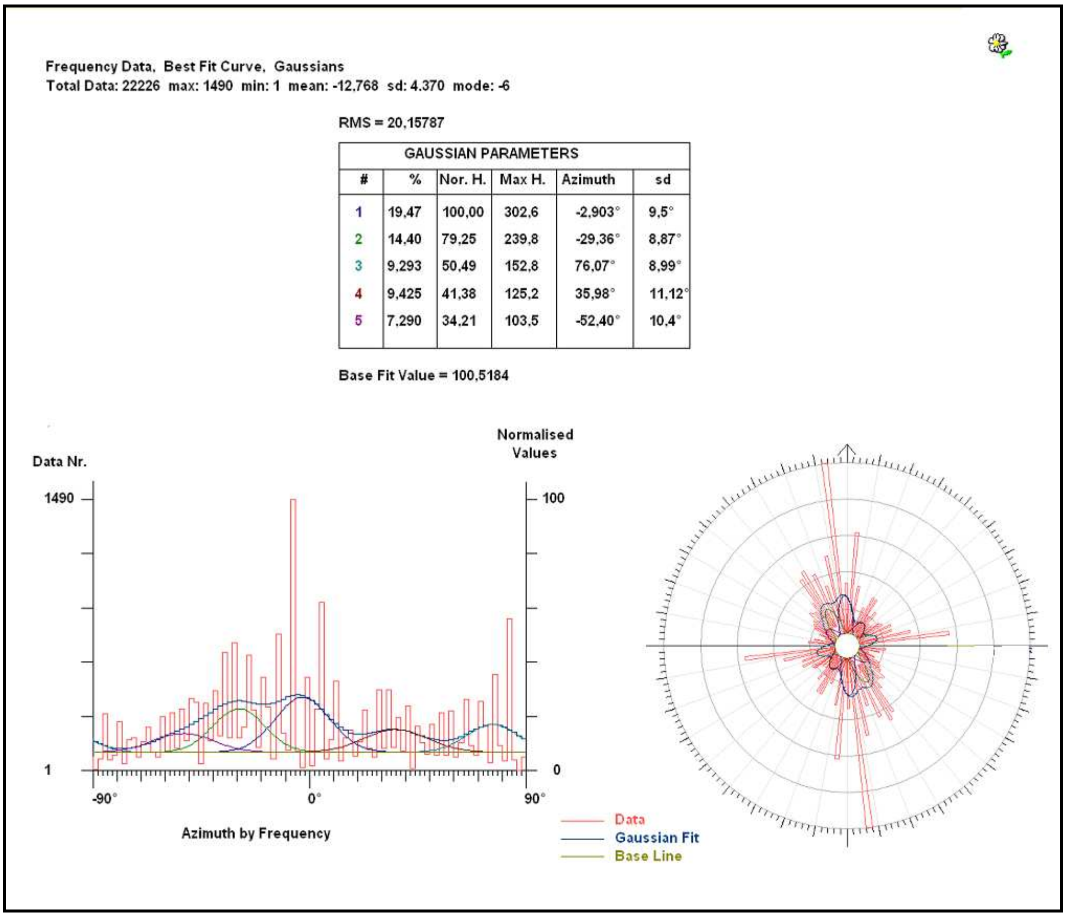

Figure 3. 18. Lineament domains obtained by merging all automatically detected data.

On top, there are the statistics parameters. On the histogram (bottom left) and on the rose diagram (bottom right) the red lines represent the data distribution. The colored curves and petals represent the gaussians correspondent to each domain.

In an attempt to obtain a better use of the these lineaments data was proceeded a comparative analysis between the results of sub-areas (Figure 3.17) and the result of the full dataset (Figure 3.18). This comparative analysis shows that the main structural trend in the study area is nearly oriented N-S to NW-SE. But the reliability of this information is little.

Thus, despite the natural risk of introducing some bias in the dataset, for the outcrops-scale analysis was proceeded a manual tracing of lineaments* (i.e, faults and joints evident in the images). For statistics purposes these data presented a much better effect (figure 3.19). The **Base Fit Value** improved significantly, from more than 100 for all automatically detected lineaments to 1.24 for the manually traced lineaments. The relative amount of elements considered on the statistics also enhanced significantly: 92% from 1339 manually traced lineaments (1227 elements) was took into account.

This quality improvement is explained by the almost impossibility of the interpreter to take non-geological aligned features as true lineaments on such high resolution images. In this case the human interpretation capability allowed to produce a noise-free dataset, resulting in lineament domains much better fitted to the data distribution (figure 3.19).

Frequency Data, Gaussians
Total Data: 1339 max: 70 min: 0 mean: -36.663 sd: 3.740 mode: -50

RMS = 1.628861

GAUSSIAN PARAMETERS

#	%	Nor. H.	Max H.	Azimuth	sd
1	55.95	100.00	56.99	-48.83°	8.74°
2	24.79	31.21	17.79	38.06°	12.4°
3	10.89	20.00	11.40	-0.6054°	8.51°

Base Fit Value = 1.23998

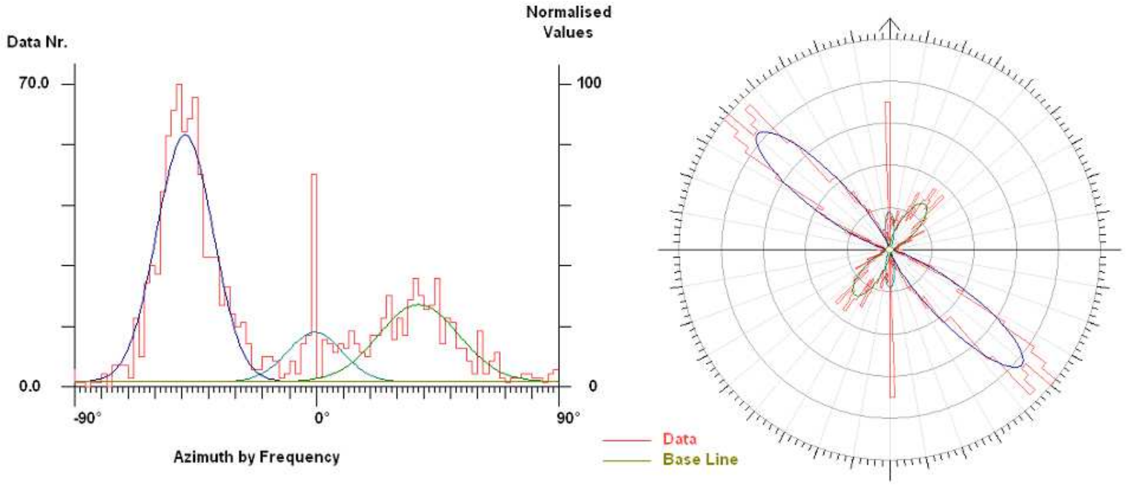

Figure 3. 19. Merging of the manually traced lineaments.

On top, there are the statistics parameters. On the histogram (bottom left) and on the rose diagram (bottom right) the red lines represent the data distribution. The colored curves and petals represent the gaussians correspondent to each domain.

* The geologist Claudia M. A. de Souza (UFRN) executed this tracing work, in order to avoid my own influence on the data set.

Even if the number of manually traced lineaments is few, in comparison with the automatically detected, the relative gain on number of elements taken into account for the statistics makes this dataset more reliable. The domains of lineaments' azimuths obtained from the frequency analysis are (Figure 3.19): N49^{o}W (56% of data); N38E (25% of data); N-S (11% of data).

6. Partial conclusions

It is interesting to notice that exists an important difference between the results obtained from the regional-scale lineaments analysis and the local-scale lineaments analysis. The main frequency domain for the regional-scale is oriented N65^{o}E, compatible with the Potiguar Basin structural framework as seen on Chapter2. However the main frequency domain for the local-scale is oriented N49^{o}W, that is nearly perpendicular (114^{o} divergent) to the regional domain.

This difference is indicative that the lineaments at the study area are probably controlled by local deformational events, related or not to the regional tectonic-structural history. To investigate the origin of such difference, it is necessary to combine the results achieved on this chapter with other information, like outcrops structural analysis, earthquakes focal mechanisms, and breakouts analysis. This investigation is presented through the next Chapter 4.

Summary

At the beginning of this chapter was presented an introduction to the concept of lineament, the possible applications for the lineaments analysis, and the main techniques of detection of these features.

Then we presented the results of the analysis of lineaments made to the Potiguar Basin and the study area of this thesis (regional and local scales) and how those results integrated with other geological information, contributed to the model proposed at the end of the study.

Chapter 4
Structural Analysis

1. Introduction

The goal of this chapter is to present the structural analysis results and the tectonic-structural model for the study area. The structural analysis was executed from outcrops data and from information about a cavern system named Furna Feia, all located at the study area (Figure 4.1). The tectonic-structural model was founded on the structural analysis results, four seismic lines available for the study area, and the information compiled on the previous chapter: earthquake focal mechanisms, fracturing testes and breakouts, and lineament analysis.

2. Outcrops structural analysis

The structural measurements were obtained from Jandaíra Formation outcrops localized close to the Baraúna village (Figure 4.1).

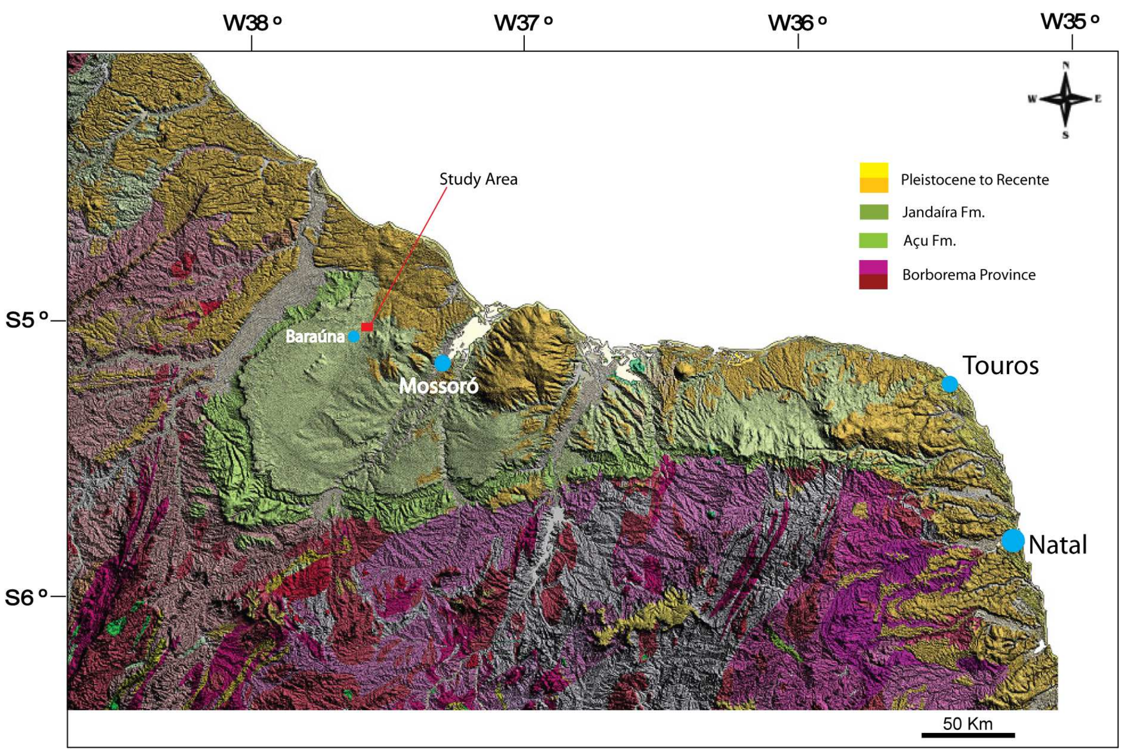

Figure 4. 1. Study area localization.

The image is composed by the SRTM3 regional data, draped by the geological map (scale 1:1.000.000; sheets Jaguaribe SB-24, and Natal SB-25). The blue circles indicate cities of reference (Natal is the capital of the Rio Grande do Norte State).

At this area occurs one of the most meaningful carbonate exposition in the whole Basin, which exhibits an impressive NW-SE and NE-SW fracturing pattern (Figure 4.2).

(Source: Google Earth Pro™)

Figure 4. 2. An overview of fracturing at the study area.

The blue-grey areas are continuous outcrops of the Jandaíra carbonates. The yellow ellipse indicates the Furna Feia entrance. The green objects correspond to vegetation. The brown areas correspond to Recent sediment deposits.

As said on the chapters 2 and 3, the Jandaíra Formation is marked by intense karstification. The karstic fabric makes difficult to distinguish on the terrain between tectonic faults and joints and other discontinuities associated to the karsting process. In addition, the existing tectonic fractures often concentrate preferentially the dissolution process, forming elongated sinkholes (Figure 4.3). These features are very common at the study area and possibly they are responsible by the absence of cinematic indicators on the faults plain, like slickensides and slickenfibers.

Figure 4. 3. Examples of sinkholes on Jandaíra Formation.

Alternatively to the missing cinematic indicators I used the geometric relationships between the measured fractures (Figure 4.4) according with the Ridel's model: (i) the longest and more penetrative fractures were taken as faults (Y fractures); (ii) the minor fractures, which make an angle nearly 30^{o} with the principal one, were taken as synthetic cleavages (R fractures). Fractures with no evidence of displacement and not related to others of minor or greater order, were classified as joints (i.e. tensile fractures).

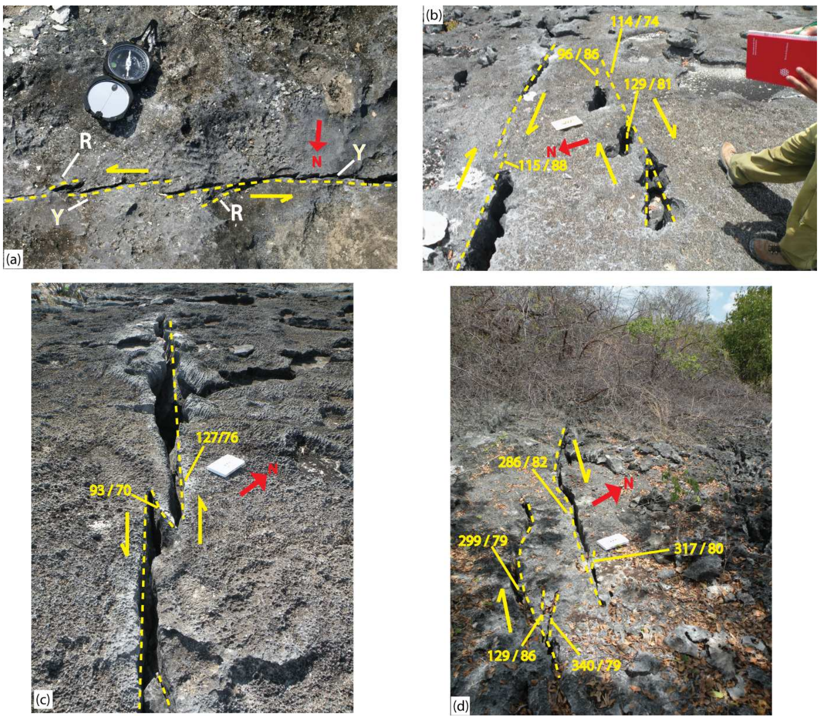

Figure 4. 4. Examples of cinematic indicators on Jandaíra's carbonates.

The notation of structural measurements (Strike/Dip) follows the right hand rule.

Notice that all the given examples indicate only strike-slip movements. Actually none normal or reverse components were identified on the faults cutting the studied outcrops. If this type of movement has occurred, the erosion and the karsting processes very likely erased all the possible indicators.

2.1. Measurements analysis

Despite the mentioned difficulties to field work, 32 outcrops were studied (Figure 4.5) and 145 structural measurements were obtained.

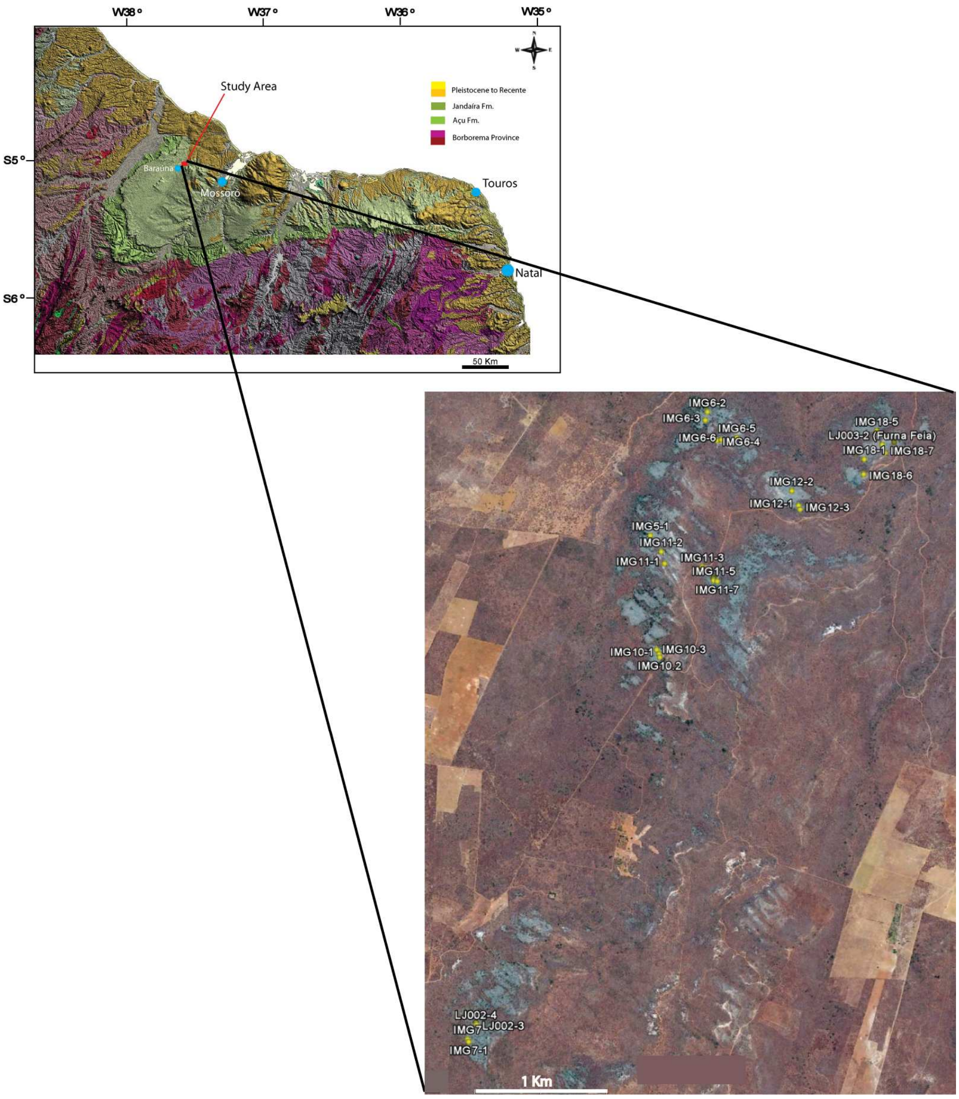

Figure 4. 5. Distribution of the analyzed outcrops.

The yellow dots represent the outcrops from where the structural measurements were obtained. The labels identify the outcrops according to the division established for the lineament analysis (Figure 3.10). For example, the label IMG06-02 indicates the second outcrop studied at the Area 6.

The simple observation of the satellite image (Figure 4.5) shows the topography in the study area is gentle. This perception is supported by measurements of bedding dip, obtained from a few outcrops in road-cuts. Such measurements show that the layers are nearly horizontal (Figure 4.6).

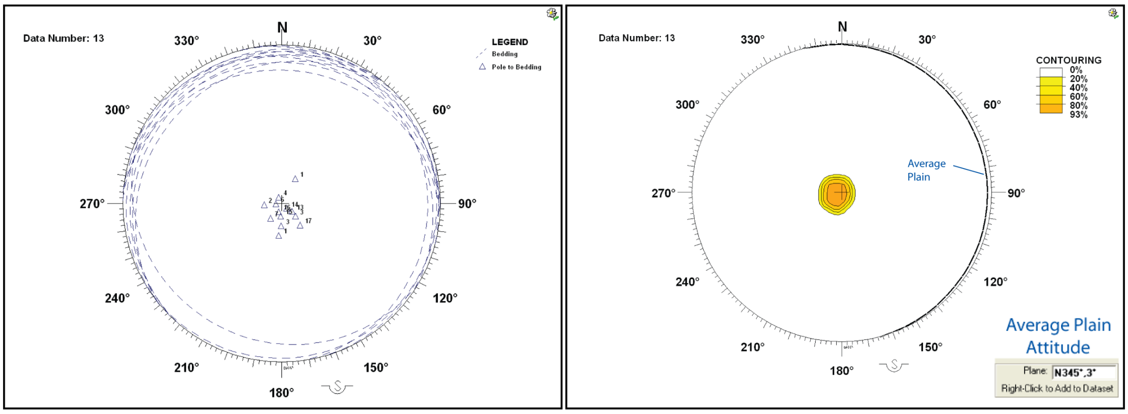

Figure 4. 6. Bedding stereographic diagram and poles contouring.

Both graphics refer to the Schmidt-Lambert Diagram, low hemisphere projection. The average plain represents an intermediate bedding attitude, referred to the center of the bedding poles contouring. The attitude annotation (345^{o}/3^{o}) follows the right hand rule.

The Figures 4.7 to 4.9 show the stereographic projections and the azimuth by frequency analysis performed from measurements of the structural elements identified through the study area (faults; synthetic cleavages; joints).

The faults and theirs respective synthetic cleavages fed into the software Daisy (©Prof. F. Salvini) offered the information necessary to estimate the principal faulting regime (Figure 4.7). Based on the relationship between these fractures the software calculated: (i) artificial slickenlines attitudes, that could have occurred on each fault plain; (ii) the rotax element, which represents the theoretical rotation around the axis described by the intersection between a given fault plain and its respective synthetic cleavage (Wise and Vincent, 1965; Salvini and Vittori, 1982).

For the study area the measured geometric indicators and the calculated cinematic indicators point to a dominant strike-slip faulting regime (Figure 4.7a and b). Despite the reduced dataset, it is noticeable how the faults' azimuths are strongly oriented NW-SE (main direction) and NE-SW (Figures 4.7 and 4.9). Apparently a preferential sense of movement (right-lateral or left-lateral) does not exist relating to the faults orientation. But this hypothesis is not conclusive once the available number of measured faults and related elements is few.

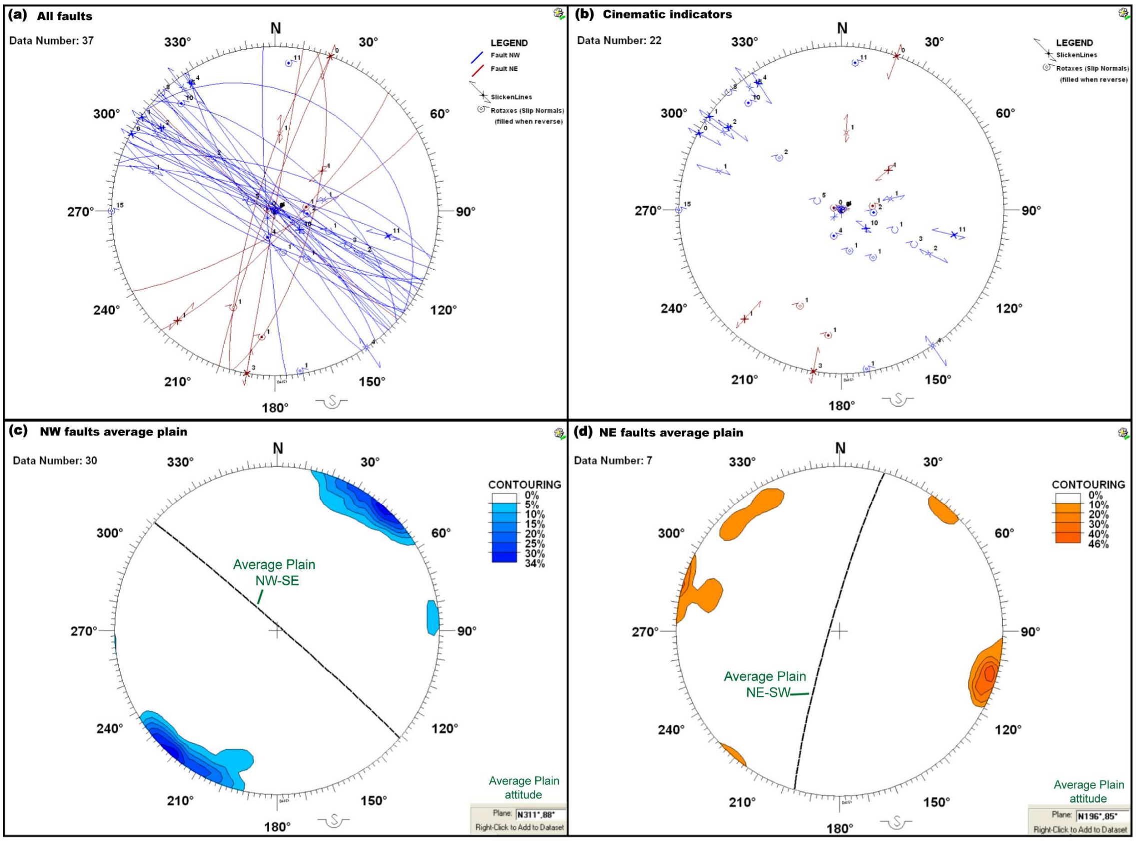

Figure 4. 7. Faults stereographic diagram and poles contouring.

The graphics refer to the Schmidt-Lambert Diagram, low hemisphere projection. Data Number is the number of elements represented on each diagram. On (b) the arrow’s tip of booth slickenlines and rotaxes symbols indicate the sense of movement (right-lateral or left-lateral). On diagrams (c) and (d) the average plains represent intermediate attitudes of the faults, referred to the center of the bedding poles contouring, and the attitude annotation in the small grey windows follow the right hand rule.

The great number of joint measurements makes their dataset (Figure 4.8) lightly more reliable. But it is possible that some of the elements classified as joints actually are faults, which movement indicators have been obliterated by the dissolution process. Although the genesis of joints is not certain, the predominance of the NW-SE direction over the NE-SW direction is still evident (Figures 4.8 and 4.9).

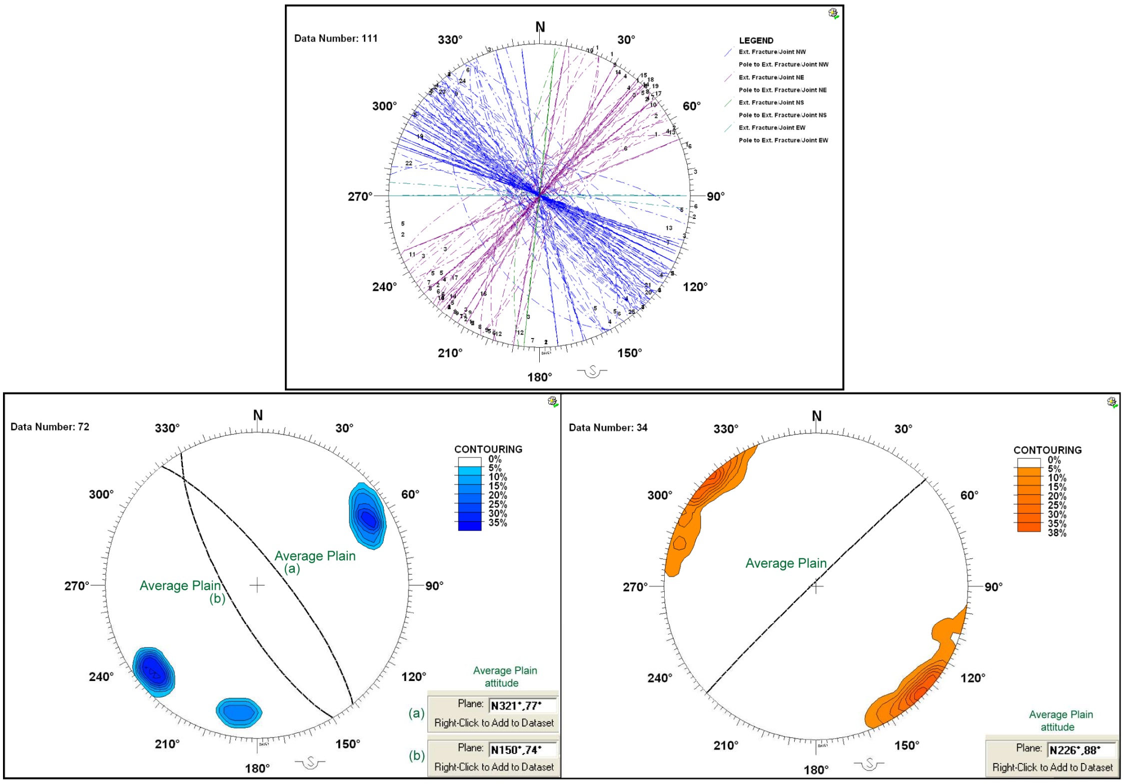

Figure 4. 8. Joints stereographic projection and poles contouring.

The Figure 4.9 compares the azimuth by frequency distribution of faults, synthetic cleavages, and joints. This comparison makes clear how the NW-SE trend is dominant over the NE-SW trend, irrespective of the type of structural element in the database. Few trends N-S and E-W appear in the diagrams. However these directions do not have enough elements, and therefore become statistically irrelevant.

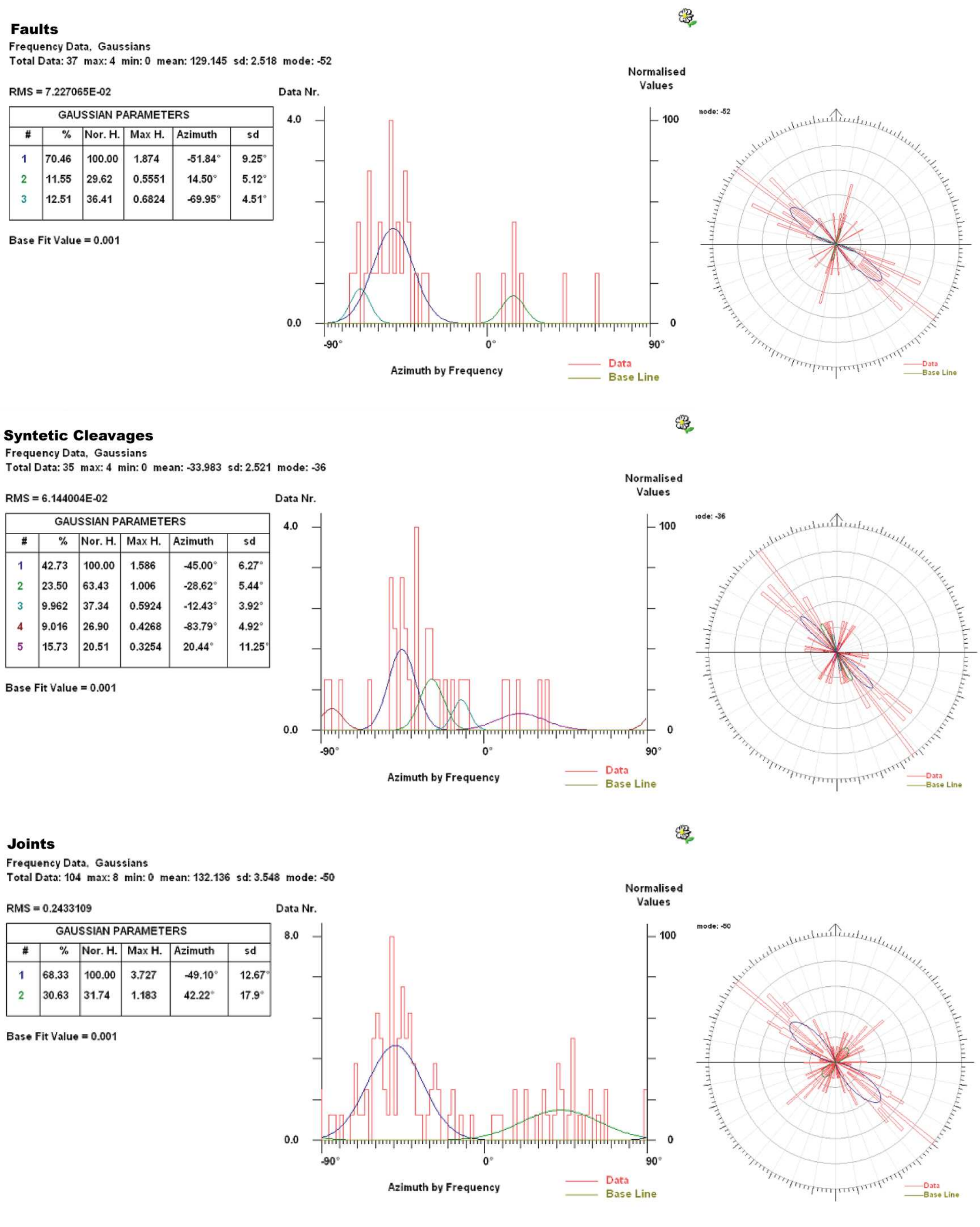

Figure 4. 9. Azimuths frequency of the more common structural elements.

The statistic parameters definition are: **max**, is the maximum frequency comprising all data; **min**, is the minimum frequency comprising all data; **mean**, is the average azimuth comprising all data; **sd**, is the mean azimuth stander deviation; mode, is the most frequent azimuth in the dataset; **RMS** (Root Mean Square), is a statistical measure of magnitude of a varying quantity, that in this case defines the number of gaussians that better fit the data distribution; **%**, the percentage of lineaments included in each domain; **Nor.H.** (Normalization High), is the maximum frequency value used to normalize the dataset, bringing them to a common scale; **Max H.** (Maximum High) defines the gaussian maximum length related to the **Nor.H.; Azimuth**, the mean orientation referred to the North calculated to each lineament domain; **Base Fit Value**, the cutoff value accepted as a reference to eliminate data that presents a high level of scattering. The red lines represent the data distribution and the colored petals are equivalent to the gaussians correspondent to each domain.

On the chapters 2 and 3 it was noticed that the Potiguar Basin’s framework architecture is strongly controlled by Paleproterozoic structures oriented NE-SW. Structures oriented NW-SE, E-W and N-S are interpreted as transfer faults or accommodation zones associated to the rift opening process.

The regional-scale analysis of lineaments, presented in Chapter 3, had highlighted that the NE-SW direction is deeply marked on topography (Figure 3.15) and remains the most important trend in the Basin (Figure 3.16).

On the other hand, at the study area the NW-SE structural elements are much more frequent and penetrative than the NE-SW. This is evident from both the analysis of structural measurements (Figure 4.9) and the analysis of lineaments on the outcrop-scale (Figure 3.19). All these evidences show that an inversion of the relative importance between these two directions exists, which points out that a more local scale tectonic-structural history occurred at the study area.

2.2. Stresses Direction in the study area

Two inversion methods, available in the program Daisy, were used to predict the direction of stresses responsible for the creation or reactivation of faults and joints in the study area.

The first method is the “inversion by rotax analysis”. The algorithm uses the available faults measurements and rotaxes information to assess the most probable stress tensor which generated a given faults population. According to this method the best stress tensor must comprise the greatest number of possibly compatible/conjugated faults, with parallel rotaxes.

The “inversion by rotax analysis” method was applied to all faults stored in the study area dataset. The best stress tensor obtained is compatible with a strike-slip faulting regime, with a maximum compression (S1) oriented NW-SE (Figure 4.10). This result is not unexpected since all measured faults present strike-slip indicators and most of them are oriented NW-SE.

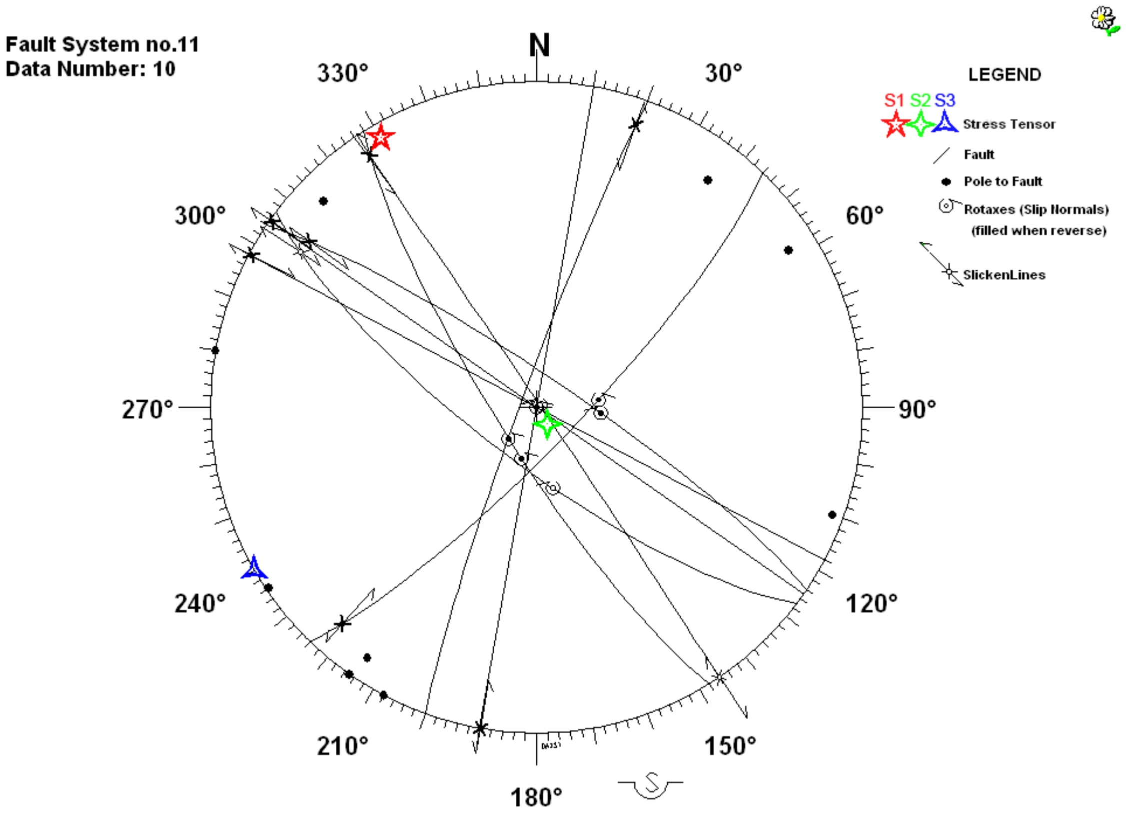

Figure 4. 10. Stress tensor according to the method inversion by rotax analysis.

The labels S1, S2 and S3 correspond to the stress components σ_1, σ_2 and σ_3, respectively. Therefore the relative magnitudes are S1 > S2 > S3.

The second method is the "Direct Inversion", which algorithm applies a convergent Montecarlo test[Appendix, 4.1] to estimate the most probable stress tensor. For a given population of faults this algorithm randomly generates tens of thousand of tensors, and for each tensor it computes the mean angular difference between the measured slip vector and the theoretical slip produced by that given stress vector. To increase the solution reliability the routine must to be run several times (for this study it was runned 10 times). Each time the software stores the new solution in the data set, to be plotted or contoured later.

Another factor that becomes the "Direct Inversion" trustful is that, in addition to the faults information, the algorithm takes into account information from other structural elements (e.g. bedding; joints; cleavages) included in the dataset. The computed stress tensor must be able to explain as much as possible the whole observed deformation.

The application of the "Direct Inversion" method on the study area dataset constrained a stress tensor compatible with a reverse faulting regime (Figure 4.11). The maximum compression component of this tensor (S1) is oriented too NW-SE.

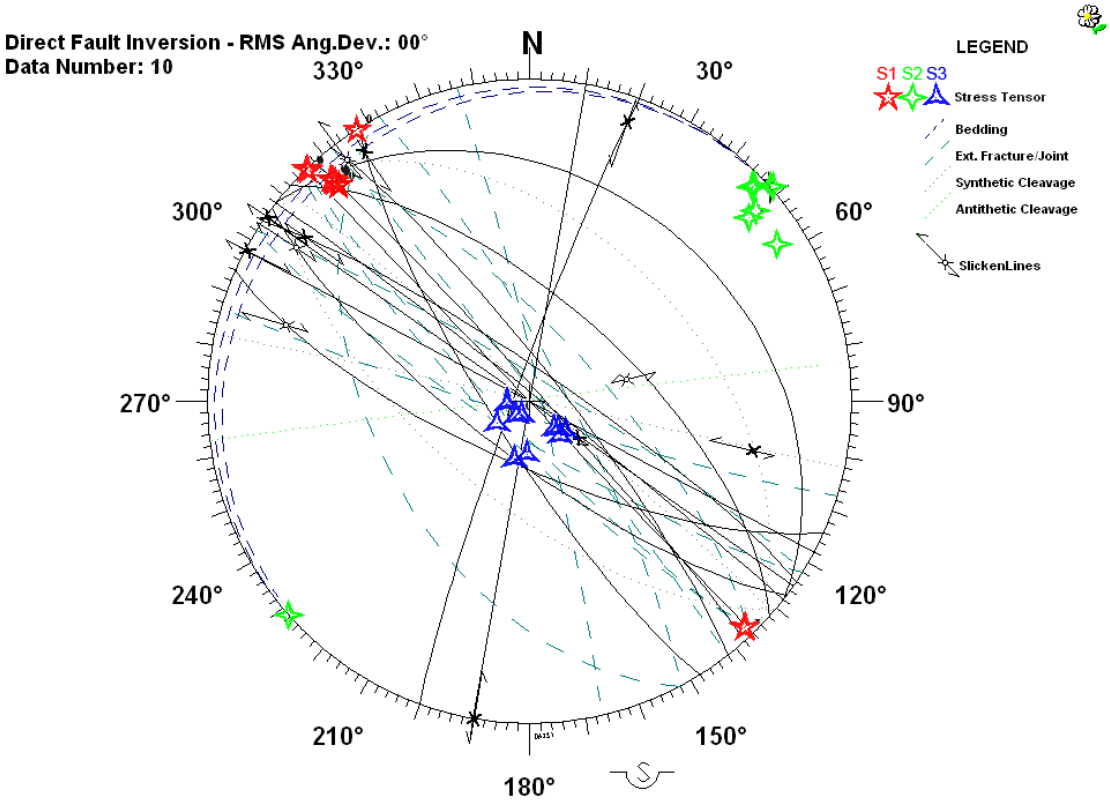

Figure 4. 11. Stress tensor according to the Direct Inversion method.

Despite both results offer stress tensors with the maximum component horizontal and oriented NW-SE, the state of stresses fixed for each method are different. Which of them is the best solution for the deformation pattern observed through the study area? I assumed that the result given by the "Direct Inversion" method (Figure 4.11) is the most reliable. Such assumption is founded in two reasons:

(i) The Motecarlo test used in the "Direct Inversion" algorithm allows comparing instantaneously several stress tensor solutions. All tensors computed for the study area dataset were constrained around a single attitude, describing a mean stress tensor that can be taken as highly accurate.

(ii) The method "inversion by rotax analysis" considers only the fault information to calculate the stress tensor, while the method "Direct Inversion" takes into account other elements. Because of this the "Direct Inversion" solution is able to explain not only the faults but the complete deformation pattern that occurred in the area.

3. The Furna Feia cavern system

On the Jandaíra Formation limestones outcropping at the study area a cavern system named Furna Feia was developed (Figure 4.12). According to Diego de Medeiros Bento (IBAMA/CECAV regional coordinator, written communication) the Furna Feia is the second biggest cavern system at Rio Grande do Norte State, totalizing approximately 739 m of linear development and achieving 30 m of depth (Figure 4.13).

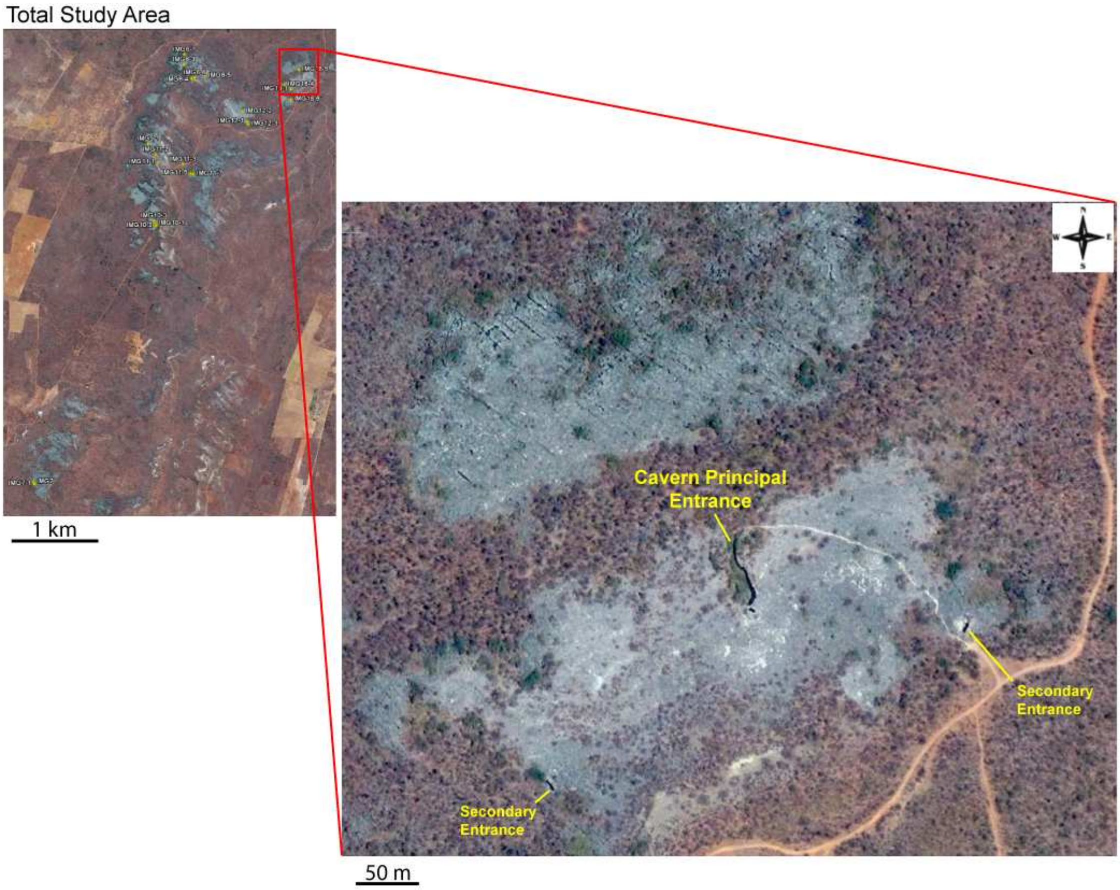

Figure 4. 12. Localization of the Furna Feia cavern.

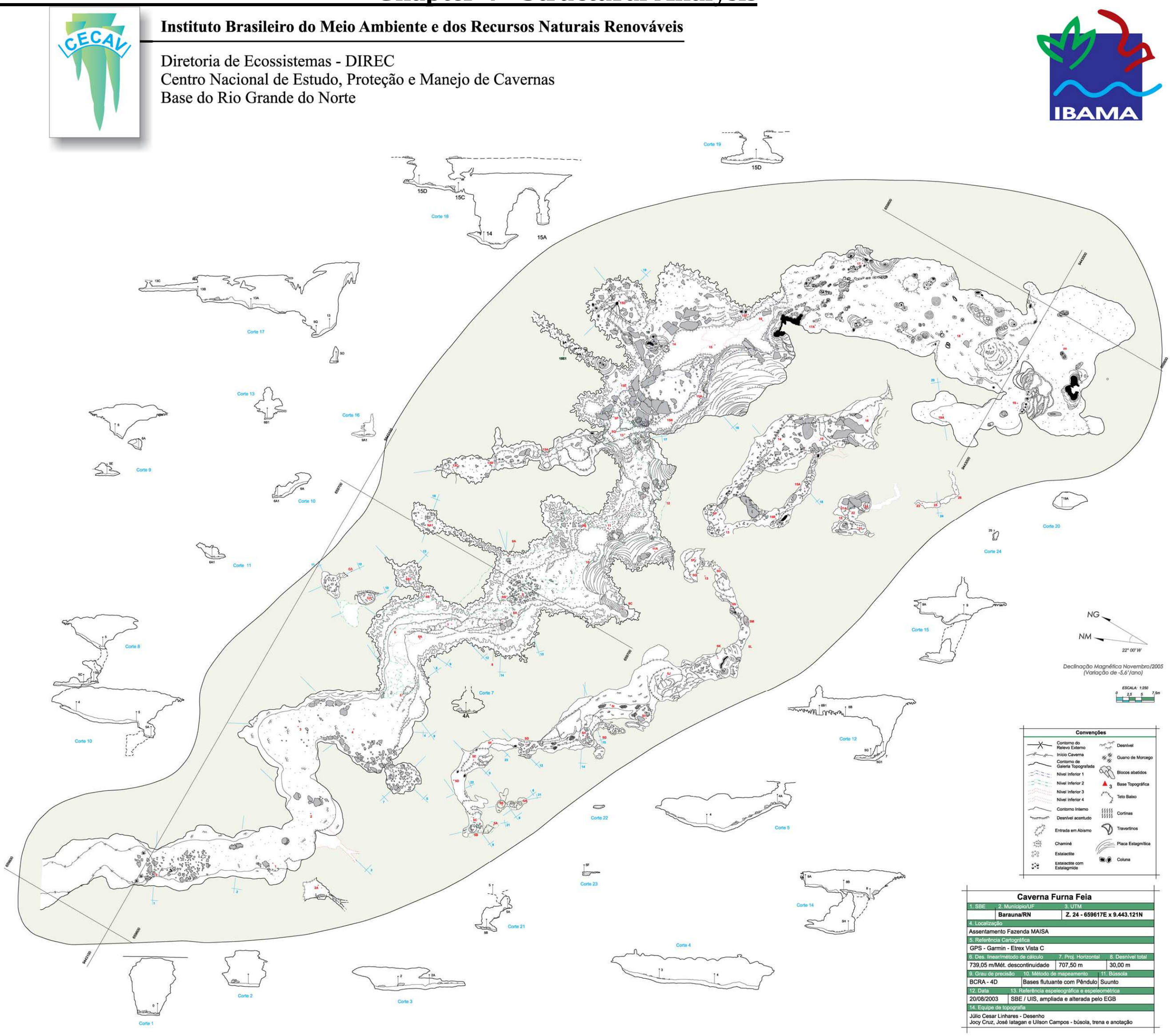

(This map was kindly provided by the IBAMA/CECAV - Rio Grande do Norte)

Figure 4. 13. The Furna Feia map.

This topic intends to verify if there is any coincidence between the structural trends at the study area and the cavern's galleries. If such coincidence exists it is an evidence that the brittle deformation process actually has an important role on the cavern development.

To achieve this objective, the azimuths of the Furna Feia galleries were measured from the map of the cavern (Figure 4.14), using a common drawing software and the algorithm LinDig (©F. Salvini). The LinDig output files provided the axis information necessary to feed Daisy (i.e. azimuth; length) to perform the statistical analysis.

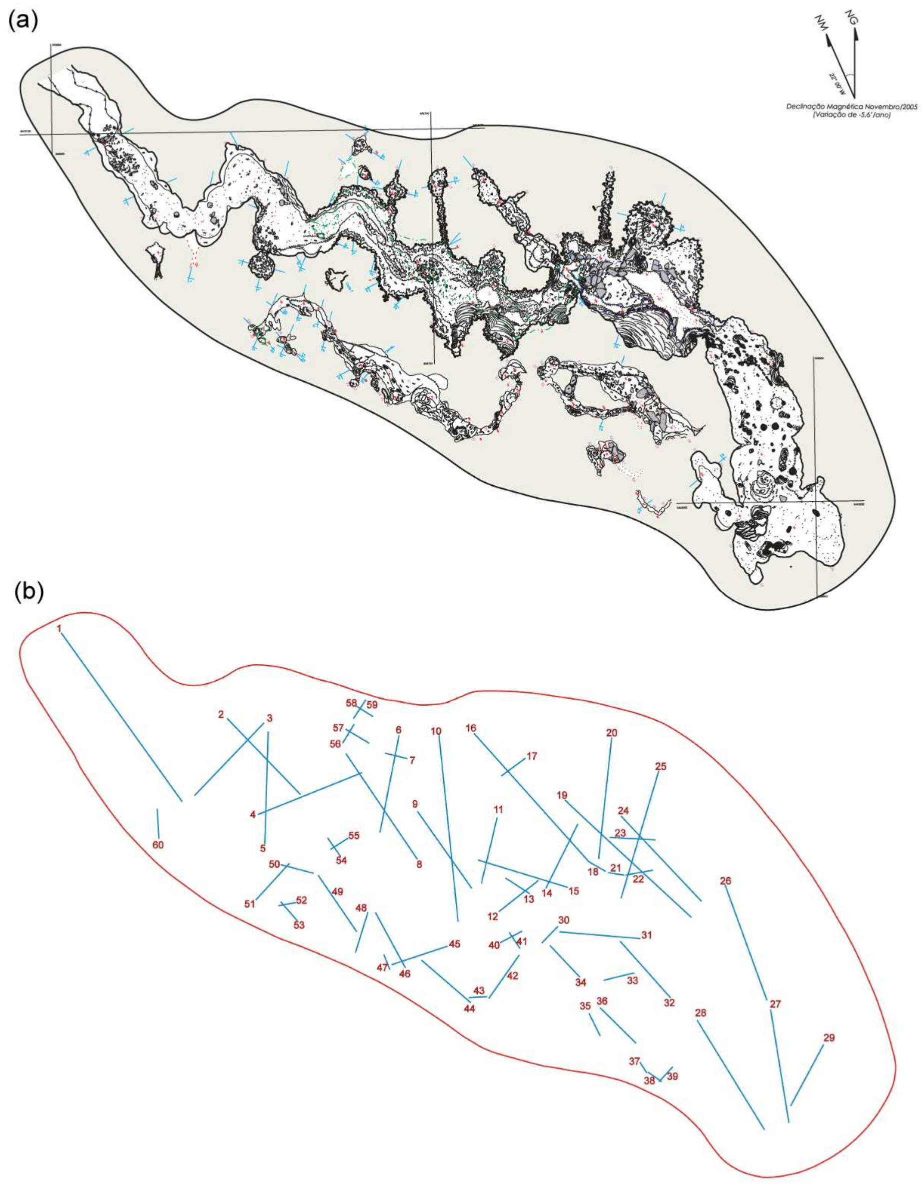

Figure 4. 14. Mean axis of the Furna Feia Galleries.

(a) The simplified cavern map. (b) The mean axis map; after digitalized using the LinDig algorithm.

It is interesting to notice the angular network pattern of the galleries axis (Figure 4.14b). Easterbrook (1999) interprets such type of geometry on carbonate caverns as a result from the intersecting fractures widened by chemical erosion.

Similarly to the outcrops and local-scale lineaments, the azimuth by frequency analysis for the Furna Feia galleries (Figure 4.15d) exhibits an important NW-SE trend (38% of axis). The second most important trend for the cavern system is the direction E-W (27% of axis), while the direction NE-SW exhibits a close frequency (21% of axis). Even if the trend N-S is the less frequent, it is well represented with 16% of the axis.

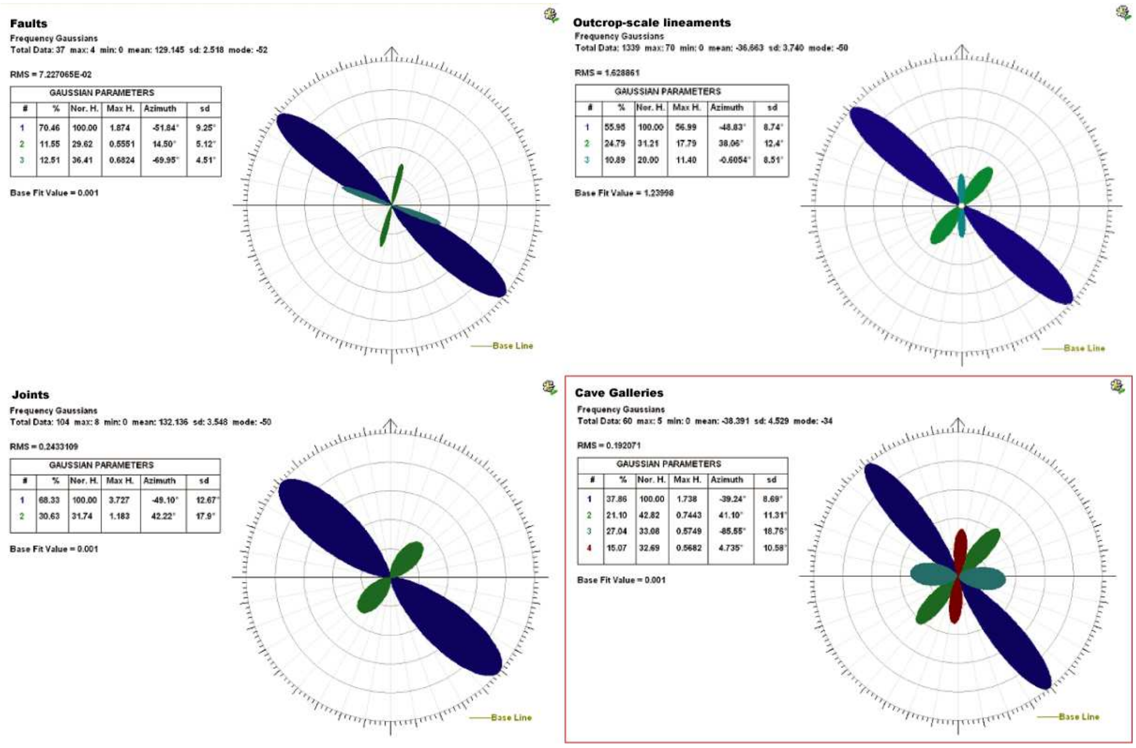

Figure 4. 15. Trends coincidence analysis.

The comparison between the azimuth by frequency diagrams of the structural elements observed on the terrain and the galleries axis (Figure 4.15) identified that the Furna Feia cavern system has an evident coincidence with the tectonic faults and joints trends.

4. Seismic line data

Four seismic lines available for the study area were authorized to be used on this thesis (Figure 4.16). However the quality of imagery obtained from these lines is very poor, due to the presence of the Jandaíra carbonates close to the ground surface (Figure 4.17). Carbonates bodies have a high seismic velocity and frequently present strong fracturing. These factors cause reverberation of the acoustic wave through the different interfaces, altering the velocity and the propagation angle of the seismic signal from the layers below carbonates. This phenomenon creates a significant amount of noise on seismic image which are very difficult to treat.

Despite the low quality of images, it was possible to identify the top of key-horizons at the onshore portion of Potiguar Basin (basement, Alagamar Formation, Assu Formation, and Jandaíra Formation) and some faults (Figure 4.17). It is important to notice that very few identifiable normal faults intersect the Jandaíra Formation.

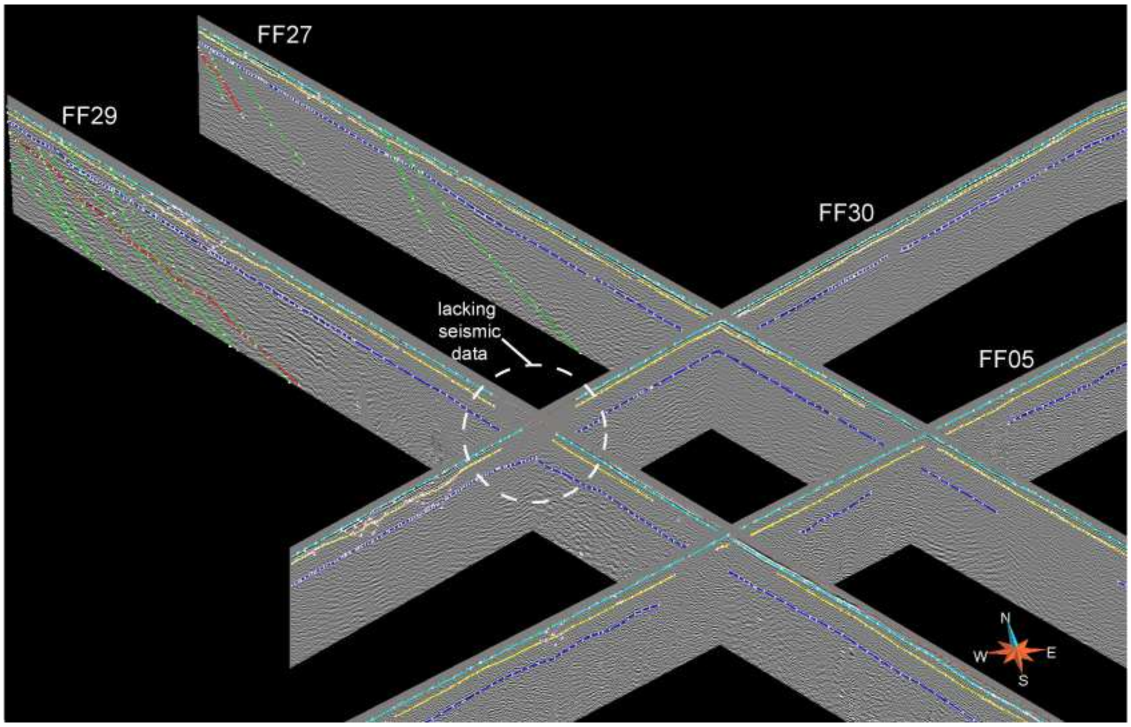

Figure 4. 16. Four seismic lines available for the study area.

The void observed on these seismic lines probably are due to: any obstacle on the ground, that has not allowed the acquisition team to pass through; some out of order receptors; low-quality data eliminated during the processing.

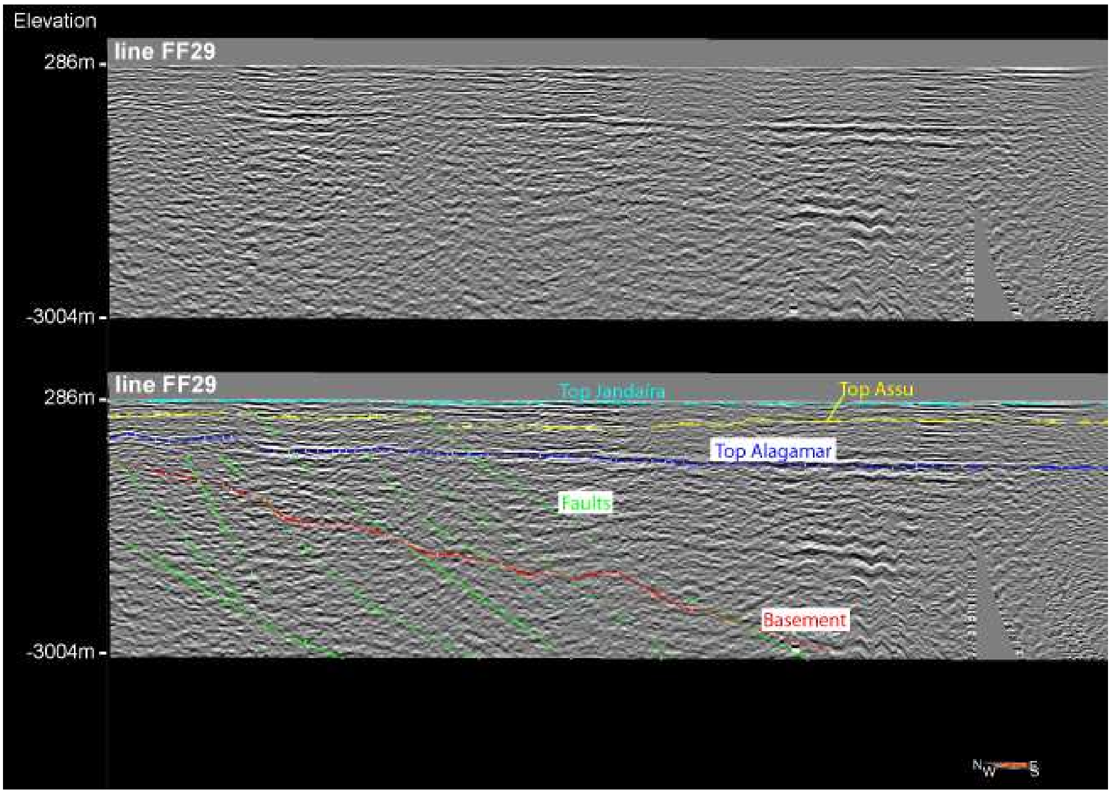

Figure 4. 17. Elements identified on the seismic lines.

On the line FF30 some small areas where the seismic sign is lightly altered were individualized. Those areas were interpreted as possible caverns existing at that position (Figures 4.18).

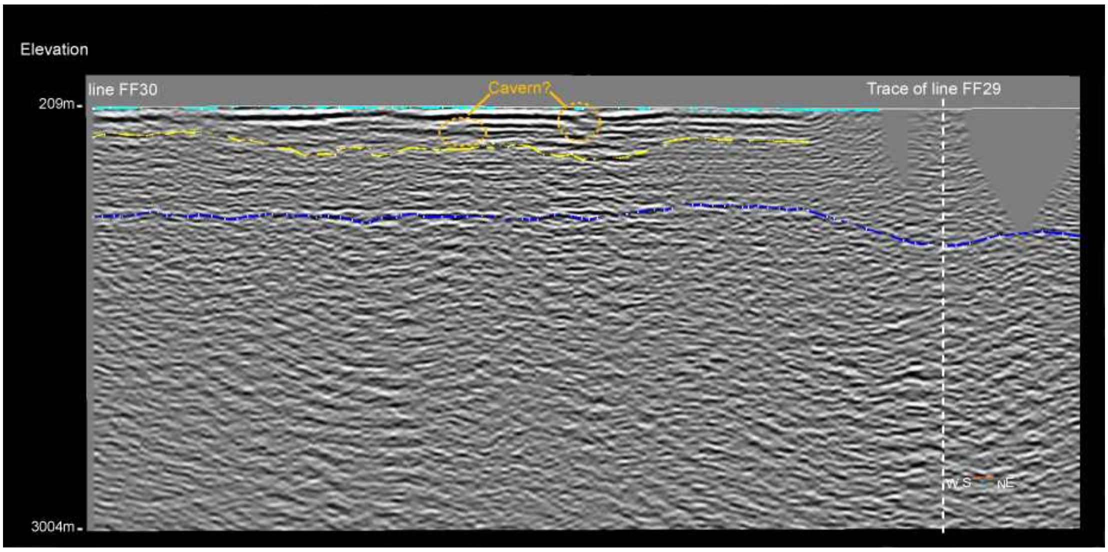

Figure 4. 18. Possible caverns observed on the seismic data.

The intense fracturing observed on Jandaíra Formation, at the area where the supposed caverns are identified, exhibits a shape mostly compatible with a strike-slip shear zone than normal faulting.
Notice that the basement, if present, can not be recognized in this image.

At the beginning of this thesis the idea was to restore[Appendix, 4.2] these seismic lines in order to identify regions of greater deformation, which were supposed to be the more permeable zones and most favorable places for caverns development. But on account of the low-quality of seismic images and all evidences that the fault regime controlling the caverns development is strike-slip, this task was abandoned.

Anyway the seismic lines offered a general view about the state of deformation on the deepest portion of the Jandaíra carbonates, contributing to the tectonic-structural model proposed for the study area.

5. Tectonic-structural Model

According to the tectonic models presented on Chapter 2, the Potiguar Rift was created under an extensional regime generally oriented toward NW-SE to E-W. During the rift opening some NE-SW Paleoproterozoic weak zones were reactivated as normal faults, while NW-SE and E-W trends become potential sites for transfer faults and accommodation zones.

Evidences about the nowadays state of stresses on the Potiguar Basin are also presented on Chapter 2. The available information from focal mechanisms, breakouts analysis, and borehole tests analysis reveal that the Basin is nowadays submitted to a maximum horizontal compression mostly oriented NW-SE (Figure 2.8). Such compressional state of stress is compatible with reverse and strike-slip faulting regimes. In this context the NE-SW faults are properly oriented to be reactivated as inverted faults, while the NW-SE, E-W and N-S faults are properly oriented to be reactivated as strike-slip faults.

Considering these regional tectonic-structural scenarios - during the rifting and today -, it seems reasonable to imagine that during the Potiguar Basin history the main NE-SW faults had their normal or inverted movements compensated by minor NW-SE, E-W and N-S structures.

Concerning the study area, three fundamental circumstances must be noticed:

(i) The relative importance between the NE-SW trend and the NW-SE trend is inverted with respect to the Basin regional architecture, suggesting the existence of a more local-scale deformational history.
(ii) The best stress tensor for the study area (Figure 4.11), computed by the "Direct Inversion" algorithm, is in conformity with the present day regional state of stress given by the seismology and the breakouts analysis.
(iii) Exits a very good coincidence among the local structural trends and the distribution of the Furna Feia axis azimuth (Figure 4.15). This strongly suggests that the cavern results from the preferential high permeability carry zones, formed by faults and joints, controlling the meteoric water circulation.

On the basis of all these information I formulated the following local-scale tectonic-structural model (Figure 4.19):
(i) There is a major not outcropping NE-SW normal fault, somewhere toward NW from the study area;
(ii) Given the estimated nowadays stresses condition, the hypothetical NE-SW normal fault was reactivated as an inverted fault;
(iii) This inversion movement caused the exhumation of the Jandaíra Formation, on the returning hanging wall of the main NE-SW fault;
(iv) The minor NW-SE strike-slip faults result from the accommodation movements due to the major NE-SW fault activity;
(v) The minor NE-SW strike-slip faults constitute conjugated pairs with the NW-SE strike-slip faults, or are related to oblique movements of the main NE-SW fault.
(vi) The fracturing associated to this brittle deformation history was responsible by the creation of oriented high permeability corridors. These corridors control the meteoric water circulation through the Jandaíra limestone rocks, conducting the dissolution process and the formation of the Furna Feia caverns system.

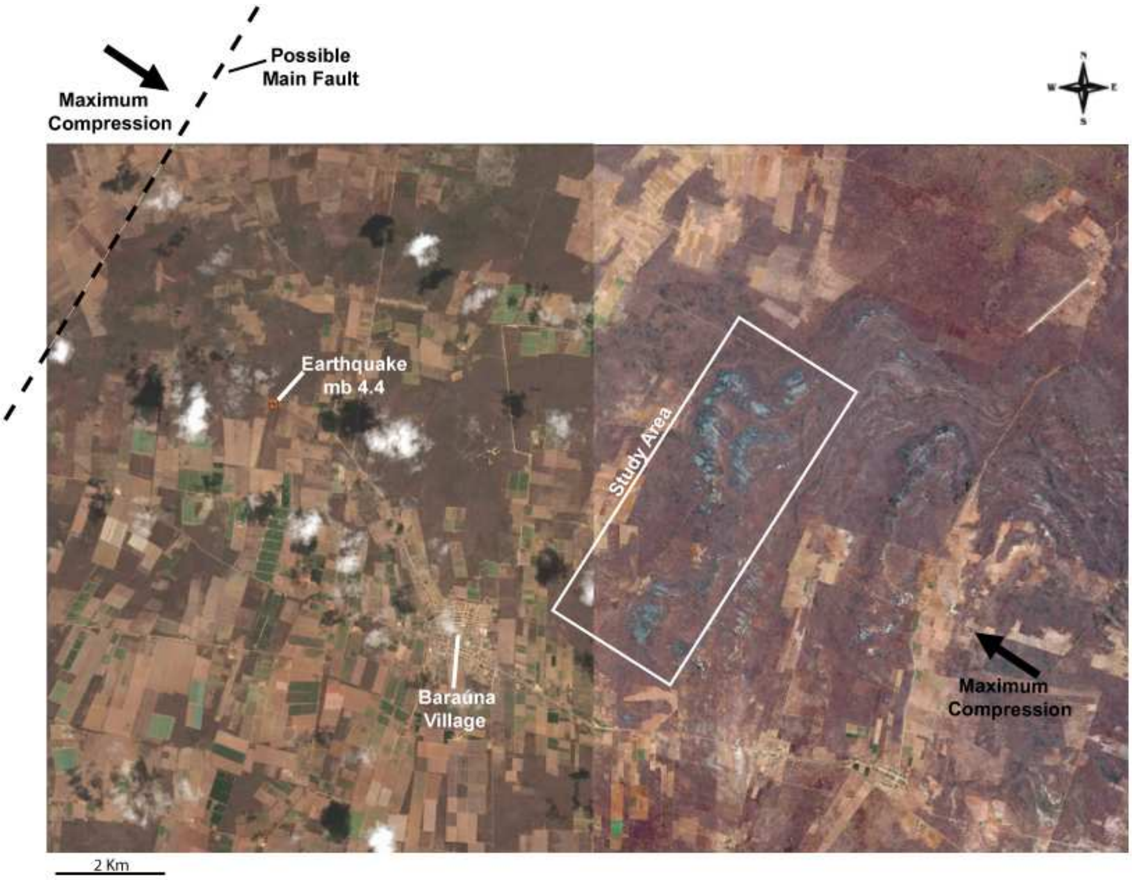

Figure 4. 19. Tectonic-structural model for the study area.

The main fault position was estimated from the 3D visualization tool available on the Google Earth application – it is traced where the 3D visualization (3x vertical exaggeration) indicates a long rupture on the topography. The earthquake information was obtained from the USGS database, but its focal mechanism was not available. This earthquake indicates that possibly the main fault had some recent activity.

This tectonic-structural model was used to guide the numerical models presented on the next Chapter 5.

Chapter 5

Numerical Modeling

1. Introduction

The importance of understanding the mechanical evolution of geological structures responsible for the basins framework and their reservoirs, justifies the necessity to perform more elaborate mechanical studies. The development of technologies for the analysis of deformation and stresses in sedimentary basins has brought significant benefits for the improvement of structural interpretation applied to the hydrocarbons exploration and production. The best mechanical knowledge about geological structures and associated fields of stress and strain provides a better geological interpretation of study areas, reducing the risk of investments.

The numerical modeling presented on this chapter intends to examine the reasonability of the theory proposed on Chapter 4, for the possible permeability increasing on the Jandaíra carbonates in consequence of the observed brittle deformation. To accomplish this task the software TECTOS was used, which has been developed in partnership between the Petrobras Researcher Center (CENPES) and the Catholic University of Rio de Janeiro (PUC-Rio). TECTOS is an integrated system of mechanical analysis by finite element method[Appedix, 5.1] for 2D simulation of processes in structural geology and tectonics.

2. Preparing the numerical modeling

The first step to prepare the numerical model was to select a comprehensive area around the Furna Feia cavern. Then, the most representative fractures at that area were mapped (Figure 5.1).

It must be noticed that at the zone adjacent to the Furna Feia cavern the number of identifiable fractures is reduced. However, even if the traces of these fractures at the surface are too discreet to allow them to be imaged, field evidences clearly sign their presence.

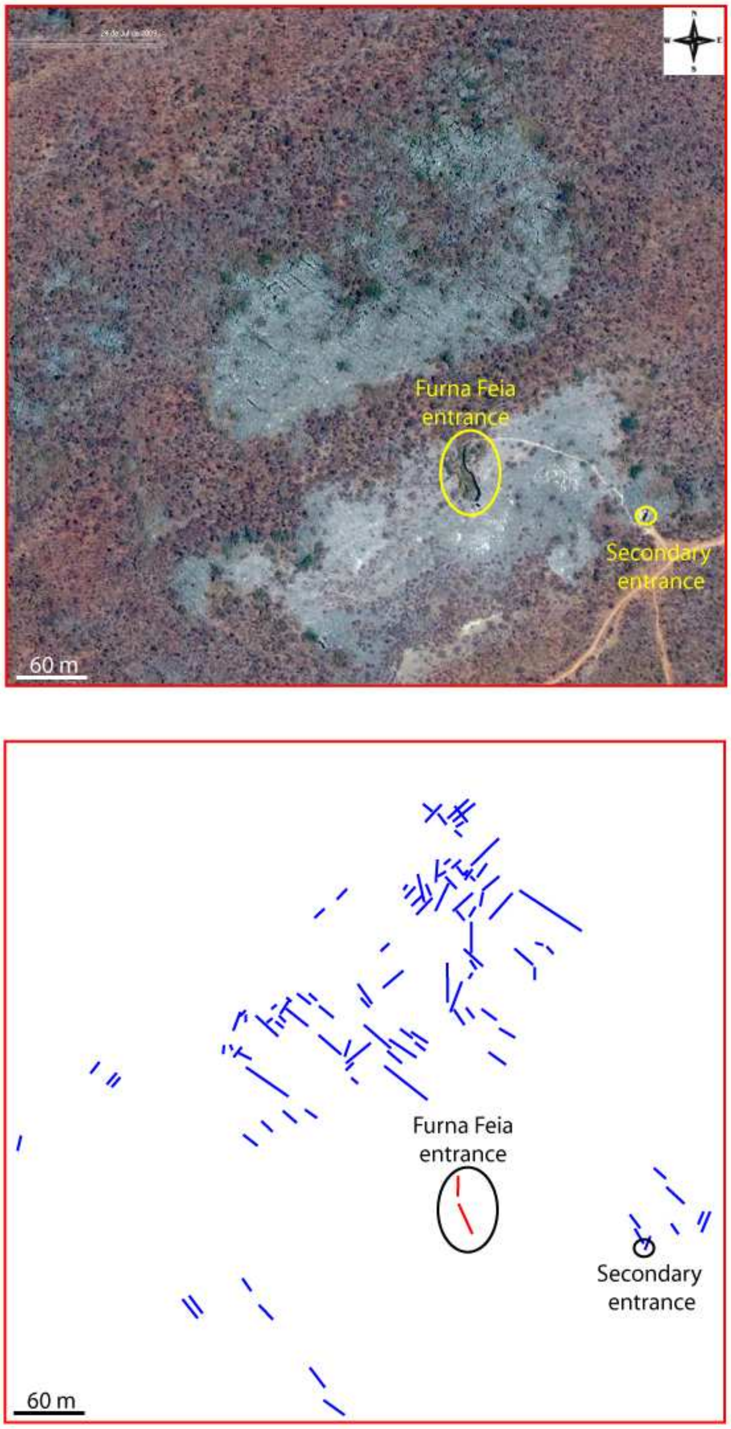

Figure 5. 1. Base for the numerical modeling.

All the line segments are fractures identified on the satellite image. The two red line segments sign two galleries axis of the Furna Feia cavern, visible on the satellite image because the cavern's ceiling at its entrance collapsed some years ago. These two axis were equally into account too for the models' mesh.

The mapped fracturing network was used to orient the building of the model's mesh (Figure 5.2). The model was built by using a non-structural linear triangular mesh. It has a non-associated elastoplastic rheology and discontinuities are represented by contact elements. The mesh accounts with 9246 nodes and 18170 linear elements.

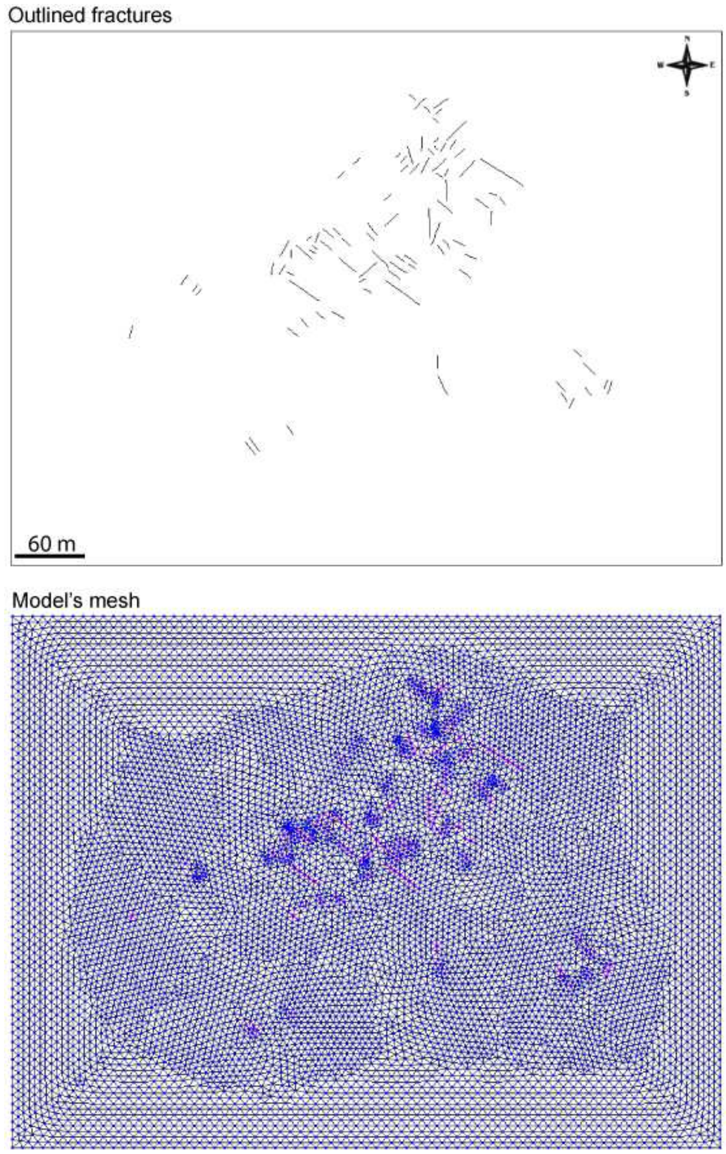

Figure 5. 2. Basic mesh for the model.

3. Setting up scenarios

For this model nine scenarios where run: three compressive (Mod1c; Mod2c; Mod3c), three right-lateral shear (Mod1s; Mod2s; Mod3s), and three left-lateral shear (Mod1ss; Mod2ss; Mod3ss). What differentiate these scenarios are the confining conditions 1, 2, and 3 (Figure 5.3) that allow model's borders movement or not according to the applied stress. Because the scenarios Mod2s and Mod2ss were stuck in all sides in horizontal X and Y axis, they did not support shear in the prescribed form.

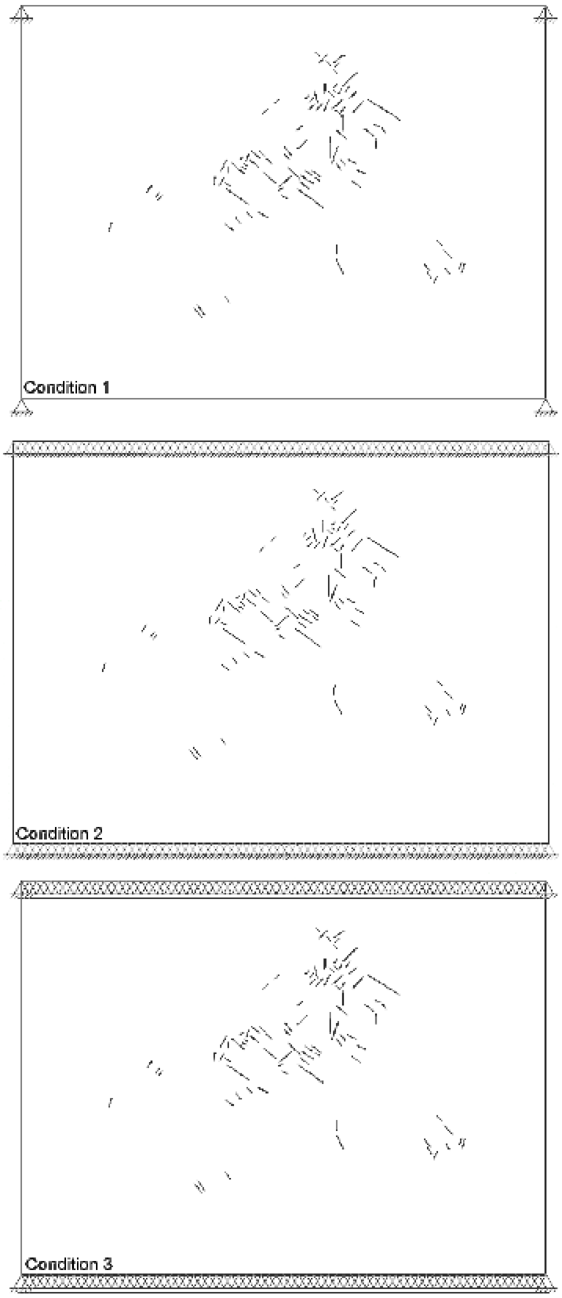

Figure 5. 3. Support conditions of the model's borders.

For all scenarios was prescribed an effective stress equal to 5 MPa, progressively implemented in ten steps of 0.5 MPa (i.e. step1 equal to 0.5 MPa, step10 equal to 5 MPa). This maximum of 5 MPa, corresponds to the minimum value from which all the models indicate imminent rupture or reactivation of almost all preexisting fractures. Also were prescribed the following mechanical properties: Young's modulus equal to 25 GPa; Poisson's ratio equal to 0.15; Cohesion equal to 5 MPa; Internal friction angle equal to 30^{o}; Dilatancy angle equal to 12.

4. Modeling results

In general the results from all the possible scenarios are not very much different. The scenarios Mod3s (Figure 5.4) and Mod3ss (Figure 5.5) better represented the proposed theory for the creation of Furna Feia cavern. Each image on figures 5.4 and 5.5 corresponds to a step that presented some significant transition on the calculated deformation distribution. The RFS values distribution shown on theses images represent how close the rock is to touch the Morh-Coulomb Envelopment (Figure 5.6). The RFS values equal or close to 1 (red zones) point out areas where associated fractures and greater dilation zones might occur.

It is intuitive that at these high deformation zones the well-known phenomenon of dilatancy, associated to the progressive increase of cumulated stress, lead to the increase on porosity and, consequently, on permeability. In this way the percolation of fluids is concentrated along these fracturing zones, working to the formation of karst (Figure 5.7).

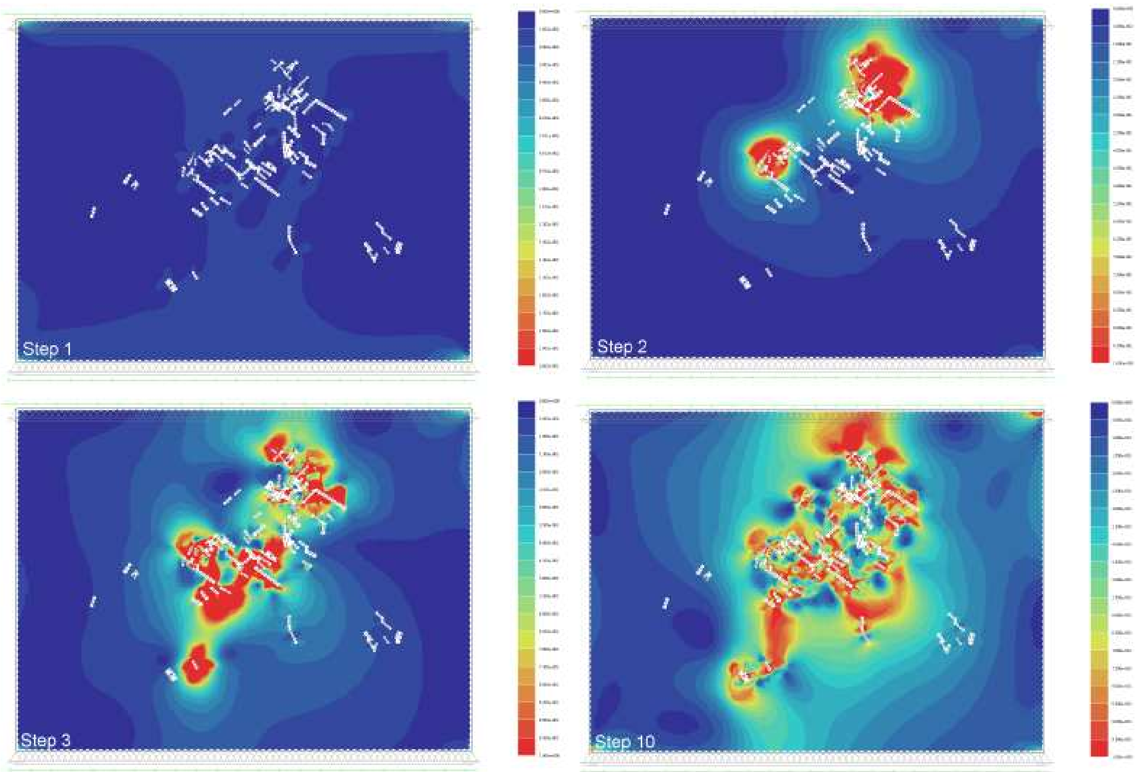

Figure 5. 4. Results RFS from the condition Mod3s right-lateral.

RFS is the shear rupture ration. As much red highest is the possibility of fracturing. Step1 = 0.5 MPa; Step 2 = 1 MPa; Step 3 = 1.5 MPa; Step 10 = 5 MPa.

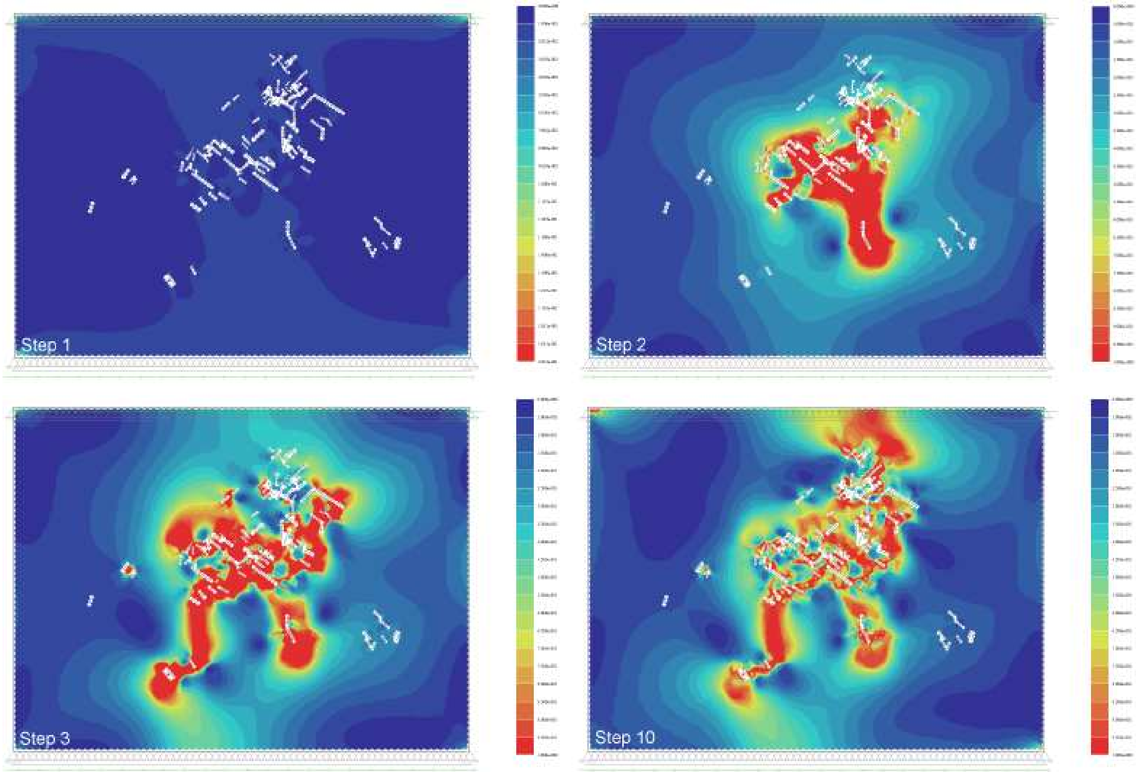

Figure 5. 5. Results RFS from the condition Mod3s left-lateral.

RFS is the shear rupture ratio. As much red highest is the possibility of fracturing. Step1 = 0.5 MPa; Step 2 = 1 MPa; Step 3 = 1.5 MPa; Step 10 = 5 MPa.

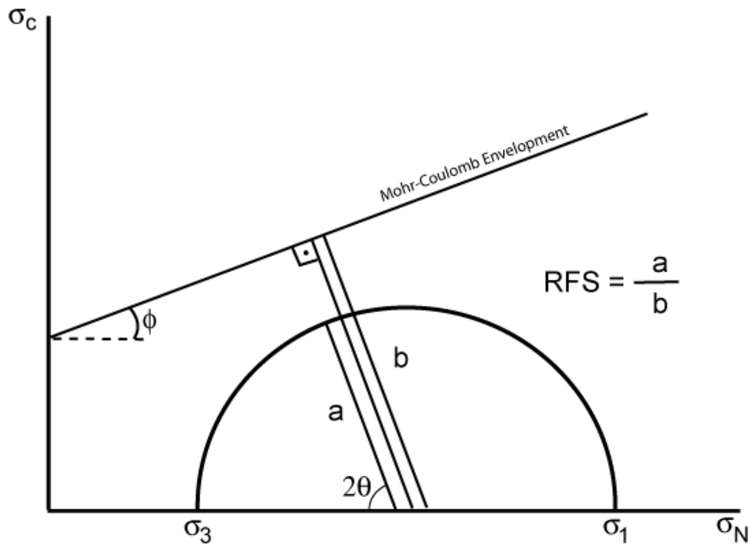

(From Moraes, 1995)

Figure 5. 6. Assessment of fracturing probability from RFS.

$\boldsymbol{\sigma_N}$ is the Norma Stress axis; $\boldsymbol{\sigma_c}$ is the shear stress axis; $\boldsymbol{\sigma_3}$ is minimum stress component; $\boldsymbol{\sigma_1}$ is the maximum stress component; ϕ is the rock internal friction angle; $\boldsymbol{\theta}$ is the angle between $\boldsymbol{\sigma_1}$ and a given plane in the space; **a** is Mohr circle's ray; **b** indicate how far the circle is to touch the Mohr-Coulomb Envelopment.

Figure 5. 7. Furna Feia location in relation to the outcrops.

This figure shows how the Furna Feia extends at depth, beneath the Jandaíra Formation outcrops. It is noticeable the geometry of the cave with the pattern of fractures in outcrop.

5. Partial conclusions

Despite the small number of fractures identified on satellite imagery surrounding the Furna Feia cavern, the numerical modeling results remain valid since they contemplate the general behavior of faults and fractures in the area.

According to this numerical modeling the deformation observed on the study area presents a directions distribution of fracturing favorable for the creation of high permeability zones by dilation with a very low amount of stress (5 MPa). This behavior was evident on both compressive and shear scenarios.

In this way, the feasibility of the theory presented in Chapter 4 for the creation of the Furna Feia cavern system is demonstrated.

Chapter 6

Conclusions

As demonstrated at the very beginning of this study, hydrocarbons are nowadays the most important source of energy in the world and carbonate reservoirs have a significant participation for the global oil and gas supply. On the other hand, the knowledge about the key elements controlling the porosity and permeability in carbonate reservoirs is incomplete. This is especially true regarding the understanding of brittle deformation contribution to the creation of secondary porosity and subsequent permeability increases.

Over four chapters of this thesis information compiled from the literature and results from analysis performed in this study were presented. These data contributed to the construction of a tectonic-structural model for the study area and a theory to explain the creation of the cavern system named Furna Feia. This cavern was developed in the carbonate rocks of Jandaíra Formation, which was used as analogue to fractured carbonate reservoirs.

From the published data were obtained information about earthquakes focal mechanism and results of tests and logs acquired from hydrocarbon wellbores. This information demonstrated that: (i) the state of stress nowadays predominant through the Basin is strike-slip, with some reverse events; (ii) the orientation of the component of maximum horizontal stress ranges from NW-SE to E–W. In such stress regime it is expectable that the NE-SW faults, inherited from the Potiguar Rift opening, are favorably oriented to be reactivated as inverted faults, while the NW-SE, E-W and N-S faults are favorably oriented to be reactivated as strike-slip faults.

From the lineaments analysis performed in this study it was identified that for the Basin (regional-scale) the main lineaments domain is oriented approximately N65^{o}E, while at the study area (local-scale) the main lineaments domain is oriented N49^{o}W. These two trends are nearly orthogonal (114^{o} divergent). Such results difference put into evidence that at the study area exist some particular structural evolution, that could be related or not to the regional tectonic-structural history.

From the analysis of outcrops measurements, the NW-SE direction was confirmed as the principal structural trend at the study area. Also were calculated two stress tensors that possibly generated the observed deformation: (i) a stress tensor oriented NW-SE and compatible with a strike-slip fault regime, that could explain only the observed faults; (ii) a stress tensor oriented NW-SE too but compatible with a reverse fault regime, that could explain the whole deformational pattern observed through the area. Both stress tensors are in conformity with the present day regional state of stress given by the seismology and the borehole data analysis, but the second stress solution was assumed as being the most reliable as a function of the Monte Carlo test included on the algorithm which calculated this tensor.

The azimuth distribution of principal axis of the Furna Feia cavern galleries was compared with the statistical analysis of structural measurements. Such comparison demonstrated that exist a clear coincidence between the principal structural trends at the study area and the galleries axis of the cavern.

On the basis of all available information was thought a tectonic-structural model for the study-area, which predicts that:

(i) Exist a major not outcropping NE-SW normal fault, somewhere toward NW from the study area;

(ii) Given the estimated nowadays stress regime, the hypothetical NE-SW normal fault was reactivated as an inverted fault;

(iii) This inversion movement caused the exhumation of the Jandaíra Formation, on the returning hanging wall of the main NE-SW fault;

(iv) The minor NW-SE strike-slip faults result from the accommodation movements due to the major NE-SW fault activity;

(v) The minor NE-SW strike-slip faults constitute conjugated pairs with the NW-SE strike-slip faults, or are related to oblique movements of the main NE-SW fault.

(vi) The fracturing associated to this brittle deformation history was responsible by the creation of oriented high fractured corridors. These corridors control the meteoric water circulation through the Jandaíra limestone rocks, conducting the dissolution process and the formation of the Furna Feia caverns system.

Afterwards a numerical model was run in order to examine the reasonability of the theory proposed for the permeability increasing on the Jandaíra carbonates. Such numerical model is based on mechanical analysis by finite element method for 2D simulation, comprised on the program TECTOS, At the end of this work it was accepted that the faults and joints observed through the whole study area, associated to a dilatancy effect, led to a porosity increasing on the Jandaíra carbonate rocks and controlled the creation of high permeability corridors. Such high permeability zones focalized the water percolation into the carbonate rocks and conditioned the growth of the Furna Feia cavern system

Under the light of these results the main conclusions of this doctoral thesis are:

1. If at the study area a real hydrocarbon reservoir would exist, possibly instead of a cavern system it could be found a superior productivity zone.
2. Taking this into account, it was demonstrated that the understanding of the fracturing processes on carbonates is fundamental for the predictability improvement of geological models, that will better support the selection of exploratory targets on carbonatic plays and the decision chain for carbonate reservoirs management.
3. The capability to recognize the fracturing pattern on a given area offered by the lineament analysis and numerical models represents an improvement on the localization of high fractured zones, consequently the detection of potential high permeability targets.

References Cited

Aadnoy, B. S., & Bell, J. S. (1998). Classification of Drilling - Induced Fractures and Their Relationship to In-Situ Stress Directions. The log Analyst Journal: 27 - 42.

Aadnoy, B.S. (1990). In-Situ stress directions from borehole fracture traces. Journal of Petroleum Science and Engineering, **4**: 143-153

Addis, M. A., Hanssen, T. H., et al. (1998). A Comparison Of Leak-Off Test And Extended Leak-Off Test Data For Stress Estimation. SPE/ISRM Eurock '98: 131-140.

Aguilera, R. (2006). Sandstone vs. carbonate petroleum reservoirs: A global perspective on porosity-depth and porosity-permeability relationships: Discussion. AAPG Bulletin **90**(5): 807-810.

Almeida, F.F.M., Hasui, Y., et al. (1977). Províncias estruturais brasileiras, paper presented at 2nd Simp. Geol. Nordeste, Anais Soc. Brás. Geol. Núcleo Nordeste, 242-258, Campina Grande, Brasil.

Araripe, P. T. & F. J. Feijó (1994). Bacia Potiguar. Boletim de Geociências da PETROBRAS. **8**: 127-141.

Arellano-Baeza, A. A., Zverev, A. T. & Malinnikov, V. A. (2006). Study of changes in the lineament structure, caused by earthquakes in South America by applying the lineament analysis to the Aster (Terra) satellite data. Advances in Space Research **37**, 690–697.

Assumpção, M. (1992). The Regional Intraplate Stress Field in South America. Journal of Geophysicl Research **97**(B8), 1.889-11.903.

Assumpção, M. (1998). Seismicity and Stresses in the Brazilian Passive Margin. Bulletin of the Seismological Society of America **88**(1), 160-169.

Babcock, E. A. & Sheldon, L. G. (1976). Structural significance of lineaments visible on aerial photos of the Athabasca oil sands area near Fort Mackay, Alberta. Bulletin Of Canadian Petroleum Geology **24**(3), 457-470.

Balaji, S. & Ramasamy, S. (2005). Remote Sensing and Resistivity Image for the Tectonic Analysis of Biligirirangan Region of Peninsular India. Geocarto International **20**(2), 55-61.

Barton, C. A., M. D. Zoback, et al. (1995). In situ stress and permeability in fractured and faulted crystalline rock. The Mechanics of Jointed and Faulted Rock, Viena / Austria.

Bell, J. S. (1990). Investigating stress regimes in sedimentary basins using information from oil industry wireline logs ans drilling records. Geological Application of

Wireline Logs. A. Hurst, M. A. Lovell and A. C. Morton, Geological Society Special Publication. **48**: 305-325.

Bertani, R. T., Costa, T. G., et al. (1991). Evolução Tectono-Sedimentar, Estilo Estrutural e Habitat do Petróleo na Bacia Potiguar. Origem e Evolução de Bacias Sedimentares. G. P. e. M. de Raja Gabaglia, E.J., Petrobras: 291-310.

Bezerra, F. H. R. & Vita-Finzi, C. (2000). How active is a passive margin? Paleoseismicity in northeastern Brazil. Geology **28**(7), 591-594.

Bezerra, F. H. R., Brito Neves, B.B, et al. (2008). "Late Pleistocene tectonic-geomorphological development within a passive margin — The Cariatá trough, northeastern Brazil." Geomorphology **97**: 555–582.

BP. (2009, June). "Statistical Review of World Energy."
(http://www.bp.com/statisticalreview)

Brudy, M. (1998). Determination of the State of Stress by Analysis of Drilling - Induced Fractures - Results from the Northen North Sea. SPE/ISRM Eurock '98, SPE/ISRM 47236, p. 141-149.

Bullard, E. C., Everett, J. E. & A.G., S. (1965). The fit of the continents around the Atlantic. In: Symposium on Continental Drift Ser. A, 258. Philos. Trans. R. Soc., London, 41-51.

Burcham, J. (2009, September 8). ""Learning about caves; how caves are formed. (http://www.amazingcaves.com/learn_formed.html)

C&C Reservoirs (1998). Chapter 1 – Overview and Summary Statistics.

Choquette, P.W., Pray, L.c. (1970). Geologic nomenclature and classification of porosity in sedimentary carbonates. AAPG Bulleting, **54**(2): 207-250.

Conceição, J. C. J., Zalán, P. V. & Wolff, S. (1988). Mecanismo, evolução e cronologia do Rift Sul-Atlantico. Bol. Geociênc. PETROBRAS **2**(2/4), 255-265.

Cremonini, O. A. (1993). Caracterização estrutural e evolução tectônica da área de Ubarana, porção submersa da Bacia Potiguar, Brasil. Dissertação de Mestrado, Universidade Federal de Ouro Preto.

Cremonini, O. A., Goulart, J. P. M. & Soares, U. M. (1996). O Rifte Potiguar: novos dados e implicações tectônicas. The Potiguar Rift: recent data and tectonic implications. In: Boletim do 4o Simpósio sobre o Cretáceo do Brasil, UNESP - Campus de Rio Claro / SP, 89-93.

Easterbrook, D.J. (1999). Surface Processes and Landforms. New Jersey, Prentice Hall, 2nd ed.

Ehrenberg, S. N. and P. H. Nadeau (2005). "Sandstone vs. carbonate petroleum reservoirs: A global perspective on porosity-depth and porosity-permeability relationships." AAPG Bulletin v. 89(no. 4): 435-445.

Ervine, W. B., & Bell, J. S. (1987). Subsurface In-Situ Stress Magnitudes from Oil Well Drilling Records: An Example from The Venture Area, Offshore Eastern Canada. Canadian Journal of Earth Sciences.

Fainstein, R., Gregory-Sloan, J., Christie, P. (1998). Capítulo 5 - A ocorrência de petróleo na costa brasileira: imagem espelho da costa oeste africana. In:Searching For Oil and Gás in the Land of Giants. Ed. Schlumberger: 81-92.

Ferreira, J. M., Oliveira, R. T., Takeya, M. K. & Assumpcao, M. (1998). Superposition of local and regional stresses in northeast Brazil: evidence from focal mechanisms around the Potiguar marginal basin. Geophys. J. Int. 134, 341–355.

Finkbeiner, T., C. A. Barton, et al. (1997). "Relationships Among In - Situ Stress, Fractures and Faults, and Fluid Flow: Monterey Formation , Santa Maria Basin, California." AAPG Bull. **81**(12): 1975 - 1999.

Françolin, J. B. L. & Szatmari, P. (1987). Mecanismo de Rifteamento da Porção Oriental da Margem Norte Brasileira. Revista Brasileira de Geociências **17**(2), 196-207.

Gleeson, T. & K. Novakowski (2009). "Identifying watershed-scale barriers to groundwater flow: Lineaments in the Canadian Shield." GSA Bulletin **121**(3/4): 333-347.

Groshong, R. (2006). "Structural Validation, Restoration and Prediction". 3-D structural geology: a practical guide to quantitative surface and subsurface map interpretation, Birkhäuser.

Guo, G., George, S. A. & Lindsey, R. P. (1999). Statistical analysis of surface lineaments and fractures for characterizing naturally fractured reservoirs. In: Reservoir Characterization-Recent Advances, AAPG Memoir 71, Chapter 16 (edited by Jordan, R. S. a. J.), 221–250.

Hobbs, W. H. (1904). "Lineaments of the Atlantic border region." Geological Society of America Bulletin **15**: 483-506.

Hubbert, M. K., & Willis, D. G. (1957). Mechanics of Hydraulic Fracturing. American Institut of Mining Eng.. Petroleum Transactions, **210**: 153-168.

IEA - International Energy Agency. (2006). World Energy Outlook - Summary and Conclusions. (http://www.iea.org/weo/2006.asp)

Jordana, G., & Schott, B. (2005). Application of wavelet analysis to the study of spatial pattern of morphotectonic lineaments in digital terrain models. A case study. Remote Sensing of Environment **94**, 31–38.

Lima, C. C., Nascimento, E. & Assumpção, M. (1997). Stress orientations in Brazilian sedimentary basins from breakout analysis: implications for force models in the South American plate. Geophys. J. Int. **130**, 112-124.

Lima Neto, F. F. (1998). Um exemplo da interferência mecânica de uma interface fraca da distribuição regional de esforços tectônicos: o campo atual de tensões da Bacia Potiguar, Nordeste Brasileiro. Author's studies, 320p.

Lima Neto, F. F. (1999). O Regime Atual de Tensões nas Bacias Sedimentares Brasileiras. In: Anais do VII SNET - Sessão 4, Lençoes - Bahia, Brasil.

Liu, W.T.H. (2007). Aplicações de Sensoriamento Remoto. Ed. UNIDERP. 908p.

Lønøy, A. (2006). "Making sense of carbonate pore systems." AAPG Bulletin 90 (9): 1381–1405.

Lucia, F. J. (2007). Carbonate Reservoir Characterization. An Integrated Approach. Springer, 2nd edition. p. 336.

Masoud, A. & Koike, K. (2006). Tectonic architecture through Landsat-7 ETM+/SRTM DEM-derived lineaments and relationship to the hydrogeologic setting in Siwa region, NW Egypt. Journal of African Earth Sciences **45**, 467–477.

Matos, R. M. D. (1992). The Northeast Brazilian Rift System. Tectonics **11**(4), 766-791.

Mastin, L. (1988) Effect of Borehole Deviation on Breakout Orientations. Journal of Geophysical Research **93**: 9187-9195.

Mckenzie, D. (1969). "The relation between fault plane solution and the directions of principal stresses." Bull Seismol Soc. Am. **59**: 591-601.

McLean, M. R., & ADDIS, M. A. (1990). Wellbore Stability Analysis: A Review of Current Methods of Analysis and Their Field Application. IADC/SPE Drilling Conference, p. 261 - 273.

Montaron, B. (2008). "Confronting Carbonates." Oil Review Middle East(5): 132-135.

Moraes, A. (1995). Estudo dos campos de tensões locais e da geração de falhas em regime extensional pelo método dos elementos finitos. Departamento de Geologia, Escola de Minas. Ouro Preto, Universidade Federal de Ouro Preto: 241 p.

Nogueira, F. C., Bezerra, F. H. R., et al. (2010). "Quaternary fault kinematics and chronology in intraplate northeastern Brazil." Journal of Geodynamics **49**: 79–91.

Onyedim, G. C. & Norman, J. W. (1986). Some appearances and causes of lineaments seen on landsatimages. Journal of Petroleum Geology **9**(2), 179-194.

Peacock, D. C. P. and A. Mann (2005). Controls on Fracturing in Carbonate Rocks. SPE 92980.

Peska, P., & Zoback, M. D. (1995) Compressive and tensile failure of inclined well bores and determination of in situ stress and rock strength. Journal of Geophysical Research, **100**: 12,791-12,811.

Pessoa Neto, O. C. et al. (2007). Bacia Potiguar. In: B. Geoci. Petrobras **15**, 357-369.

Plumb, R. A., & Hickmann, S. H. (1985). Stress-Induced Borehole Elongation: A Comparison Between the Four - Arm Dipmeter and the Borehole televiewer in the Auburn Geothermal Well. Journal of Geophysical Research, **90**: 5513-5521.

Popoff, M. (1988). Du Gondwana à l'Atlantique sud: les connexions du fossé de la Bénoué avec les bassins du Nord-Est brésilien jusqu'a l'overture du golfe de Guiné au Crétacé inférieur, in The West African Connection. J. Afric. Earth Sci. **7**(2), 409-431.

Pradhan, B., Singh, R. P. & Buchroithner, M. F. (2006). Estimation of stress and its use in evaluation of landslide prone regions using remote sensing data. Advances in Space Research **37**, 698–709.

Rabinowitz, P. D. & La Brecque, J. L. (1979). "The Mesozoic South Atlantic Ocean and Evolution of Its Continental Margins." Journal of Geophysical Research **84**: 5973 - 6002.

Raghavan, V., Masumoto, S., Koike, K. & Nagano, S. (1995). Automatic lineament extraction from digital images using a segment tracing and rotation transformation approach. Computer & Geosciences **21**(4), 555-591.

Rahiman, T. I. H. & Pettinga, J. R. (2008). Analysis of lineaments and their relationship to Neogene fracturing, SE Viti Levu, Fiji. GSA Bulletin **120**(11/12), 1544–1555.

Raleigh, C.B., Healy, J.H., Bredehoeft, J.D., (1972). Faulting and crustal stress at Rangely, Colorado. In Flow and Fracture of Rocks, Geophys. Monogr. Ser., 16. Eds., H.C. Heard et al. 275-284, AGU, Washington.

Regali, M.S.P. & Viana, C.F. (1989). Late Jurassic-Early Cretaceous in Brazilian Sedimentary Basins: Correlation with the International Standard Scale. Eds. Petróleo Brasileiro S.A.

Salvini, F. & Vittori, E. (1982). Analisi strutturale della linea Olevano - Antrodoco - Posta (Ancona - Anzio Auct.): metodologia di studio delle deformazioni fragili e presentazione del tratto meridionale. Memorie della Società Geologica Italiana **24**, 337-356.

Sarkisyan, S. G., Politykina, M. A., et al. (1973). Efect of Postsedimentation Processes on Carbonate Reservoir Rocks in Volga-Urals Region, USSR. AAPG Bulletin. **57**: 1305 - 1313.

Schlumberger. (2007). "Carbonate Reservoirs." 2010.
(http://www.slb.com/services/industry_challenges/carbonates)

Solomon, S., & Ghebreab, W. (2006). Lineament characterization and their tectonic significance using Landsat TM data and field studies in the central highlands of Eritrea. Journal of African Earth Sciences **46**, 371–378.

Souza, Z.S., Vasconcelos, P.M., et al. (2004). Geocronologia e geoquímica do magmatismo cretácico a terciário do NE do Brasil. In: Congresso Brasileiro de Geologia, Araxá, Minas Gerais. CD ROM.

Szatmari, P., Françolin, J. B. L., et al. (1987) Evolução tectônica da margem equatorial brasileira. Rev. Bras. Geosc. **17**(2): 180 - 188.

Takeya, M., Ferreira, J. M., et al. (1989). "The 1986-l 988 intraplate earthquake sequence near João Câmara, northeast Brazil-evolution of seismicity." Tectonophysics **167**: 117-131.

Tibana, P.; Terra, G.J.S. 1981. Sequências carbonáticas do cretáceo da Bacia Potiguar. Boletim Técnico da PETROBRÁS **24** (3), 174-183.

Unternehr, P., Curie, D., Olivet, J. L., Goslin, J. & Beuzart, P. (1988). South Atlantic fits and intraplate boundaries in Africa and South America. Tectonophysics **155**, 169-179.

VanderBrug, G. J., 1976, Line detection in satellite imagery. IEEE Transactions on Geosciences and Electronics **14**, 37-43

Wester, K. & Lundén, B. (1996) Digital Elevation Data, Ladsat TM and Magnetic Data for Visualization of Geomorphological and Geological Features. In Remote Sensing and GIS for Site Characterization: Applications and Standards, ASTM STP 1279, V.H. Singhroy, D.D, Nebert, and A.I. Johnson, Eds., American Society for Testing and Materials, 29-37.

Wiprut, D. Zoback, M. D. (2000). "Fault reactivation and fluid flow along a previously dormant normal fault in the northern North Sea." Geology **28**(7): 595–598.

Wise, D. U. & Vincent, R. J. (1965). Rotation axis method for detecting conjugate planes in calcite petrofabric. American Journal of Science **263**, 289-301.

Wise D.U. (1969). Pseudo-radar topographic shadowing for detection of subcontinental sized fracture systems. Proceedings of the Sixth International Symposium in the Remote Sensing of Environment, Univ. Michigan, 603-615

Wise, D. U. (1982). Linesmanship and the practice of Linear Geo-art. Geological Society of America Bulletin **93**, 886-888.

Wise, D. U., Funiciello, R., Parotto, M. & Salvini, F. (1985). Topographic lineament swarms: Clues to their origin from domain analysis of Italy. Geological Society of America Bulletin **96**, 952-967.

Zoback, M. D., Moos, D., et al. (1985). Well Bore Breakouts and In Situ Stress. Journal of Geophysical Research, **90**: 5523-5530.

Zoback, M. L. (1992). First- and second-order patterns of stress in lithosphere: the World Stress Map Project. Journal of Geophysical Research, **97**: 11,703 -11,728.

Zoback, M.D. & Peska, P. (1995). In-Situ Stress and Rock Strength in the GBRN/DOE Pathfinder Well, South Eugene Island, Gulf of Mexico. SPE 29233.

Appendix

Definition of Terms

Chapter 1- Problem Presentation

[1.1] C&C Reservoirs (http://ccreservoirs.com) captures, distills and delivers lessons learned in the upstream E&P industry, and documents the experiences of thousands of geoscientists and reservoir engineers.

[1.2] The term "natural fractures" is here used to distinguish the tectonic fractures from those artificially induced in some operation in the petroleum industry (hydraulic fractures).

[1.3] The term "water breakthrough" refers to the arrival of the injected water at the producer well. This occurs naturally when it is necessary to inject water through the reservoir to impel the oil toward the producer wells. Eventually the water arrives before the predicted time, what is usually supposed be caused by not detected fractured high permeability zones.

[1.4] Mud is a general name for the fluids used while drilling wells for hydrocarbons exploration and production, to reduce the heat produced by the friction on the drilling tool, and to keep the well stability by preventing the formation falling into the hole. There are three main categories of drilling fluids: water-based mud, that is the most common; oil-based mud; gaseous drilling fluid.

Chapter 2 – The Potiguar Basin

[2.1] The Late Jurassic to Early Cretaceous sediments on Brazilian basins is marked by the absence of marine fossils, as a result of its fluviolacustrine origin and evolution. For years this fact created many difficulties on establishing an accurate chronocorrelation between these nonmarine sequences and the International Standard Chronostratigraphic Scale. Based on palynological and micropaleontological (ostracodes) information, obtained from hydrocarbon prospection in Brasil and worldwide, Regali and Viana (1989) established six local Stages equivalent in age to marine sediments of Europe and Canada: Dom João (Tithonian); Rio da Serra (Berriasian to Early Hauterivian); Aratu (Hauterivian to Early Barremian); Buracica (Middle Barremian); Jiquiá (Late Barremian to Early Aptiano); Alagoas (Aptian to Early Albian).

[2.2] Sabkha environment refers to restrict lakes formed along an arid coastline, characterized by evaporite-carbonate deposits with some siliciclastics.

[2.3] The focal mechanism solution of a single earthquake does not give directly the orientation of the principal stresses acting in the lithosphere, but only the directions of that part of the stress released by the earthquake (McKenzie, 1969; Assumpção, 1992). However, the experience has shown that the differences between the orientations of the P and T axes of focal mechanism solution and the principal directions of the stress field are not usually more than about 30^o (Raleigh et al., 1972; Assumpção, 1992).

[2.4] The World Stress Map (WSM) is a collaborative project between academia, industry and government that aims to characterize the stress patterns and to understand the stress sources (http://www.world-stress-map.org).

Chapter 3 Lineament Analysis

[3.1] SRTM3 means Shuttle Radar Topography Mission, with a 3 arc-second resolution (equivalent to 90m).

Chapter 4 – Structural Analysis

[4.1] Monte Carlo methods (or Monte Carlo experiments) are a class of computational algorithms that rely on repeated random sampling to compute their results. Monte Carlo methods are often used in simulating physical and mathematical systems. Because of their reliance on repeated computation of random or pseudo-random numbers, these methods are most suited to calculation by a computer and tend to be used when it is unfeasible or impossible to compute an exact result with a deterministic algorithm.

[4.2] In structural geology section restoration is a technique used to progressively undeform a geological section in an attempt to validate the interpretation used to build the section. It is also used to provide insights into the geometry of earlier stages of the geological development of an area. A section that can be successfully undeformed to a geologically reasonable geometry, without change in area, is known as a balanced section(Groshong, 2006).

Chapter 5 – Numerical Modeling

[5.1] Finite element method (FEM) is a numerical technique for finding approximate solutions of partial differential equations (PDE) as well as of integral equations.

The solution approach is based either on eliminating the differential equation completely (steady state problems), or rendering the PDE into an approximating system of ordinary differential equations, which are then numerically integrated using standard techniques such as Euler's method, Runge-Kutta, etc.. Its practical application often known as finite element analysis (FEA).